Strangers in a strange land: bacteria provide mechanistic insight into eukaryotic ubiquitination

by

Tyler G. Franklin

A DISSERTATION

Presented to the Department of Molecular Microbiology and Immunology

and the Oregon Health and Science University

School of Medicine

in the partial fulfillment of

the requirements for the degree of

Doctor of Philosophy

November 2023

School of Medicine

Oregon Health & Science University

CERTIFICATE OF APPROVAL

This is to certify that the PhD dissertation of

Tyler Franklin

has been approved.

_____

Advisor: Jonathan Pruneda

_____

Chair: Eric Barklis

_____

Member: David Farrens

_____

Member: Isabella Rauch

_____

Member: Scott Landfear

_____

Member: Michael Cohen

_____

Member: Liman Zhang

Table of Contents

List of Figures

List of Tables

Acknowledgments

First, I must express my gratitude to my advisor and friend, Jonathan Pruneda, who has been with me on this journey since day 1. It's been a glorious ride, with countless cups of seasoned coffee, long nights of crystallography fueled by beer and a bottomless pit of hopes and dreams, and so much more. We've shared so many successes and endured even more failures, but we did all of it together. You have shaped me into the scientist I will be moving forward, which I know wasn't always easy, and I will always owe you a debt of gratitude for your patience, support, and encouragement. The lab's future is incredibly bright.

My irreplaceable grad school comrades, Thomas and Taylor, who together with me formed the infamous Triple-T academy, and Kristen, Lauren, FliC and Eve, who kept the Triple-T academy in check… mostly. Without you all, graduate school would have lacked all color.

My honorary advisor Jeff, who has provided me with laughs, guidance, a seat at the table for Thanksgivings, Christmases, birthdays, and the Macy's parade, as well as plenty of strife when I forget which TLR recognizes flagellin. *Go Buffs!*

My former advisors and dear friends Michael Guarnieri (Mikey G.) and Calvin Henard (the immortal C-money), Karolin Luger, and Guillaume Gallier, all without whom I would never have had the confidence to go to graduate school, brew beer, navigate life, and not take myself too seriously.

My lab mates Justine, Cam, Gus (*Go Avs!*), Madeline (*let's ride!*) and Will (can I get a *Shigell*-yeah?) who made coming to work so much easier.

My best friends back home, Josh and Jordan, who are forever my best buds, the most creative individuals I've ever known and who both provide me a source of happiness and

great music recommendations. We will never be able to go as hard as we did when we were younger, but we're going to try at Jordan's and Chloe's wedding.

Marin, you have taken me on so many adventures, kept my head and heart above water and steered the ship for me in the murky waters of a sunsetting graduate student. *So anyway*, I can't summarize all you've meant to me here. Here's to many more years of getting skunked in cribbage and nulled in Tennis. You are loved and deeply cared-for.

Rick, we love you, miss you, and will always cherish the beautiful memories you gave us.

Britt Britt, my dearest, amazing little sister who breathes life and fun into everything she touches, has so much potential, and I can't wait to see what the future holds for your mighty ambitions!

Riley, you have been my closest friend since the beginning, from our little mermaid fashion show to our chaotic Los Angeles adventures. Thank you for everything, especially being able to summarize my entire 5-year dissertation and scientific ramblings into a single, beautiful piece of art, arguably of which will be more coherent than this document.

Mom (guy, buddy, friend), you have always offered me the kind of blind love and loyalty that isn't meant to exist on Earth, and I know full-heartedly I could always drop everything and return to your home, no questions asked. I couldn't have done this without you.

Dad, you've always given me unfailing support in grad school and helped guide me in all things with your infinite wisdom. You are the lighthouse, and without you, I would be lost. Someday we will both be retired and fish the days away with bushy fisherman's beards.

Now, in the infamous words of Mikey G.: *And with that, it's business time…*

Abstract

Ubiquitin (Ub) is a critical post-translational modifier that is used in the regulation of virtually every cellular pathway. Ubiquitination occurs when an E3 Ub ligase, such as a Homologous-to-the-E6AP-C-terminus (HECT) Ub ligase, catalyzes the transfer of Ub onto a lysine (Lys or K) residue of its substrate. E3 Ub ligases can attach multiple Ub monomers together to generate poly-ubiquitin (polyUb). Because Ub has seven Lys residues (K6, K11, K27, K29, K33, K48, and K63), and can be linked through its N-terminal methionine (M1), at least eight different types of polyUb exist. Following Ub ligation, a diverse set of Ub-regulating proteins recognize only very specific polyUb assemblies and signal for downstream events, with each polyUb signal thought to result in distinct cellular outcomes. A final layer of regulation exists with the deubiquitinating enzymes, which can cleave polyUb nonspecifically, or with exquisite specificity for only a single type of polyUb. This polyUb specificity intimately links ligases, deubiquitinases, and other Ub regulators, to a particular signaling pathway. For example, HECTs in the protein degradation pathway generate K48-linked polyUb onto targets, and these K48-linked polyUb modifications are specifically recognized by protein degradation machinery. Other well-described polyUb signaling outcomes with known E3 Ub ligases include K63-linked polyUb (cellular trafficking) and M1-linked polyUb (the innate immune response). However, the Ub ligases and signaling outcomes for other chains, like K6, are unclear. Concurrently, because of the critical and emerging roles of Ub in responding to pathogen invasion, several viruses and bacteria have evolved their own Ub regulating enzymes, despite not encoding Ub themselves. Though the Ub ligation mechanism and functionality remains unclear, one of these enzymes, NleL, assembles the mysterious K6-linked polyUb, representing a potential

inlet into understanding K6-linked polyUb signaling. NleL is found in the diarrhea-causing pathogen Enterohemorrhagic *Escherichia coli* (EHEC), and appears to mimic HECT Ub ligases. However, because NleL has poorly resolved cellular targets, disputed functionality in the literature, and also generates, confoundingly, K48-linked polyUb, it is difficult to study the signaling role of K6-linked polyUb by NleL.

Here, I present a comprehensive assay termed UbiReal for monitoring each step of the Ub signaling cascade, including linkage-specific polyUb ligation and deubiquitination. Next, I use bioinformatic tools and recombinant protein expression to identify additional, HECT-like ligases from human and plant pathogens, and validate these ligases using UbiReal. I apply structural biology and biochemical techniques to elucidate the mechanism of Ub ligation by the bacterial HECT-like ligases, and capture a rare glimpse of a linkage-specific polyUb ligation interface. I leverage insights from the linkage-specific polyUb interface to engineer an NleL specific for K6-linked polyUb, and show that similar rules influence the ligation of K6-linked polyUb in humans. Finally, through analysis of a family of deubiquitinating enzymes in bacteria, I demonstrate the utility of the deubiquitinase LotA as a tool for detecting the presence of K6-linked polyUb. Collectively, this dissertation provides the critical tools for understanding K6-linked polyUb biology, and in particular sets the stage for elucidating the enigmatic role of K6-linked polyUb at the host-pathogen interface.

Chapter 1 – Introduction

Franklin, T.G., and Pruneda, J.N. (2021). Bacteria make surgical strikes on host ubiquitin signaling. *PloS Pathogens* 17, e1009341. 10.1371/journal.ppat.1009341.

Roberts, C.G., Franklin, T.G., and Pruneda, J.N. (2023). Ubiquitin-targeted bacterial effectors: rule breakers of the ubiquitin system. *EMBO Journal*. 42, e114318. 10.15252/embj.2023114318.

Abbreviations: Ub, ubiquitin; monoUb, monoubiquitin; polyUb, polyubiquitin; Lys or K, lysine; Cys or C, cysteine; Met or M, methionine; RING, Really Interesting New Gene; RBR, RING-between-RING; HECT, Homologous to E6AP C-terminus; LUBAC, linear ubiquitin assembly complex; RCR, RING-Cys-relay; NleL, non-LEE(locus of enterocyte effacement) encoded ligase; NEL, novel E3 ligase; DUB, deubiquitinase; OTU, ovarian tumor deubiquitinase; USP, ubiquitin specific protease; EHEC, enterohemorrhagic *Escherichia coli*; EPEC, enteropathogenic *Escherichia coli*; DDR, DNA damage response; UPS, ubiquitin proteasome system; PDB, protein data bank.

The Ub signaling pathway

A general overview

Our cells are composed of dynamic networks that enable rapid, complex responses to various stimuli, such as hormones stimulating cell division, insulin increasing sugar metabolism, or even a more dangerous stimulus such as the presence of a pathogen that instigates an immune defense pathway. These rapid responses are mediated by the messengers and workers of our cells: proteins. Proteins themselves can require additional modifications to regulate their activities and enable dynamic responses to new cellular stimuli. For example, a protein may face the surface of the cell, but, following an extracellular stimulus, another protein will *modify* the previously surface-facing protein with an additional signal that brings it back into the cell (through a process called endocytosis) for a new intracellular task. Proteins that are able to perform these modifications through biochemical reactions are known as enzymes. One of the most abundant and versatile protein modifications is known as ubiquitination.

Ubiquitination is achieved through the coordinated effort of the E1, E2, and E3 enzymatic cascade, which attaches ubiquitin (Ub), a small protein itself, onto lysine residues of targeted proteins (**Fig. 1.1**). Ubiquitination is an essential eukaryotic post-translational modification that regulates a gamut of cellular processes, including classical roles in proteasomal degradation (the 'recycling can' of the cell), newly established roles in endocytosis and protein trafficking, and emerging roles in immunity and the response to invading pathogens[1]. The crucial role of ubiquitination in cellular signaling is reflected by the fact that about 5% of the human protein-coding genome is dedicated to the regulation

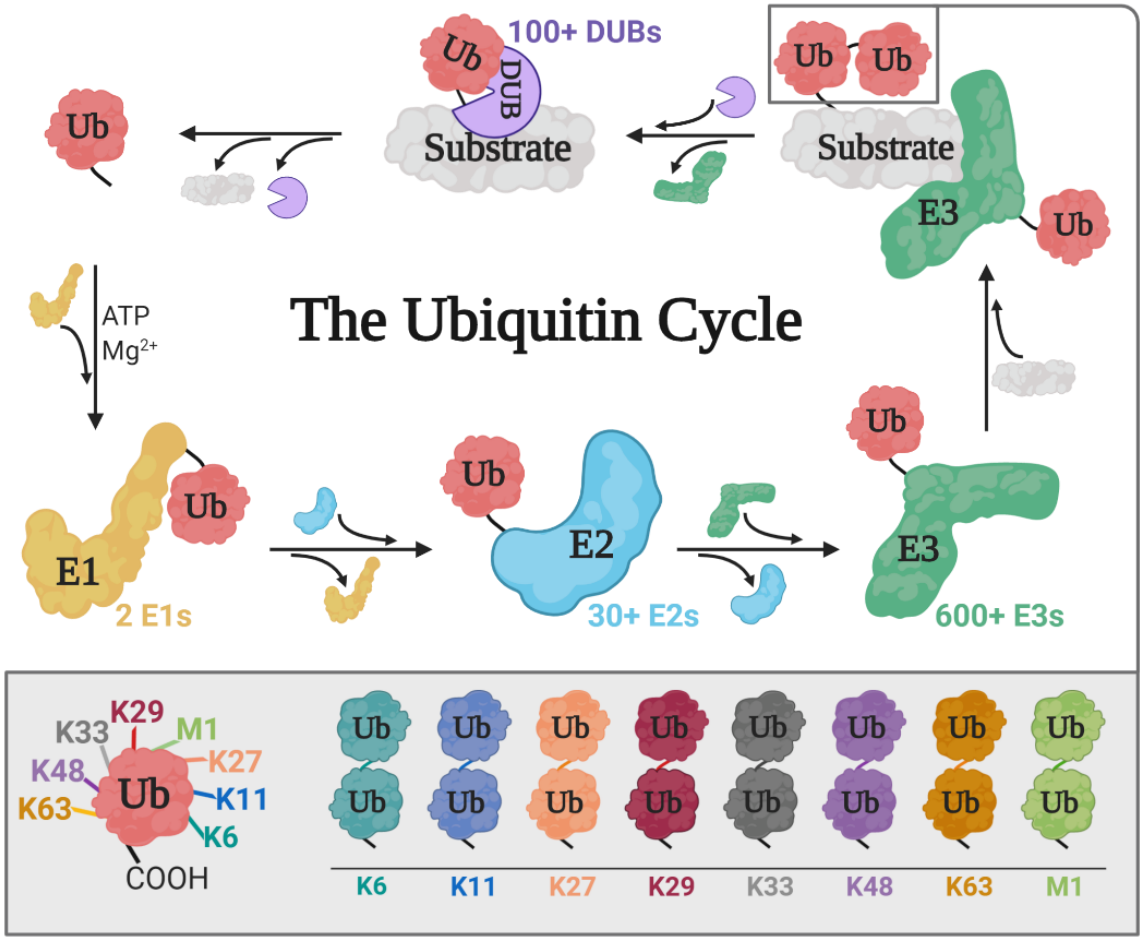

Figure 1.1 The Ub cycle.

A schematic demonstrating the enzymatic cascade governing ubiquitination. The E1 Ub-activating enzyme, utilizing ATP and Mg^{2+} as cofactors, activates Ub through adenylation and forms the E1~Ub conjugate. E1~Ub transfers Ub to different E2 Ub-conjugating enzymes to from the critical E2~Ub conjugate. The E2~Ub conjugate may then work with Really Interesting New Gene (RING)-type ligases to attach Ub onto a target substrate or, as depicted here, transfer the Ub to a Cys-dependent E3 (such as a HECT-type E3) to generate the E3~Ub conjugate that then ligate the Ub to its target substrate. Following the initial monoUb modification, an additional Ub can be utilized to further modify the monoUb into several different types of polyUb (K6, K11, K27, K29, K33, K48, K63, or M1). These polyUb modifications can be cleaved by DUBs to return free monoUb. The amounts of different E1, E2, E3, and DUB regulators that are known to exist are indicated.

of ubiquitination[2]. In particular, the enzymatic cascade features over 30 E2s and a whopping 600+ E3s (**Fig. 1.1**). The large number of E3s, which dictate target selection, partly explain the extensive reach of ubiquitination.

Critically, the breadth of different signaling roles for Ub stems partly from the unique ability of Ub to be linked into complex polyUb chains through any of its seven lysine residues or the amino-terminus (**Fig. 1.1**)[1,3,4]. The emerging theme thus far is that diverse and distinct cellular messages are encoded in each polyUb chain-type, but identifying the regulators that maintain each different polyUb chain-type, and the and the exact signaling outcomes they encode, is an active area of research[5].

He who controls the spice controls the universe: a closer look at the many flavors of polyUb

Ub contains lysine (Lys or K) residues which can serve as the target of ubiquitination, resulting in the potential formation of the eight distinct polyUb chain-types: K6, K11, K27, K29, K33, K48, K63, and M1, a special case where Ub is linked through its N-terminal methionine (M1) residue[1]. While it is helpful to think of Ub as a complex Lego with 8 attachment sites that can support complex assemblies limited only by the builder's imagination, it is perhaps more fun (for some) to imagine polyUb as the *spice* from Frank Herbert's Dune series, except here the *spice* comes in many distinct flavors. Modification with some *flavors* of polyUb frequently initiate protein degradation pathways (K11, K48), but non-degradative *flavors* of polyUb also exists in endocytic processes (K63), the innate immune response (M1, K63), and several other biological pathways[1]. As noted, a massive 5% of the human protein-coding genome is dedicated to Ub signaling, and, on a more

serious note, the dysregulation (mutation, etc.) of these regulators are implicated in numerous cancers, neurodegenerative diseases, and autoimmune disorders[2]. This large number of regulators and the vastly different cellular outcomes that are possible exemplifies the importance of having meticulous control over polyUb (the *spice*). But, regardless of the *flavor* of the Ub, at a staggering 1.3% of the total cellular proteome [2], *the spice must flow*. The E3s from the enzymatic cascade are the "writers" of polyUb (or the *merchants of the spice*) and require specialized domains, such as the Homologous to the E6-AP C-terminus (HECT) domain, that enable them to ligate specific polyUb chains onto their targets (**Fig. 1.1**). Because of the vastly different cellular outcomes that result from different polyUb, it is critical that the writers reproducibly ligate the same type of polyUb, which additionally requires the writer to properly orient Ub so that the desired Lys residue (such as K48) is used in the ligation of the desired polyUb (or *spice flavor*). Thus, because of the powerful signal that is polyUb (the *spice*), it is both a great power and a great burden to be a writer of polyUb (or *merchant of the spice*), because *he who controls the spice controls the universe* (i.e., the cell).

Elucidating the cellular roles (protein degradation, endocytosis, etc.) for many of the polyUb chains was enabled by the identification and analysis of their E3s. Conversely, the failure to identify the E3s of other, so-called 'atypical' polyUb, like K6-linked polyUb, which has been implicated in both degradative[6,7] and non-degradative[8] pathways, is a recurring obstacle impeding their direct study. This lack of robust regulators for atypical polyUb extends beyond the E3 writers, but also to the 'erasers', or deubiquitinases (DUBs), which break down linkage-specific polyUb to return monoUb (**Fig. 1.1**). Thus, the lack of

characterized regulators represents a major impedance towards the understanding of many polyUb linkage-types and their roles in cellular signaling and human diseases. This limitation of knowledge has been tackled by some of the most intelligent minds of our time, and only through creative and collaborative methods of approach will we be able to fill in the many gaps of knowledge surrounding polyUb signaling.

Bacteria make surgical strikes on host Ub signaling

What are their motives?

Despite not encoding a functional Ub system of their own, some pathogenic bacteria have evolved the remarkable ability to regulate discrete host polyUb signals through the action of secreted effector proteins, providing them with a significant strategic advantage during infection. For example, the ability to induce the Ub-dependent degradation of host response factors is an important component of *Shigella flexneri* infection[9–11]. Meanwhile, the ability of *Salmonella* Typhimurium to remove Ub signals offers it a competitive advantage[12]. The evolutionary pressure to target host Ub signaling is so strong that entirely convergent mechanisms of regulation have arisen, and in some cases these methods of Ub manipulation make up a sizeable proportion of a bacterium's virulence factor repertoire[13].

In his book *Strangers in a Strange Land*, Robert A. Heinlen describes a protagonist from the planet Mars who is forced to learn how to live on Earth, though he quickly realizes his own Martian abilities exceed those of the strange Earthlings. Analogously, as *strangers* inside their hosts, forced to survive by adapting to the *strange-land* of eukaryotic ubiquitination, infectious bacteria represent an excellent alternative approach for studying Ub signaling, and may hold key insights into the unresolved functions of Ub (**Fig. 1.2**).

Figure 1.2 Strangers in a strange-land.

Artistic rendition of an infectious bacterium (the “stranger”) learning to live among its human hosts and utilize their tools of ubiquitination (the “strange-land”), depicted here as the bacteria sharing in a drink with the host and proposing a “cheers!”. Artwork “When in Rome…” by Riley Franklin.

The bacterial arsenal

Ub is typically attached to Lys residues of target proteins after passing through an E1, E2, E3 enzyme cascade. Classically, polyUb chain specificity is determined by the last enzyme to form a labile cysteine (Cys)-linkage with the Ub carboxy-terminus. In the case of Really Interesting New Gene (RING)-type E3 ligases, this means that polyUb specificity is encoded by the E2 Ub-conjugating enzyme. The previously introduced HECT-type E3 ligases, as well as the RING-between-RING (RBR)-type E3 ligases, however, form one final Cys-linkage with Ub and thus dictate chain specificity themselves. Bacterial pathogens such as *Shigella flexneri*, *Salmonella* Typhimurium, *Legionella pneumophila*, and enterohemorrhagic *Escherichia coli* (EHEC) have all acquired E3 ligases that transfer Ub through a Cys-based mechanism and can dictate polyUb chain specificity[14–17]. Remarkably, aside from some similarities, these bacterial E3 ligases are structurally and mechanistically distinct from any analogous eukaryotic enzymes, suggesting convergent evolution of mechanisms for chain-specific polyUb signaling.

In eukaryotes, ubiquitination is reversed through the action of proteases termed DUBs that hydrolyze the (iso)peptide linkages of Ub signals. Some DUBs demonstrate exquisite polyUb chain specificity, while others show more relaxed preferences or no chain specificity at all[18]. Bacterial DUBs have been identified in a range of pathogens including *Salmonella*, *Legionella*, and *Chlamydia trachomatis*[12,19,20]. While some bacterial DUBs distantly resemble examples in eukaryotes, others appear to have arisen through convergent evolution in order to manipulate discrete Ub signals during infection[21–23].

In addition to modifying polyUb signals directly, bacteria have also acquired methods to modulate the activities of host Ub regulators and responders. In this way, bacteria can block specific Ub signaling pathways or mask the signal from being read[24,25]. In fact, some of the post-translational modifications that bacteria use to inactivate components of the Ub system are entirely foreign to eukaryotic biology, essentially making them irreversible[25].

Bacterial ligases destroy key targets

K48-linked polyUb is the canonical message for proteasomal degradation, and bacterial E3 ligases frequently take advantage of this process to selectively degrade target host proteins[5]. Specificity for assembling the K48-linked polyUb signal has been evolved by a range of structurally-distinct folds, including the bacterial HECT-like family of ligases (e.g., *Salmonella* SopA) and the bacterial novel E3 ligase (NEL) family of ligases (e.g., *Shigella* IpaH9.8), both of which depend upon a Cys-based mechanism to facilitate direct ubiquitination of a target[14,15].

SopA from *Salmonella* uses a familiar HECT-like mechanism to assemble K48-linked polyUb chains onto the host E3 ligases TRIM56 and TRIM65, which may be related to SopA's role in enteritis[26,27]. The NEL family also assembles K48-linked polyUb chains onto substrates, though NELs are more structurally and mechanistically distinct from any eukaryotic E3 ligases[28,29]. NELs are widely used by *Salmonella* and *Shigella*, which encode 3 and 12 family members, respectively. Aside from one report of K27 specificity[30], the majority of NELs are believed to be K48-specific and induce degradation of their targets. For example, *Salmonella* SspH1 has been shown to target the host serine/threonine kinase

PKN1 in order to dampen the host inflammatory response to infection[14,31]. *Shigella* has evolved a remarkable expansion of NEL effectors, which provide a means to selectively target a number of host factors for degradation, including components of inflammatory signaling and cytosolic defense[10,11,30,32,33]. Notably, some bacterial ligases have been reported to target multiple host factors for ubiquitination, thus expanding their reach for host manipulation even further.

K48-specific E3 ligases are a powerful and popular strategy of manipulating host responses, as they allow bacteria to tap into the Ub-proteasome system for targeted protein degradation (**Fig 1.3**, **Table 1.1**).

Bacteria cut off host communications

Beyond its role in targeted protein degradation, select polyUb chain types can serve diverse signaling functions in, for example, immune signaling pathways. Innate immune signaling relies heavily upon several types of polyUb signals. Cytokine and pattern recognition receptors often require the addition of K63-linked polyUb chains to the receptor signaling complex for a downstream transcriptional response[5]. The generation of K63-linked polyUb in these contexts requires the chain-specific E2 Ub-conjugating enzyme UBE2N. To surgically block K63-linked polyUb signaling pathways, *Shigella* has evolved the effector protein OspI that deamidates a key surface residue on UBE2N, leading to its inactivation and subsequently an impaired inflammatory response[24]. The activity of UBE2N is also tightly regulated by *Legionella* through the competing actions of MavC and MvcA, which catalyze the noncanonical (de)ubiquitination of UBE2N through a transglutamination

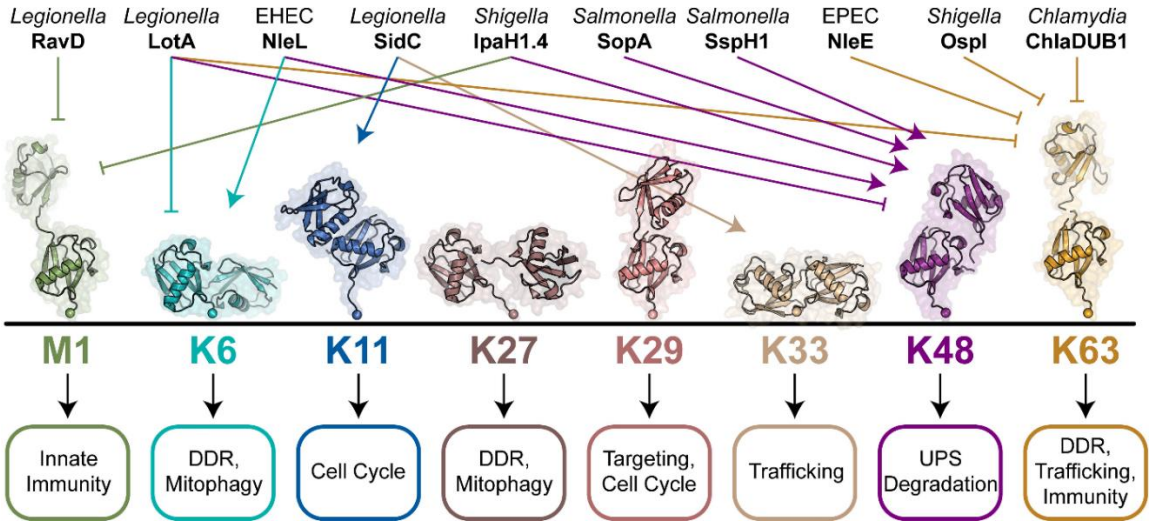

Figure 1.3 Bacteria manipulate specific polyUb signals.

Secreted bacterial effectors are shown positively or negatively regulating specific polyUb signal types. Individual polyUb chains are represented by their diUb crystal structures (PDB codes 2W9N, 2XK5, 2XEW, 6QML, 4S22, 4XYZ, 5GOI, and 2JF5). Current models for the signaling roles of each polyUb chain type are shown below. DDR, DNA damage response; UPS, Ub–proteasome system.

Pathogen	Effector	Activity	Specificity	Target	Outcome	Reference
Salmonella Typhimurium	SopA	E3 Ligase	Lys48	TRIM56, TRIM65	Degradation	[15,26]
Salmonella Typhimurium	SspH1	E3 Ligase	Lys48	PKN1	Degradation	[14,31]
Shigella flexneri	IpaH9.8	E3 Ligase	Lys48	GBPs, NEMO	Degradation	[10,11,30]
Shigella flexneri	IpaH4.5	E3 Ligase	Lys48	TBK1	Degradation	[32]
Shigella flexneri	IpaH0722	E3 Ligase	Lys48	TRAF2	Degradation	[33]
Shigella flexneri	IpaH1.2, 2.5	E3 Ligase	Lys48	HOIP	Degradation	[34]
Legionella pneumophila	SidC, SdcA	E3 Ligase	Lys11, 33	Vacuolar proteins	Remodeling	[16]
EHEC	NleL	E3 Ligase	Lys6, 48	JNK	Unknown	[17,35]
Legionella pneumophila	MavC	Ligase/ Transglutaminase	Lys63	UBE2N	Signal inhibition	[36]
Legionella pneumophila	MvcA	DUB/ Transglutaminase	Lys63	UBE2N	Signal activation	[37,38]
Salmonella Typhimurium	SseL	DUB	Lys63	Various	Signal elimination	[12,21,39]
Chlamydia trachomatis	ChlaDUB1	DUB	Lys63	Various	Signal elimination	[20,21,40]
Legionella pneumophila	SdeA	DUB	Lys63	Vacuolar proteins	Signal elimination	[19]
Legionella pneumophila	RavD	DUB	Met1	Vacuolar proteins	Signal elimination	[23]
Legionella pneumophila	LotA	DUB	Lys6, 48, 63	Vacuolar proteins	Unknown	[41]
Shigella flexneri	OspI	Deamidase	Lys63	UBE2N	Signal inhibition	[24]
EPEC	NleE	Methyltransferase	Lys63	TAB2, TAB3	Signal masking	[25]

Table 1.1 Linkage-specific Ub-targeted bacterial effectors.

A table of linkage-specific polyUb-targeted bacterial effectors. The table shows the effectors' pathogen of origin, polyUb activity and specificity, known host target, signaling outcome (if known), and the referenced studies.

reaction[36–38]. Downstream of K63-linked ubiquitination, TAB2 and TAB3 specifically recognize the K63-linked signal through Ub-binding domains and activate TAK1. To block this step of inflammatory signaling, enteropathogenic *E. coli* (EPEC) has acquired NleE, a Cys methyltransferase that modifies the Ub-binding domains of TAB2 and TAB3, thereby blocking their ability to recognize K63-linked polyUb[25]. Another common strategy for interrupting K63-linked polyUb signaling is through its specific reversal by bacterial DUBs. The CE clan of bacterial DUBs appear to have convergently evolved a preference for the hydrolysis of K63-linked polyUb, and these effectors have demonstrated roles in inhibiting inflammatory signaling, blocking autophagy, and maintaining the bacteria-containing vacuolar compartment in *Chlamydia*, *Salmonella*, and *Legionella*, respectively[19,21,39,40].

M1-linked polyUb chains also play roles in the innate immune response, often immediately downstream of K63-linked polyUb signaling. These Ub chains are solely assembled by the linear Ub chain assembly complex (LUBAC), and play an important role in the response to bacterial invasion[5]. As with K63-linked chains, *Shigella* has also developed a means to block the formation of M1-linked polyUb signals. The NELs IpaH1.4 and IpaH2.5 attach K48-linked polyUb to the catalytic subunit of LUBAC, targeting it for proteasomal degradation and thereby preventing M1-linked polyUb chain formation and subsequent inflammatory signaling[34]. Using IpaH9.8, a separate NEL effector, *Shigella* also targets the M1-linked polyUb sensor protein NEMO for Ub-dependent proteasomal degradation, thus blocking activation of the IκBα kinase complex required for NF-κB signaling[30]. M1-linked polyUb can also stimulate inflammatory signaling from the surface of a pathogen-

containing vacuole. *Legionella* counteracts this by directing the M1-specific DUB RavD to the cytosolic face of the *Legionella*-containing vacuole[23].

Thus, for both K63- and M1-mediated polyUb signaling processes, bacteria have evolved unique strategies to specifically block a signal's formation, mask its sensing, or remove it altogether (**Fig. 1.3, Table 1.1**).

Bacterial code talkers transmit cryptic messages

For some polyUb chain linkages, such as K33 and K6, the specific regulators, substrates, and signaling outcomes are not fully understood[5]. Curiously, although many aspects of these atypical polyUb chains remain a mystery, bacteria appear to have selected for mechanisms that specifically interact with these signal types. *Legionella* has acquired a novel E3 ligase fold that uses a Cys-dependent mechanism to assemble K11- and K33-linked polyUb chains, which are proposed to remodel the *Legionella*-containing vacuole[16]. Though K11-linked signals are thought to be primarily degradative, the proposed functions of SidC and the related SdcA may be more congruent with the connection between K33-linked polyUb and protein trafficking. K6-linked polyUb signals, which have been loosely tied to the DNA damage response and mitophagy, are also targeted during bacterial infection. EHEC, as previously noted, encodes a HECT-like E3 ligase called NleL that assembles K48- and K6-linked polyUb, though the relevance of these specificities has not been tied to its potential role in regulating pedestal formation[17,35]. On the other hand, *Legionella* has acquired an effector protein called LotA that encodes dual DUB domains, one of which specifically hydrolyzes K6-linked polyUb at the surface of the *Legionella*-

containing vacuole[41]. Why EHEC and *Legionella* have evolved opposing mechanisms to regulate K6-linked polyUb, and how these processes align with current models of this signal's function, remain unknown.

Given how little we understand about the roles and regulation of atypical polyUb chains, it is interesting to consider what evolutionary pressures led to the acquisition of atypical linkage-specific effector proteins and how future research can leverage these enzymes to study human biology (**Fig 1.3, Table 1.1**).

Gathering strategic intelligence

From an evolutionary perspective, it is remarkable that bacteria have evolved unique strategies for manipulating the eukaryote-specific post-translational modifier Ub, and even more astounding that they have gone to the lengths of targeting specific types of polyUb signals so as to enact surgical strikes on cellular processes in the infected host. With mechanisms that are both familiar and foreign to our understanding of eukaryotic Ub regulation, bacterial pathogens have the capability to tap into our system of targeted protein degradation, block our ability to signal and respond to infection, and manipulate certain polyUb signals that we don't yet fully understand. Additional work at this complex host-pathogen interface has the potential to not only provide strategic insight into bacterial pathogenesis and mechanisms of disease, but also explain cryptic facets of human Ub signaling.

A closer look at the HECT-type E3 Ub ligases

The Human side:

Unlike RING-type E3 ligases that facilitate direct transfer from activated E2~Ub to substrate, Cys-dependent E3 ligases first receive Ub from the E2 onto an active site Cys, forming one final thioester intermediate before ultimately transferring Ub onto a substrate. Humans encode ~40 known Cys-dependent E3 ligases, the bulk of which fall into the previously mentioned HECT and RBR families[42,43], but also include the newly described RING-Cys-relay (RCR) and RNF213-ZNFX1 families[44,45]. Though structurally each family is unique, a common theme among Cys-dependent E3 ligases is a multi-domain architecture that allows flexibility between an E2-binding domain and a catalytic domain that presents the active site Cys. For example, HECT E3 ligases are characterized by an E2-binding N-lobe that is flexibly linked to a catalytic C-lobe (**Fig. 1.4A-B**). The movement between these domains is important for recruitment of an activated E2~Ub conjugate and subsequent transfer of Ub onto the E3 active site. The resulting E3~Ub thioester intermediate can then carry out substrate ubiquitination and, in some cases, polyUb chain formation (**Fig. 1.4B**). One key property allowed by HECTs and the other Cys-dependent ligase mechanisms is that it they impart control over both substrate and polyUb chain specificity to the E3.

Before being realized as the founding member of the HECT family of Ub writers, E6AP was only known for its role as the host target of E6, the Human Papilloma Virus protein that mediates oncogenic p53 degradation. Since then, 28 human examples of HECTs have been validated and appreciated for their critical roles in Ub regulation. All of the HECT ligases contain their HECT domain at the C-terminus, and therefore feature their substrate-

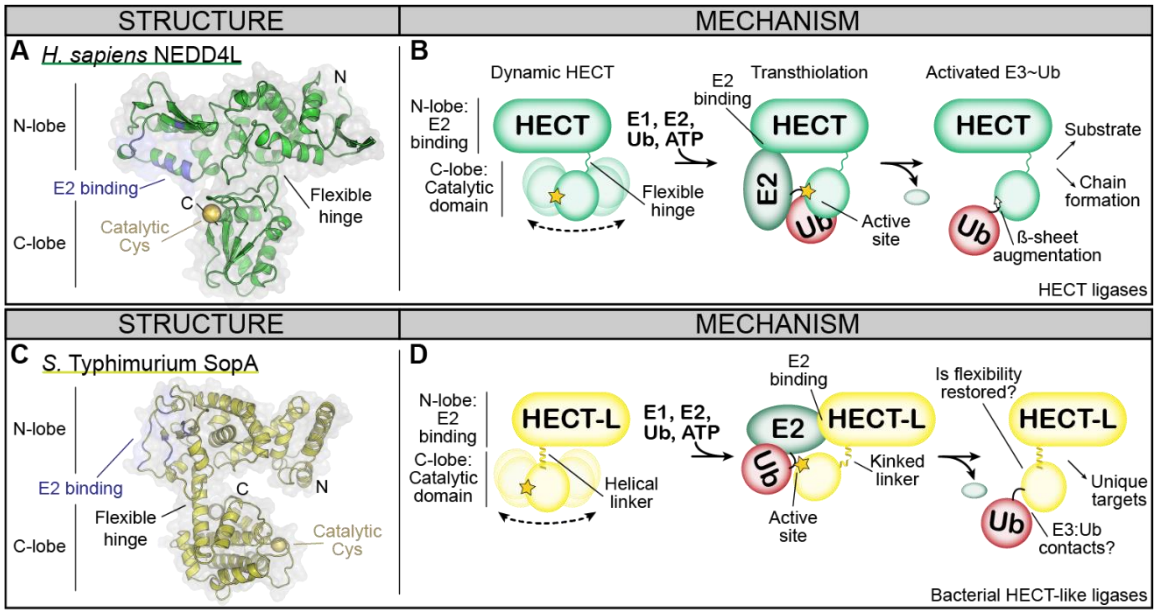

Figure 1.4 HECT-type ligation in humans and bacterial pathogens.

A. Structure of the human HECT E3 ligase NEDD4L (PDB 3JVZ[46]), with the E2-binding region and active site colored in blue and gold, respectively. **B**. Mechanism of HECT E3 ligases, highlighting flexibly-linked N- and C-lobes that facilitate docking and transfer of Ub from an E2, as well as activation of Ub for substrate ubiquitination and/or polyUb chain formation[46–48]. **C**. Structure of the *Salmonella* Typhimurium HECT-like E3 ligase SopA (PDB 2QYU[49]), highlighting topologically analogous E2-binding region and active site. **D**. Mechanism of bacterial HECT-like E3 ligases, highlighting common themes including inter-lobe flexibility and E2 transthiolation[17,49–51].

binding regions upstream of the HECT domain. While the HECT domain is highly conserved, the type and number of domains upstream of the HECT domain vary greatly, but the presence of certain domains are the basis for categorizing the HECT subfamilies, such as the NEDD4 family. Of the well-characterized HECT ligases, there appears to be a predominant specificity for Ub ligation of either K48- or K63-linked polyUb.

The pathogen side:

The bacterial HECT-like E3 Ub ligases were previously composed of just two members: SopA from *Salmonella* Typhimurium and NleL from enterohemorrhagic *Escherichia coli*, however Chapter 3 of this dissertation identifies additional members of this family. SopA, before being described as a HECT-like Ub ligase, was primarily appreciated for its critical role among several other effectors in inducing inflammatory responses and enteritis during *S.* Typhimurium infection[27,52]. Another study found that N-terminal regions of SopA could localize to the mitochondria in several cancer cell lines, and reported that SopA shared a 29% amino acid homology to a protein of unknown function from EHEC[53]. This EHEC protein of unknown function would next be characterized as the secreted effector protein EspX7, and finally later as NleL[17,54]. A different group, in search of a host target of SopA, performed a yeast two-hybrid screen and identified the RING ligase HsRMA1[55]. During the characterization of SopA and HsRMA1, an inexplicable Ub ligation activity was observed and a follow-up study revealed that SopA is a Ub ligase with an active site Cys 30 residues upstream of its C-terminus, an amino acid signature shared by all eukaryotic HECT ligases[15]. At last, a crystal structure of SopA suggested the structural mimicry of the SopA HECT-like domain to the eukaryotic HECT domains, despite the poor sequence

homology between them, as SopA appeared to contain two distinct lobes joined by a linker (**Fig. 1.4C**)[17,49]. Following the fascinating discovery of the HECT-like Ub ligation style of SopA, a structure was solved of its ortholog, NleL from EHEC, which was revealed to also have a HECT-like architecture[17]. Using insights from the structures of NleL and SopA, as well as sequence features of both, Chapter 3 of this dissertation expands the family of bacterial HECT-like E3 Ub ligases to include additional examples from both human and plant pathogens.

Another study revealed how extensively SopA and NleL mimicked eukaryotic HECTs, by solving the structure of these effectors bound to the HECT-specific E2 UBE2L3[50]. The structures with UBE2L3 revealed that both NleL and SopA have *de facto* N-lobe, C-lobe, and linker architectures, similar to eukaryotic HECTs. Both SopA and NleL contact UBE2L3 at their most N-terminal lobe, each making strong intermolecular contacts to F63 of UBE2L3, a residue known to be critical for interaction between UBE2L3 and other HECTs[46,50,56]. However, it is worth noting that both NleL and SopA bind UBE2L3 at their N-lobe in a manner that is spatially orthogonal to that of an analogous eukaryotic structure of E6AP bound to UBE2L3[50]. Fortuitously, the NleL-UBE2L3 structure, when compared with the previous apo NleL structure, showed that the C-terminal lobe of the NleL HECT domain had adopted an entirely different conformation, demonstrating a large rearrangement with its linker domain as the axis[50]. The SopA C-lobe in the SopA-UBE2L3 structure was also observed to undergo movement relative to the apo SopA structure. This observation demonstrated that, not only do NleL and SopA share the architecture of eukaryotic HECT domains, but that their C-lobes also demonstrated the ability to undergo

large rearrangements as they theoretically rotate to face the E2~Ub bound to the N-lobe in one conformation, take the Ub from the E2~Ub, and undergo a rearrangement to ligation-primed NleL~Ub or SopA~Ub conformations (**Fig. 1.4D**); however, the actual Ub ligation mechanism of NleL and SopA was unknown. Chapter 3 of this dissertation captures catalytic intermediates of NleL, SopA, and a novel third member of this family, that demonstrate some shared mechanisms of Ub ligation among the bacterial HECT-like and eukaryotic HECT ligases. These structural observations make NleL and SopA clear rule-followers to the analogous conformations observed in eukaryotic HECTs (**Fig. 1.4B**). Like eukaryotic HECTs, NleL and SopA also encode their HECT domains as the very C-terminal domain, with the substrate binding regions located upstream[42].

One notable deviation from eukaryotic HECTs, however, is that the linker domain bridging the N-lobe and C-lobes is considerably longer, as NleL and SopA have a linker domain around 23 amino acids, relative to the more commonly observed linker domain size of 3 to 4 amino acids in eukaryotic HECTs[17,42]. Another interesting observation is that SopA appears to preferentially ligate K48-linked polyUb chains[26], similar to many eukaryotic HECTs, while NleL demonstrates the unusual ability to ligate K6-linked polyUb at about a 50:50 preference along with K48-linked polyUb[17,57]. Chapter 3 of this dissertation explores how mutations of the HECT-like domain can be used to alter the ligation specificity of NleL and other HECT E3s.

While SopA had first been observed to target the RING Ub ligase HsRMA1[55], two recent studies separately identified the RING Ub ligases TRIM56 and TRIM65, components of

interferon signaling in innate immune responses, as additional targets of SopA[26,58]. The first study found this targeting of TRIM ligases by SopA to be non-degradative and stimulate interferon responses, while the second study concluded oppositely that SopA was degrading these targets, which may resonate with the observation that SopA preferentially ligates the degradative K48-linked polyUb signal[26]. Interestingly, the second study identified the substrate binding region to be the β-barrel region of SopA, located immediately upstream of the HECT domain[26]. NleL, on the other hand, has been observed to target at least one of its substrates using the disordered region upstream of its β-barrel region, which typically encodes the secretion signal, making it unclear if NleL and SopA employ the same domains for substrate targeting[35]. NleL has been studied for its contributions to the attaching and effacing mechanism of EHEC, which is used by EHEC to adhere to host epithelial cells during infection, but conflicting results from separate studies make the exact function of NleL in this pathway unclear[35,59]. Lastly, a more recent study has also provided evidence that NleL may be targeting components of the NF-κB innate immunity signaling pathway[60].

Interestingly, the effector protein TRP120 from *Erlichia chaffennesis* was recently reported to have Ub ligase activity that was dependent on a Cys residue located ~30 amino acids upstream from its C-terminus[61]. While TRP120 otherwise has no other identifiable HECT-like features, future work on TRP120 may hold interesting insights into its unexpected Ub ligase activity. The discovery of TRP120, alongside NleL and SopA, indicates that more HECT-like ligases may exist in the repertoire of other pathogenic bacteria. Chapter 3 of this dissertation investigates many outlying questions of the bacterial HECT-like E3 Ub

ligases, such as their commonalities with eukaryotic HECTs, such as β-sheet augmentation of the thioester-linked Ub and/or the determinants of polyUb chain specificity, among other interesting questions. Altogether, however, the strong structural and apparent mechanistic similarities to the eukaryotic HECTs establish the HECT-like effectors NleL and SopA as mimics of the human HECTs despite their distinct evolutionary origins.

DUBs make the final call

Up to now, I have primarily discussed the E3 Ub ligases and the critical importance of their polyUb specificity. A final layer of regulation follows the formation of polyUb onto a substrate, however, wherein DUBs are able to remove the polyUb signal, also in a chain-specific manner (**Fig. 1.1**). This means that DUBs canonically get the 'final call' as to the nature of the polyUb on a substrate. As a foundational example, DUBs in the proteasomal degradation pathway cleave the polyUb degradation signal at the proteasome, rescuing Ub from degradation and returning it to the pool of cellular Ub. Perhaps more interestingly, however, are examples of ligase and DUB "partners" that feature similar polyUb specificities, presumably to 'fine-tune' and ultimately regulate the final polyUb assembly that is put on the substrate, one attaching polyUb and the other removing it. For example, the RBR-type ligase Parkin is recruited to damaged mitochondria, where its ligation of polyUb promotes clearance by autophagy. Concurrently, the mitochondria-resident DUB USP30 works to counteract the polyUb ligation activity of Parkin, resulting in a regulatory tug-of-war[62–65].

Six different DUB families, categorized by their unique protein folds, feature an active site

Cys-based mechanism—including the Ub specific proteases (USPs) and ovarian tumor proteases (OTUs)—and a seventh family are metalloproteases that rely on Zinc as a cofactor for activity[18,66]. Though there are several exceptions, the Cys-based DUBs typically employ a catalytic Cys-His-(Asp/Glu/Asn) triad, wherein the active site Cys cleaves the Ub-Ub linkage, with the His and acidic residues working to increase the nucleophilic nature of the Cys. Extensive biochemical and structural work have elucidated many of the determinants of polyUb linkage-specificity of DUBs. PolyUb linkage-specificity of DUBs can be partly explained by the S1 and S1' sites that are positioned topologically adjacent to the active site. For a linkage-specific DUB, the S1 site binds to the distal, or terminal, Ub on a polyUb chain, and so the S1 site frequently binds to common surfaces of Ub, such as the I44 patch[18,66]. The S1' site, however, binds to the proximal Ub, linked to the distal Ub, and must feature a nuanced binding motif for Ub that enables it to decern different types of polyUb[18,66]. This requirement of the S1' site goes back to the previously discussed logic surrounding the seven Lys residues (and N-terminus) native to Ub that enable the different forms of polyUb: polyUb attached via K48 largely occludes binding surfaces next to the K48 linkage site, while polyUb attached via K63 occludes a much different binding surface. These differentially available binding surfaces mean that the S1' site can be extremely specific for one type of polyUb, or ultimately be entirely non-specific. Interestingly, many of the USP family of DUBs are non-specific and can cleave all types of polyUb, while many highly linkage-specific examples exist in the OTU family of DUBs, including OTULIN for M1-linked polyUb[67,68], Cezanne (OTUD7B) for K11-linked polyUb[69], OTUB1 for K48-linked polyUb[18,66,70,71].

As was the case for the E3 Ub ligases, many pathogens have also evolved secreted effector proteins that feature DUB activity, and these can show convergent evolution that results in bacterial DUBs mimicking eukaryotic DUB families[72]. Using this knowledge of effector proteins evolving in bacteria, and the knowledge that OTU DUBs can demonstrate highly linkage-specific activity, Chapter 4 of this dissertation will explore a new family of OTU DUBs from bacteria, focusing on the characterization of their linkage-specificity and use as a diagnostic tool for determining polyUb linkage-types in complex polyUb samples.

Statement of objectives

The introductory chapter highlights the complexity of the Ub code that results from the diverse polyUb chain-types and argues the importance of their study, especially the poorly resolved linkage types like K6-linked polyUb. This chapter also seeks to highlight the utility of leveraging effector proteins, which bacteria are known to employ in their combat with host Ub signaling, as a rich and underutilized resource that could aid in the effort to more completely understand eukaryotic Ub signaling. This approach is also particularly compelling considering the growing evidence that K6-linked polyUb plays a role at the host-pathogen interface.

Accordingly, the overarching goals of this dissertation are to contribute to the science of Ub signaling primarily by providing new tools, including both E3 Ub ligases and DUBs, to dissect the roles of K6-linked polyUb chain-types, and by researching the incompletely-resolved ligation mechanisms of the bacterial HECT-like E3 ligases, especially as they pertain to atypical ubiquitination. This dissertation aims to achieve these goals through the

following objectives:

1) Develop a new, comprehensive and high-throughput methodology based on fluorescent polarization to monitor the entire Ub signaling cascade, from E1-mediated Ub activation all the way through to E3 chain-specific polyUb ligation and deubiquitination. This work is featured in Chapter 2.

2) Use structural biology and biochemical techniques to dissect the ligation mechanisms of the HECT-like family of Ub ligases (initially from *Salmonella* and EHEC but expanded here) which have demonstrated ligation of atypical K6-linked polyUb, with the objective of leveraging the data to build tools for studying K6-linked polyUb biology and better understanding HECT-type ligation. This work is featured in Chapter 3.

3) Validate DUBs from several bacterial pathogens as potential tools for studying typical and atypical polyUb linkage-types, especially K6-linked polyUb. This work is featured in Chapter 4.

The presentation of these goals in Chapters 2, 3, and 4 are followed by a general discussion and outlook section at the end, in Chapter 5.

Chapter 2 – A high-throughput and comprehensive tool to monitor ubiquitin signaling

Franklin, T.G. & Pruneda J.N. (2019) A high throughput assay for monitoring ubiquitination in real time. *Frontiers in Chemistry*, 7,816.

Author Contributions: TF and JP conceptualized the approach. TF performed all experiments. TF and JP analyzed the data and wrote the manuscript.

Abbreviations: Ub, ubiquitin; FP, fluorescence polarization; DUB, deubiquitinase; HTS, high-throughput screen; T-Ub, TAMRA-Ub; F-Ub, Fluorescein-Ub.

Introduction

Post-translational regulation through attachment of the small protein modifier ubiquitin (Ub) is a conserved and essential process among all eukaryotic life. Protein ubiquitination can regulate diverse cellular processes including proteasomal degradation as well as protein trafficking, cell cycle regulation, and immune signaling[1]. Ub is typically attached via its carboxy-terminus to a lysine residue on a target protein, resulting in a monoUb modification. The vast diversity of Ub signaling roles arises from additional customization of the monoUb signal. Unlike binary post-translational modifications such as phosphorylation or acetylation, Ub itself is a protein and can thus be further post-translationally modified by, e.g., ubiquitination. Ubiquitination of Ub can occur at any of eight classical sites (seven lysine positions and the amino-terminus), creating an array of polymeric Ub (polyUb) chains. MonoUb as well as each polyUb chain type are believed to serve distinct signaling roles, for example chains linked through K48 are the classic proteasomal degradation signal, whereas Met1-linked polyUb serves a specialized role in innate immune signaling[1,5]. Additionally, target proteins can be ubiquitinated at multiple sites, further diversifying the versatility of Ub signaling.

In humans, the Ub system is controlled by hundreds of regulatory proteins[2]. Ubiquitination occurs via a cascade of Ub 'writing' enzymes that include an E1 Ub-activating enzyme, an E2 Ub-conjugating enzyme, and an E3 Ub ligase (**Fig. 2.1A**). The E1 Ub-activating enzyme (of which there are two in humans) consumes ATP to activate the Ub carboxy-terminus onto an E1 active site cysteine, creating a high-energy thioester linkage (E1~Ub). Next, through a transthiolation reaction the Ub is transferred from the

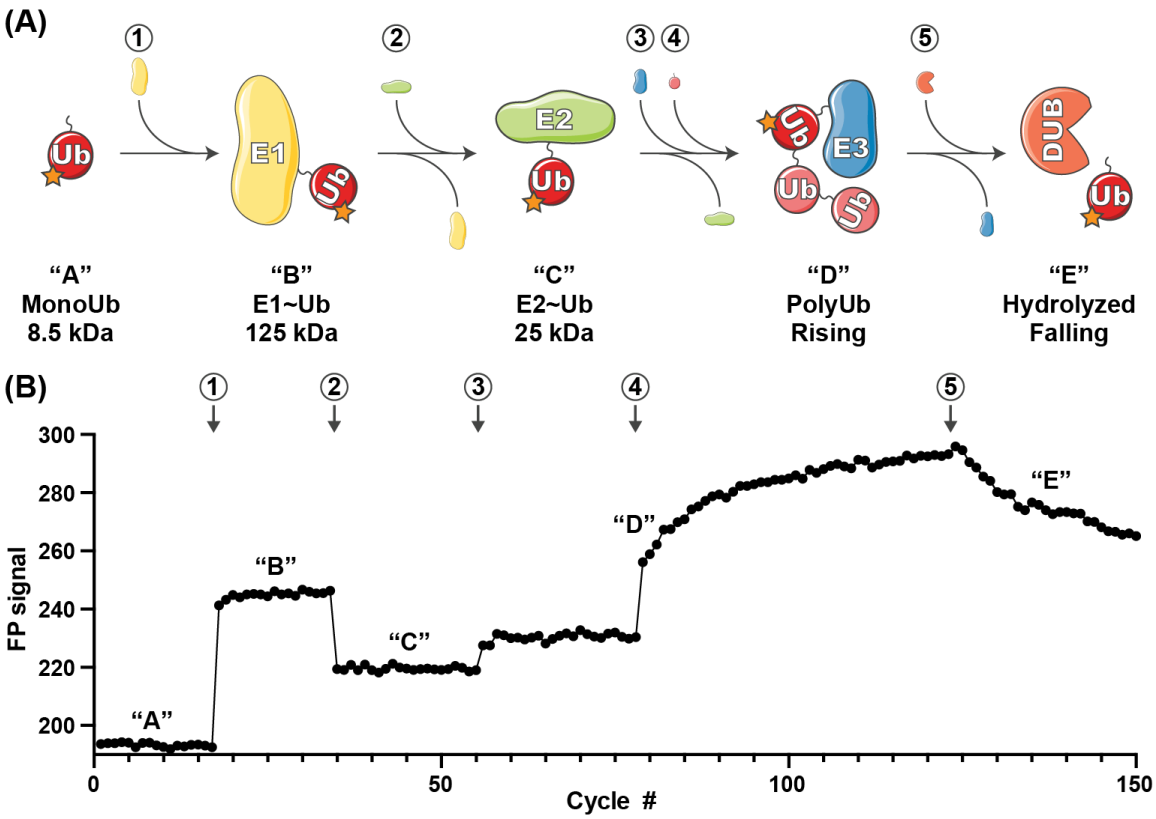

Figure 2.1 Overview of the UbiReal approach.

A. Schematic depicting the sequential states of ubiquitin conjugation that are monitored using UbiReal. Circled numbers indicate the addition of substrate and correspond to the data in part **B.** Letters in quotations indicate the state of the ubiquitin substrate complex and also correspond to the changes in FP signal observed in **B.** Approximate molecular weights of the complexes are provided and reflect the amplitude of the expected FP signal. "Rising" in "D" corresponds to the rising FP signal from the ligation of chains by the E3 enzyme, and "falling" in "E" corresponds to falling FP signal from the activity of a DUB enzyme. **B.** Data representing the ability of UbiReal to comprehensively monitor the sequential steps of the ubiquitination pathway. Numbers and letters correspond to enzyme/substrate additions and the states of ubiquitin complexes, respectively, as described in **A.** For clarity, data are presented as cycles separated by 30 seconds. In this representative assay, "1" is the E1 UBA1, "2" is the E2 UBE2D3, "3" is the E3 NleL, "4" is WT Ub, and "5" is the DUB USP21. Graph is the average of two identical, parallel experiments and representative of multiple other UbiReal experimental curves.

E1 to the active site cysteine of an E2 Ub-conjugating enzyme (of which there are ~35 in humans), forming the E2~Ub conjugate. At this stage, the Ub can either be transferred directly onto a substrate lysine in a reaction catalyzed by E3 ligases of the RING/U-box family (of which there are hundreds in humans), or via one additional intermediate in the cases of the HECT and RBR families of E3 ligases (28 and 14 examples in humans, respectively) which utilize their own active site cysteine to receive and transfer Ub onto a substrate. The resulting Ub signals are discriminately interpreted by Ub binding domains (of which there are >150 in humans) that specifically 'read' the modification and direct cellular outcomes. Finally, Ub signals can be 'erased' by specialized proteases termed deubiquitinases (DUBs, of which there are ~100 in humans) that can edit or recycle the Ub signal back to its monomeric state (**Fig. 2.1A**).

In total, approximately 5% of human genes encode regulators of Ub signaling. This significant evolutionary investment is illustrative of the strict regulation maintained over Ub signaling across its broad involvement in cellular processes. Perhaps unsurprisingly, breakdown of this regulation can often lead to disease[73]. Defects in Ub signaling are linked to many cancers, as the dysregulation of E3 ligase or DUB activities can directly impact the stabilities of tumor suppressors or oncogene products[74]. Ub proteasome system defects are also linked to neurodegenerative disorders, which arise from an inability to degrade toxic protein aggregates[75]. In addition to affecting protein stability, aberrant ubiquitination can result in constitutive activation of signaling pathways such as NF-κB, leading to autoimmune diseases or tumor formation[76].

The Ub system is a major focus of recent pharmaceutical research as it offers the opportunity to "drug the undruggable", for example by stabilizing tumor suppressors or inducing the degradation of oncogene products[77]. The posterchild of successful therapeutics targeting the Ub system is bortezomib (Velcade), which blocks proteasomal degradation of ubiquitinated substrates and is an effective treatment for multiple myeloma[78]. Other efforts have instead targeted the stability of individual proteins. For example, inhibitors of the E3 ligase MDM2 show great promise in preventing p53 ubiquitination, thus rescuing it from degradation[79]. Inhibitors have also been designed to specifically block USP7, a deubiquitinase that would otherwise protect MDM2 from Ub-mediated degradation[80–84]. In an alternative approach, protein-targeting chimeric molecules (PROTACs) can be used to induce the degradation of target proteins by recruiting an E3 Ub ligase[85]. Thus, we are entering a new era of biomedical research centered around controlling the Ub system as a means to correct disease states.

The development of small molecule modulators of ubiquitination activities hinges upon the availability of robust high-throughput screens (HTS)[86]. Currently, screens for DUB activity are much more advanced than those for Ub conjugation. The most widely used substrates for high-throughput DUB assays are Ub-AMC or Ub-Rhodamine, which fluoresce only after cleavage[87,88]. Newer classes of mono- or di-Ub substrates contain a bona fide isopeptide linkage and allow for reaction monitoring through either fluorescence polarization (FP) or FRET[67,89,90]. Still, the available DUB substrates for HTS are very simplified, and do not always accurately reflect the genuine ubiquitinated substrate. In the case of Ub conjugation, screens are much less standardized. It seems that no single method

can be applied universally to measure the activities of E1, E2, or E3 enzymes[91–94]. Further, most assays require a development step which precludes any kinetic measurement in real time[94,95]. A robust and universal HTS to monitor inhibition or activation along each point in the E1-E2-E3 enzyme cascade would be extremely enabling for both mechanistic studies of Ub transfer as well as small molecule modulator screens.

We present a simple HTS, which we term 'UbiReal', that can track all stages of Ub conjugation and deconjugation in real time. Using fluorescently-labeled Ub, we show that every step of the Ub cascade can be measured by FP in a low volume, high-throughput format. Specifically, we demonstrate the utility of UbiReal for measuring E1 activation, E2~Ub discharge and specificity, E3-dependent Ub chain formation, and DUB-dependent hydrolysis. We highlight the utility of UbiReal for studying small molecule modulators by recapitulating the IC50 value of the E1 inhibitor PYR-41[96], as well as for answering basic biochemical questions such as E2-E3 pairing and Ub chain specificity. With minimal adjustment, we are confident that this assay could be applied to any E1/E2/E3/DUB system across both Ub and Ub-like (e.g., NEDD8 or SUMO1/2/3) signaling systems, enabling real time measurement of enzyme activities.

Results

Drug screen demonstration using UBA1 and inhibitor PYR-41

FP is a sensitive measure of a molecule's tumbling behavior in solution. Though primarily used to study protein-protein interactions, previous studies[67,90,97,98] using FP to discriminate monomeric Ub from polyUb chains led us to reason that FP could be used to monitor the

passage of fluorescent Ub through the entire ubiquitination cascade (**Fig. 1A**). Using Ub labeled with tetramethylrhodamine (TAMRA) at its amino-terminus (T-Ub), we could show that conjugation onto the E1 active site resulted in a large shift in FP (**Fig. 2.1B**, step 1). Addition of the E2 Ub-conjugating enzyme UBE2D3 led to rapid formation of the E2~Ub conjugate, with an intermediate molecular weight and corresponding FP value (**Fig. 2.1B**, step 2). Subsequent addition of the bacterial HECT-type E3 ligase NleL resulted in a modest increase in FP (**Fig. 2.1B**, step 3), which dramatically increased over time following the addition of excess unlabeled Ub into the system (**Fig. 2.1B**, step 4). These Ub modifications (most likely polyUb) could then be removed with the nonspecific DUB USP21, which was evident by a decrease in FP value with time (**Fig. 2.1B**, step 5). Thus, the entire Ub conjugation and deconjugation cycle could be observed in real time simply by tracking the FP of labeled Ub. Our subsequent work with this method focused on analyzing the discrete steps of Ub conjugation and deconjugation to evaluate the utility of UbiReal for measuring activity and specificity.

Focusing first on Ub activation, we measured E1 activity in response to increasing concentrations of the previously described chemical inhibitor PYR-41[96]. By incubating E1 with PYR-41 and subsequently initiating the reaction with ATP (**Fig. 2.2A**, step 1), E1~T-Ub complex formation could be monitored over time (**Fig. 2.2A**). Data were normalized to FP values before ATP addition (0%) and to the endpoint of the DMSO-only control (100%). Effects of PYR-41 addition could be observed as a loss in activity ranging from no to complete inhibition (**Fig. 2.2A**). We noted a moderate degree of variability in our FP measurements, possibly arising from the addition of DMSO, but still calculated an overall

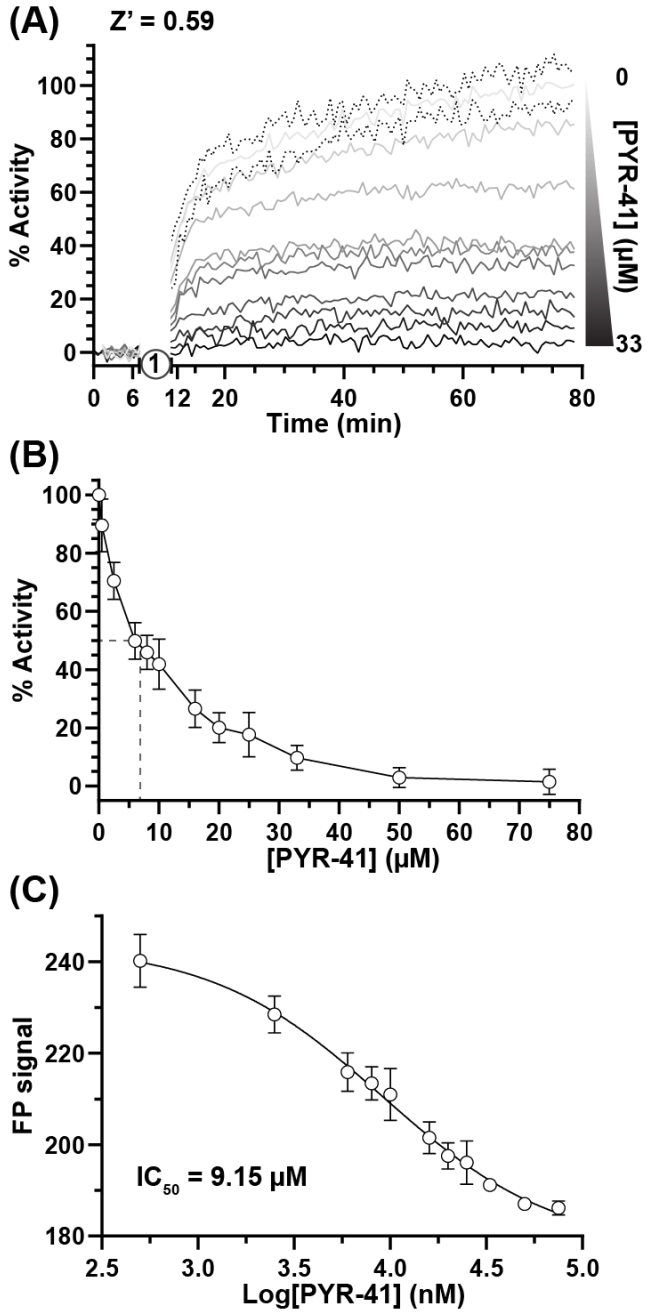
(A)
Z' = 0.59
% Activity
Time (min)
[PYR-41] (μM)
0
33
(B)
% Activity
[PYR-41] (μM)
(C)
FP signal
IC50 = 9.15 μM
Log[PYR-41] (nM)

Figure 2.2 Small molecule inhibition of E1 Ub-activating activity.

A. E1~T-Ub complex inhibition by PYR-41 monitored over time with the UbiReal assay. "1" indicates the addition of ATP to initiate formation of the E1~T-Ub complex. Increasing concentrations of PYR-41 correspond to reduced E1~T-Ub complex formation, represented by % Activity. Data points are normalized to FP values after PYR-41 addition, but before ATP addition, and to the FP signal from samples treated with DMSO instead of PYR-41, representing 100% activity. Connected lines represent Mean values, while representative error of ± SD is shown for the 0 μM PYR-41 (DMSO addition) sample. Data are the average of 3 technical replicates for each concentration and representative of all PYR-41 inhibition experiments. **B.** Inhibition of E1~T-Ub complex by PYR-41 represented using the end-point FP values at each PYR-41 concentration. The dashed lines represent the approximate PYR-41 concentration at which 50% E1~T-Ub complex inhibition occurs. Data are normalized as in A**.** Data are from 3 separate experiments that each include 3 technical replicates for all PYR-41 concentrations (see section Methods). Data are reported as Mean ± SD. **C.** IC50 graph generated using the end-point FP values as in B. Data was fitted and an IC50 value was calculated using a non-linear regression in GraphPad Prism. Data are from the same experiments as B., with data reported as Mean ± SD.

Z' value of 0.59 (a measure of signal-to-noise in HTS where values in the range of 0.5-1.0 are considered 'excellent'[99]. E1 activities reported by our assay showed a logarithmic trend with increasing concentration of PYR-41 (**Fig. 2.2B**). Using a non-linear regression, an IC50 value for inhibition of E1~Ub conjugation by PYR-41 under our assay conditions was determined to be 9.15 μM (**Fig. 2.2C**), in agreement with previously reported values[96].

Monitoring E2~Ub transthiolation

Gel-based Ub discharge assays have been used previously to measure the ability of E2 enzymes to transfer Ub onto free amino acids as a simplified model for substrates[100–102]. Using Ub labeled with fluorescein at all primary amines (F-Ub), amino acid reactivity and specificity were measured for the E2 enzymes UBE2D3 and UBE2L3 (**Fig. 2.3A**). Using activated E2~F-Ub as a starting material, the free amino acids Cys and Lys were added and discharge was measured as the return to unconjugated F-Ub FP values over time (**Fig. 2.3B-C**). As expected from previous work[102], UBE2D3 demonstrated the ability to transfer F-Ub to both Cys and Lys amino acids (**Fig. 2.3B**), whereas UBE2L3 was largely Cys-specific (**Fig. 2.3C**), indicating that it cannot directly ubiquitinate substrate Lys residues but must act through a HECT/RBR E3 intermediary. As an E2 that can directly ubiquitinate Lys residues, UBE2D3 functions with RING/U-box E3 ligases to efficiently transfer Ub. Addition of the U-box E3 ligase E4BU to the UBE2D3~F-Ub conjugate already promoted discharge of the thioester linkage (**Fig. 2.3B**, step 1), and in the presence of free Lys resulted in an enhanced rate of Ub transfer (**Fig. 2.3B**, step 2) as observed in previous gel-based assays[101]. Overall, the UbiReal method provides a new, straightforward approach for observing the specificity and activation of the family of E2 Ub-conjugating enzymes.

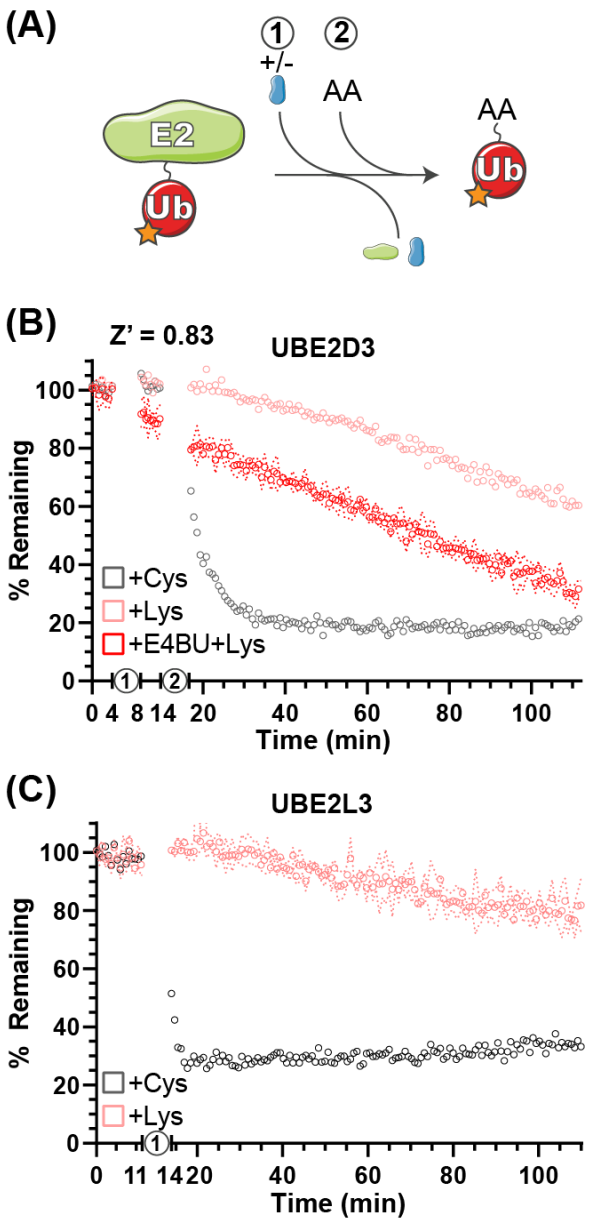

Figure 2.3. Amino acid reactivity and activation of E2 Ub-conjugating enzymes.

A. Reaction schematic depicting E2~F-Ub discharge onto a substrate amino acid (AA). **B**. Monitoring discharge of the E2 Ub-conjugating enzyme UBE2D3 from E2~F-Ub to Lys~F-Ub or Cys~F-Ub using UbiReal. "1" indicates the addition of ± E4BU, and "2" indicates the addition of amino acid. Samples are monitored over time, and data are normalized to samples not treated with amino acid (100% remaining) and samples with amino acid but lacking ATP (0% remaining). Data are reported as the Mean values from an experiment with 3 technical replicates, and representative error of Mean ± SD is reported for the UBE2D3+E4BU+Lys sample. **C**. Discharge of UBE2L3~F-Ub to Lys~F-Ub or Cys~F-Ub over time. "1" represents the addition of amino acid. Data are reported and normalized as in B., with representative error reported for the UBE2L3+Lys sample.

Observing ubiquitination by HECT E3 Ub ligases

E3 ligases traditionally facilitate the final transfer of Ub onto a substrate, but even in the absence of substrate, E3s will often autoubiquitinate themselves or form free Ub chains in vitro. Gel-based assays typically report this activity as a "smear" of Ub modifications in the high molecular weight range that is difficult to reliably quantify. As shown in **Fig. 2.1B**, the UbiReal approach can be used to monitor E3 ligase activity, particularly after the addition of excess unlabeled Ub that continually builds high molecular weight products that contain T-Ub. Using a different HECT-type E3 ligase, NEDD4L, we could again show robust ubiquitination activity that builds with time (**Fig. 2.4A**). Importantly, this activity was dependent upon known E2-E3 specificity[46], as UBE2D3 could generate large ubiquitinated products with NEDD4L but not UBE2N, an E2 that typically functions with UBE2V2 and RING/U-box ligases (**Fig. 2.4A**).

NEDD4L, as a HECT-type E3 ligase, controls the context of the final ubiquitinated product, i.e., mono- versus polyubiquitination as well as the Ub chain specificity[**103**]. As the bulk of the ligase-dependent ubiquitination signal develops after an influx of unlabeled Ub, we sought this opportunity to instead supplement mutated Ub that could inform on the type of Ub modification. By supplementing the reaction with K0 Ub (in which all seven Lys residues are mutated to Arg) or Me-Ub (in which all primary amines have been methylated), the FP signal rose to only 50% of that observed with WT Ub (**Fig. 2.4B**). Interestingly, these results suggested that approximately half of the FP signal originated from mono- or multi-mono-autoubiquitination, with the remaining activity originating

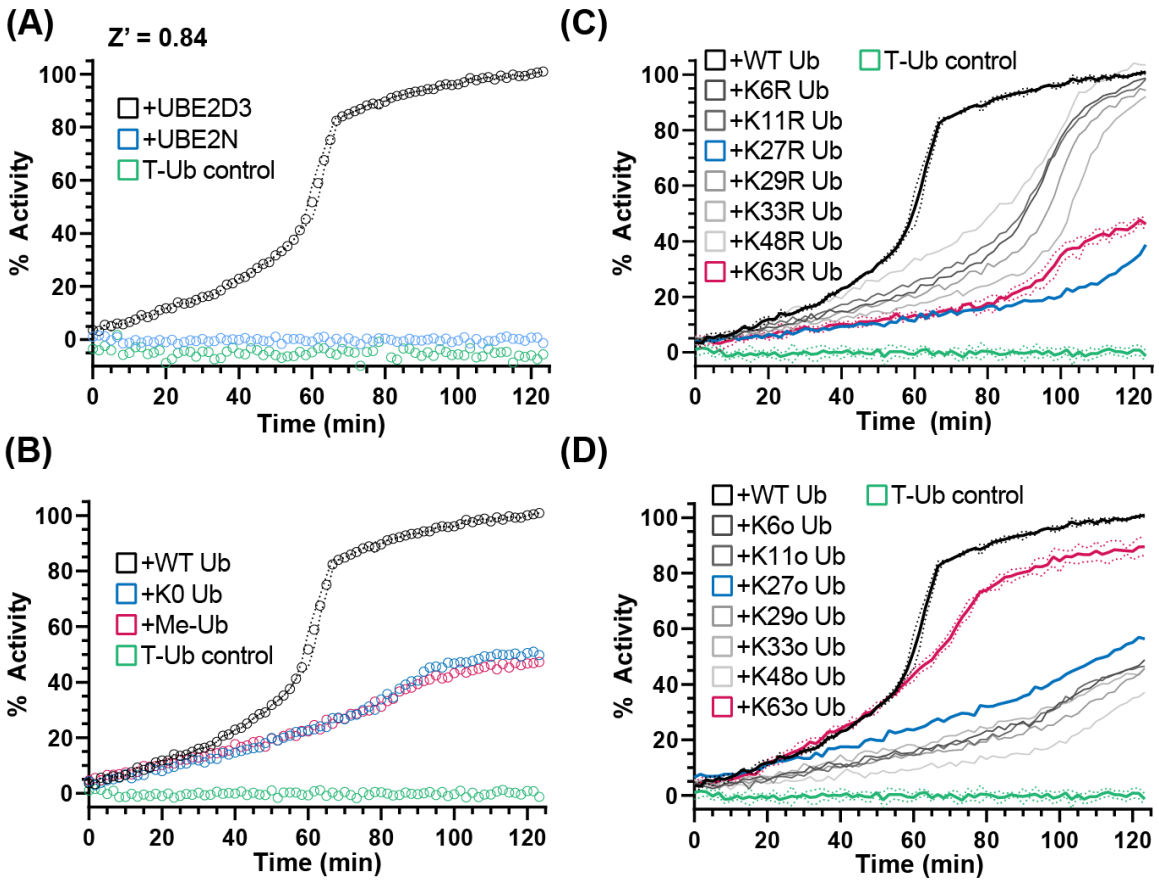

Figure 2.4. NEDD4L E3 polyUb ligation and chain specificity.

A. Ub chain ligation by K63-chain specific NEDD4L and the E2 enzyme UBE2D3 or UBE2N monitored over time using UbiReal. Reactions are initiated with ATP at time 0. Data for each sample is normalized to its starting FP value before ATP addition (0% activity) and to the final values of the NEDD4L+UBE2D3+WT Ub sample (100% activity). Data are reported as the Mean from an experiment with 3 technical replicates, with representative error reported as Mean ± SD for the NEDD4L+UBE2D3+WT Ub sample. Data for this and subsequent panels were collected together, and the UBE2D3 and T-Ub data are included as positive and negative controls, respectively, in the panels to follow. **B.** Monitoring polyUb vs. monoUb formation by NEDD4L and UBE2D3 over time. Reactions are initiated with ATP at time 0. K0 Ub is a mutant lacking all Lys; Me-Ub is methylated at each primary amine. Data are reported and normalized as in **A. C.** Ub chain ligation by NEDD4L and UBE2D3 over time using a mutant KR Ub panel that has individual Lys residues mutated to Arg (K63R has every Lys except K63, etc.). Reactions are initiated with ATP at time 0. Data are reported and normalized as in **A.**, with representative error reported as Mean ± SD for some samples. **D.** The same experiment as **C.**, but using a mutant Ko Ub panel that contain only a single Lys residue, with all other Lys mutated to Arg (K63o contains only K63, etc.). Data are reported and normalized as in **A.**, with representative error reported as Mean ± SD for some samples.

from chain-building activity of NEDD4L.

To probe the type of polyUb chain formation observed in the NEDD4L reaction, two additional sets of mutated Ub were used. The first set consists of all possible Lys-to-Arg mutants, each eliminating one potential site of chain linkage (e.g., K63R). As expected for the K63-specific ligase NEDD4L, addition of the K63R mutant Ub decreased the ubiquitination signal to levels consistent with the K0 Ub control, whereas most other Lys-to-Arg mutants had little effect on product formation (**Fig. 2.4B-C**). Interestingly, the K27R mutant Ub also produced less ubiquitination signal and could indicate a local disruption in the Ub structure (K27 is the most buried of all Lys) or in some interaction with the conjugation machinery. The second set consists of Ub K-only mutants, in which six of the seven Lys residues have been mutated to Arg leaving only one behind (e.g., K63o). With this panel, only the K63o mutant could generate a ubiquitination signal similar to WT, whereas all other mutants behaved like the K0 Ub control (**Fig. 2.4B**, **2.4D**). Together, these experiments confirm the K63 specificity of NEDD4L[47] and illustrate the utility of the UbiReal approach for studying E3 ligase activity.

Applying the UbiCRest assay to the UbiReal methodology

In our initial experiments addressing the measurement of DUB activity, we observed an incomplete reduction in FP signal using the DUB USP21 (**Fig. 2.1B**, step 5), though we expected the non-specific activity of USP21 toward both mono- and polyubiquitination[104] to return the FP signal to unconjugated T-Ub values (**Fig. 2.1A**) To understand the discrepancy, several control experiments were prepared to observe the behavior of USP21

under our assay conditions. The Ub conjugation assay components (T-Ub, E1, UBE2D3, NEDD4L, and WT Ub) were incubated with or without ATP, and this was used as the starting substrate to which each DUB was added. Interestingly, when combined with the -ATP sample that could not support Ub conjugation, the USP21-treated sample increased in FP over time, most likely a result of noncovalent interactions between T-Ub and USP21 (**Fig. 2.5A**). The +ATP sample treated with USP21 decreased to the same FP value as the -ATP sample by the end of the time course, indicating that complete deubiquitination had occurred (**Fig. 2.5A**). For other DUBs like ChlaDUB1, an effector protein from *Chlamydia trachomatis* that preferentially cleaves K63 chains[21], the background present in the -ATP samples was not as significant as for USP21 (**Fig. 2.5A**), but a -ATP sample was prepared nonetheless for each DUB in subsequent experiments to control for potential background binding. These experiments established a key foundation for the following DUB assays, but also suggest that USP21 most likely suffers from product inhibition resulting from a high affinity for free Ub, as has previously been shown for USP2[105].

UbiCRest is a powerful method that has been used to determine the type of ubiquitination present in a sample through treatment with Ub chain-specific DUBs[104]. Though normally interpreted using a gel-based readout, we applied the UbiCRest strategy to NEDD4L-generated ubiquitination in order to detect DUB activity through the release of T-Ub. Using AMSH, an endosome-associated DUB that preferentially cleaves K63 chains, cleavage of the NEDD4L assembly was observed to approximately 40% remaining FP signal, and when combined with USP21, complete cleavage was observed (**Fig. 2.5B**). This result then indicated that while AMSH can cleave the K63-linked polyUb, it cannot remove monoUb

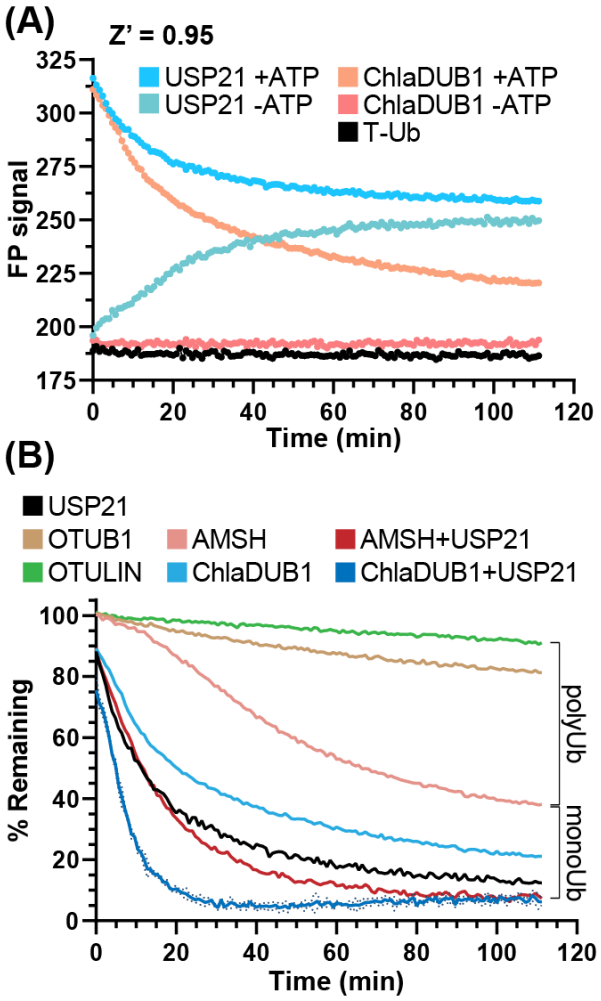

Figure 2.5. DUB activity and UbiCRest analysis of polyUb chain types.

A. Monitoring deubiquitination over time with DUBs USP21 and ChlaDUB1 using UbiReal. Curves show the raw FP signal of USP21 or ChlaDUB1 activity against samples containing a NEDD4L ligation mixture ± ATP. +ATP samples represent DUB activity against NEDD4L-generated chains while –ATP samples represent background FP signal where no ligation activity could occur. Reactions were initiated by addition of the DUB at time 0. +ATP samples are reported as the Mean of 3 technical replicates while –ATP samples are a representative single sample. **B.** Monitoring deubiquitination over time with DUBs USP21, OTUB1, OTULIN, ChlaDUB1 ± USP21, and AMSH ± USP21. The polyUb and monoUb brackets indicate the observed contributions of monoUb and polyUb in the NEDD4L ligation mixture. Data are from the same assay as **A.**, and are reported in the same manner, with representative error reported as Mean ± SD for the ChlaDUB1+USP21 sample.

modifications which likely account for the ~40% remaining signal (consistent with **Fig. 2.4B**). ChlaDUB1 alone cleaved the Ub assembly to around 20% remaining, and together with USP21 could completely remove all modifications (**Fig. 2.5B**). This suggested that ChlaDUB1, unlike AMSH, appears to be more promiscuous toward monoubiquitination. K48-specific OTUB1 and Met1-specific OTULIN were used as negative controls that should not have deubiquitinating activity towards NEDD4L-generated chains, and the slight drift observed in these samples could be an experimental artifact or low-level cleavage (**Fig. 2.5B**). Taken altogether, the UbiCRest approach for characterizing ubiquitination in our assay was effective at identifying both the amount and type of polyUb present.

Discussion

In an effort to address a longstanding need for a robust HTS for Ub conjugation, we have designed and tested UbiReal as a real-time assay for monitoring all ubiquitination activities. UbiReal uses commercially-available fluorescently-labeled Ub to track the progression through E1, E2, and E3 enzymes by the molecular weight and resulting fluorescence polarization changes associated with each step. Using this approach, ubiquitination activities can be observed in a highly parallel manner that consumes remarkably little material (on the order of 10 ng of labeled Ub per reaction). Unlike other more specialized approaches, UbiReal offers a universal method that allows the user to directly observe each consecutive step of Ub conjugation, from the E1 through to the E2, E3, and substrate ubiquitination. Furthermore, the ubiquitination products assembled using this method provide a more complex, realistic substrate that can be used to monitor DUB

activity. In our trials, we found that UbiReal was able to provide both quantitative measurements of activity as well as qualitative insights into mechanisms and specificities of Ub transfer.

As a test of its power to assay small molecule modulators, we used UbiReal to monitor the inhibition of E1 Ub-activating function in response to the PYR-41 inhibitor. In a dose-response experiment, we determined the IC50 of PYR-41 to be 9.15 μM, consistent with the reported estimation of <10 μM from a radioactive gel-based assay[96] and a fluorescent activity-based probe assay[106]. We chose to analyze this experiment as an endpoint assay as PYR-41 is an irreversible inhibitor, but the same experiment provides kinetic information as well and could easily be used to measure effects of competitive inhibitors on initial velocity. From our experimental control data, we determined Z' values in the range of 0.59-0.95 for all of our directed UbiReal experiments measuring E1, E2, E3, and DUB activities, indicating that under these conditions UbiReal provides excellent signal-to-noise ratios that are compatible with HTS. With minor adjustments, we expect that the UbiReal approach could be an effective HTS for any regulator of ubiquitination.

The UbiReal method was also useful for determining several qualitative aspects of Ub conjugation and deconjugation. Simplified amino acid reactivity assays provide a straightforward measure of E2 enzyme activity, and we showed that UbiReal is able to recapitulate both the reactivity profiles of several E2 enzymes as well as the reactivity enhancement mediated by RING/U-box E3 ligases. By supplementing the reaction with unlabeled Ub, we observed robust E3 ligase activity in the form of autoubiquitination. By

changing the nature of the supplemented Ub, we were able to distinguish mono- versus polyubiquitination as well as determine the preferred Ub chain type. To corroborate this chain type determination, we applied a simplified UbiCRest approach to our assay in order to observe which chain-specific DUBs could reduce the FP of our samples back to a monoUb value. Just as in the gel-based UbiCRest approach, by treating with DUBs singly or in combination, we observed complete, partial, or negligible collapse of FP values that indicate both the chain type and mono- versus polyUb architecture present in our complex ubiquitinated sample. These proof-of-principle studies indicate the applicability of UbiReal across the entire Ub cascade. Though we focused on aspects of Ub transfer specificity, the same approach could be used to study the mechanisms of Ub transfer, for example by incorporating structure-guided mutations. As an alternative to conventional gel-based assays, UbiReal can provide quantitative information in less time with less material. Furthermore, by separating each stage of Ub transfer, in one assay the user can isolate the precise step (e.g., E2~Ub formation versus discharge) that is affected by perturbations such as mutations or small molecule modulators.

Existing HTS for Ub conjugation have primarily focused on observation of the final ubiquitinated substrate. The bulk of these methods rely on either direct detection of Ub following enrichment of substrate (e.g., ELISA), or detection of Ub in close proximity to substrate (e.g., FRET or AlphaScreen). Because these assays are specialized for detecting ubiquitinated substrate, they are not well-suited for monitoring each stage of Ub conjugation separately. Fluorescence polarization provides the unique opportunity to track Ub based on its tumbling rate in solution vis-à-vis its molecular weight. This approach has

been used to track different aspects of the Ub system before. By either placing the label on the substrate or the Ub itself, E2- or E3-mediated polyUb chain formation has been observed by increasing FP[97,98]. Specialized Ub substrates can also be used to directly monitor the activities of HECT- or RBR-family E3 ligases by FP, in the absence of E1 or E2 enzymes[92,93]. DUB activities have been measured using defined, fluorescently-labeled Ub chains[67,90]. Interestingly, FP has even been used to track the proteasomal degradation of ubiquitinated substrates[107]. It is based on these observations that we developed UbiReal as a generalized approach to observe all consecutive steps of both Ub conjugation and deconjugation in real time.

As with any method, UbiReal does have certain caveats. The most glaring is the dependence on large differences in molecular weight that are required for significant changes in FP. In particular, size similarities between E2, E3, or substrate proteins could pose challenges. One solution to this problem could be to incorporate protein tags, such as GST, to shift molecular weights. A second caveat to our approach is the location of the fluorophore. Though labeling the amino-terminus is routine practice and practically inert for most purposes, it obviously precludes the formation of M1-linked polyUb. In this case, we expect that the label could instead be conjugated through maleimide chemistry to a Cys residue introduced at, for example, position 20[97]. Our tests with two varieties of fluorescent Ub (F-Ub and T-Ub) suggest that other dyes and sites of attachment will also be amenable to UbiReal. Lastly, we recognize that our ability to track fluorescent Ub through each stage of the conjugation process requires a molar excess of conjugating enzymes, which may preclude certain applications of the method. However, if the desired readout does not

depend on observing each transfer event (e.g., E2~Ub formation versus polyUb formation), the concentrations of each enzyme component can be tuned to suit the reaction requirements.

In sum, we present a simple method that addresses a need for a universal HTS for Ub conjugating activity. UbiReal requires no specialized reagents, only a fluorescently-labeled Ub which is readily available in multiple forms. With only minor optimization, we were able to apply the UbiReal method to measure E1, E2, E3, and DUB activities in separate, controlled experiments. We believe that the robust and scalable nature of this assay will make it useful in HTS for small molecule modulators, and its convenience and quantitative nature makes it a compelling alternative to the conventional gel-based assays for mechanistic work.

Experimental procedures

Protein expression and purification

Fluorescein-Ub (F-Ub), labeled at all primary amines, was purchased from Boston Biochem (U-590). TAMRA-Ub (T-Ub), labeled only at the amino-terminus, was a kind gift from P. Geurink (Leiden University Medical Centre). Wild-type and mutant Ub proteins were prepared according to Pickart and Rassi, 2005[108], with slight modifications. Briefly, Ub was expressed from the pET-17b vector by autoinduction at 37 ˚C for 48 hrs. Cells were resuspended in 25 mM Tris (pH 8.0), 200 mM sodium chloride and lysed by sonication. The clarified lysate was acidified with perchloric acid to a final concentration of 0.5% v/v. Some Ub mutants were more sensitive to acid precipitation, and in these cases

the acid content was limited to 0.2%. The soluble fraction from the acid precipitation was dialyzed into 50 mM sodium acetate (pH 5.0), loaded onto a HiPrep SP FF 16/10 ion exchange column (GE Life Sciences), and eluted with a linear gradient to 500 mM sodium chloride. Ub-containing fractions were pooled, concentrated using an Amicon centrifugal filter (3K MWCO, EMD Millipore), and further purified with a HiLoad Superdex 75 pg size exclusion column equilibrated in 25 mM sodium phosphate (pH 7.4), 150 mM sodium chloride. Purified Ub fractions were pooled, concentrated, and flash frozen for storage at -80 ˚C.

Human E1 (UBA1) was purified by activation to a GST-Ub column, according to Gladkova *et al.*[109]. UBE2D3, UBE2L3, UBE2N, and NEDD4L were purified from the pGEX6P-1 vector following overnight induction at 18 ˚C with 0.2 mM IPTG. Cells were resuspended in 25 mM Tris (pH 8.0), 200 mM sodium chloride, 2 mM β-mercaptoethanol and lysed by sonication. The clarified lysate was applied to glutathione agarose resin (Pierce) and washed according to the manufacturer's recommendations. E2s were eluted from the resin by overnight cleavage with GST-3C protease at 4 ˚C, and the resulting protein was dialyzed into 25 mM sodium phosphate (pH 7.4), 150 mM sodium chloride, 1 mM DTT, flash frozen, and stored at -80 ˚C. NleL was purified according to Hospenthal *et al.*[57]. E4BU was purified according to Nordquist *et al.*[110]. USP21 was purified according to Ye *et al.*[90] with the SUMO tag left intact. OTUB1* and AMSH* were purified according to Michel *et al.*[111]. ChlaDUB1 was purified according to Pruneda *et al.*[21]. All proteins were quantified by absorbance at 280 nm.

General assay parameters

T-Ub assays were monitored using fluorescence polarization (FP) on a BMG LabTech ClarioStar instrument using settings suitable for the TAMRA fluorophore with an excitation wavelength of 540 nm, an LP 566 nm dichroic mirror, and an emission wavelength of 590 nm. F-Ub assays were similarly monitored, with an excitation wavelength of 482 nm, an LP 504 nm dichroic mirror, and an emission wavelength of 530 nm. FP experiments were typically 1-2 hrs in length and FP values were read every 30-60 seconds with 20 flashes per sample well, unless otherwise noted. FP experiments were performed using Greiner 384-well small-volume HiBase microplates, with samples in 25 mM sodium phosphate (pH 7.4), 150 mM sodium chloride, 10 mM $MgCl_2$ at a final volume of 20 µL unless otherwise noted.

Generally, depending on the assay, a master starting solution was prepared with each component shared by all samples in the assay (e.g., E1, $MgCl_2$, T-Ub), and distributed to each sample well. The master solution components were calculated so that desired concentrations would be achieved in a final 20 µL volume and a volume of <20 µL master solution could be added to each well. Then, the experimental components (e.g., inhibitors, E2s, ATP, etc.) or buffer were added to sample wells such that the final desired volume of 20 µL was achieved.

Complete UbiReal curve generation

T-Ub at a final concentration of 100 nM in 25 mM sodium phosphate (pH 7.4), 150 mM sodium chloride, 10 mM $MgCl_2$ and 5 mM ATP was monitored for 17 cycles. After cycle

17, E1 was added to a final concentration of 125 nM and monitored. After cycle 34, UBE2D3 was added to a final concentration of 300 nM and monitored. After cycle 57, NleL was next added to a final concentration of 700 nM and monitored. After cycle 78, unlabeled WT Ub was added to a final concentration of 25 µM and monitored. Finally, after cycle 124, USP21 was added to a final concentration of 250 nM and monitored to cycle 150. FP readings were paused prior to the addition of protein, and resumed after protein had been added to the sample wells. The UbiReal curve shown is the average of two identical sample wells and is representative of several experiments.

E1 inhibition

0.5 µL of E1 inhibitor PYR-41 (Sigma-Aldrich, N2915) dissolved in DMSO at various dilutions was added to sample wells containing 125 nM E1 and 100 nM T-Ub to final PYR-41 concentrations of 75, 50, 33, 25, 20, 16, 10, 8, 6, 2.5, or 0.5 µM. FP was briefly monitored for 10 cycles before initiating the E1~Ub charging reaction with a 1 µL addition of ATP to a final concentration of 5 mM. FP was continuously monitored for approximately 1 hr, at which point it had stabilized. An uninhibited control sample that received 0.5 µL of DMSO instead of PYR-41 was used to determine the maximal E1~Ub charging FP signal.

To determine the inhibition of the E1, the FP values for each PYR-41-treated sample were normalized to its starting FP signal before ATP addition (0% activity), and to the final signal of the uninhibited DMSO control, which served as the maximum FP signal in the assay (100% activity). The initial signal in each sample was determined by averaging the

10 values before ATP addition, and the final signal for each sample was determined by averaging the final 10 values. Each sample was prepared in triplicate, and the experiment was performed separately 3 times.

To construct the IC_{50} curve, the unnormalized FP values were used. The final 10 FP values for each sample were averaged and this was used as the final value to plot against the PYR-41 concentration. This was done for each of the 3 separate experiments as before, giving 3 values at each concentration except the 33 μM PYR-41 sample, which had 2 final values. The non-linear regression calculation in GraphPad Prism was used to fit the curve and calculate the final IC_{50} value.

E2 amino acid reactivity

Master solutions resulting in final concentrations of 25 mM sodium phosphate (pH 7.4), 150 mM sodium chloride, 100 nM F-Ub, 10 mM $MgCl_2$, 125 nM E1 and either 5 mM ATP or no ATP were incubated at RT for 10 mins before addition to sample wells. FP was monitored for 5 cycles before addition of either UBE2D3 or UBE2L3 to a final concentration of 300 nM, while a subset of UBE2D3 samples also received an addition of E4BU to a final concentration of 2.5 μM. Samples next received an addition of either no amino acid (buffer alone), lysine, or cysteine to a final concentration of 0, 37.5 mM, or 37.5 mM, respectively. Samples were monitored by FP for approximately 2 hrs.

E3 ligase assay

A master solution resulting in final concentrations of 25 mM sodium phosphate (pH 7.4),

150 mM sodium chloride, 10 mM $MgCl_2$, 100 nM T-Ub, 125 nM E1, 2 µM E2 (UBE2D3 or UBE2N) and 2 µM E3 NEDD4L, or a master solution lacking E3 NEDD4L as a control, was added to sample wells. Samples then received a 3 µL addition of either 250 µM WT Ub, lysine-less Ub, methylated Ub, one of the seven Ub K-only mutants, or one of the seven K-R Ub mutants, resulting in a final concentration of 37.5 µM unlabeled Ub in each sample well. The control lacking NEDD4L received WT Ub. FP was monitored for 5 cycles, before initiating the Ub cascade with a 1 µL addition of ATP to a final concentration of 5 mM. FP was monitored for an additional 75 cycles over the course of approximately 2 hrs. Each sample was prepared in triplicate, with the FP values averaged at each timepoint. The FP value at each time point was normalized to the average of the sample's initial 5 FP values before ATP addition (0% activity), and to the final 5 FP values of the WT Ub sample (100% activity).

DUB treatment

Ub chains were created in a master solution resulting in final concentrations of 25 mM sodium phosphate (pH 7.4), 150 mM sodium chloride, 10 mM $MgCl_2$, 100 nM T-Ub, 125 nM E1, 2 µM E2 UBE2D3, 2 µM E3 NEDD4L, 50 µM WT Ub, and 5 mM ATP, or a master solution lacking ATP as a control. The master solutions were incubated at 37 ˚C for 1 hr while shaking at 500 rpm, and then distributed into sample wells containing a final concentration of 10 mM DTT. FP signal was monitored for 10 cycles before DUB addition.

DUBs were incubated at room temperature for 15 mins in 25 mM sodium phosphate (pH 7.4), 150 mM sodium chloride, 10 mM DTT, and 30 mM EDTA. After incubation, DUBs

were added to the sample wells containing NEDD4L-generated Ub/T-Ub ubiquitination products. In this assay AMSH had a final concentration of 250 nM, while ChlaDUB1, OTUB1, OTULIN, and USP21 had final concentrations of 600 nM. Following DUB addition, deubiquitination was monitored for approximately 2 hrs. The FP values at each timepoint were normalized to the sample's averaged FP value prior to DUB addition (0% activity), and to a corresponding control sample that contained all components except for ATP, representing an unconjugated Ub signal (100% activity).

Data analysis

Data was first analyzed using the MARS data analysis software from BMG LABTECH. The fluorescence polarization values were calculated by the MARS software using the equation:

$$\boldsymbol{FP} = 1000 \times \frac{\parallel - \perp}{\parallel + \perp}$$

where ∥ and ⊥ are the measured values from the parallel and perpendicular channels, respectively, both in units of mP. Averages and standard deviations of FP data were calculated and plotted using GraphPad Prism.

Z' values were calculated for each assay according to the equation:

$$\boldsymbol{Z'} = 1 - \frac{(3\sigma_{c+} + 3\sigma_{c-})}{|\mu_{c+} - \mu_{c-}|}$$

where μ_{c+} and μ_{c-} are the means of the positive and negative controls, respectively, and σ_{c+} and σ_{c-} are the standard deviations of the positive and negative controls, respectively.

Acknowledgements

We thank members of the Pruneda Lab for reagents and discussion, and P. Geurink (Leiden University Medical Centre) for providing the TAMRA-Ub reagent.

Chapter 3 – Bacterial mimicry of eukaryotic HECT Ub ligation

A version of the following chapter is *accepted* at the journal *Molecular Cell*, and an earlier version is available online at *bioRxiv*.

Franklin, T.G., Brzovic, P.S., and Pruneda, J.N. (2023). Bacterial mimicry of eukaryotic HECT ubiquitin ligation. bioRxiv, 2023.06.05.543783. **DOI**: 10.1101/2023.06.05.543783.

Author contributions: TGF and JNP conceptualized the approach. TGF performed all experiments with guidance from PSB and JNP. TGF and JNP analyzed the data and wrote the manuscript with input from PSB.

Abbreviations: Ub, ubiquitin; monoUb, monoubiquitin; polyUb, polyubiquitin; Ub^{D}, donor ubiquitin; Ub^{A}, accepter ubiquitin; Lys or K, lysine; Cys or C, cysteine; Met or M, methionine; RING, Really Interesting New Gene; RBR, RING-between-RING; HECT, Homologous to E6AP C-terminus; eHECT, eukaryotic HECT; bHECT, bacterial HECT; FH, Full-HECT; NleL, non-LEE(locus of enterocyte effacement) encoded ligase; SNc, SopA-NleL chimera E3 ubiquitin ligase; HUWE1, HECT, UBA and WWE domain-containing protein 1; NEL, novel E3 ligase; DUB, deubiquitinase; EHEC, enterohemorrhagic *Escherichia coli*; PDB, protein data bank.

Introduction

Ubiquitination is a critical post-translational modification that regulates a gamut of cellular processes ranging from targeted protein degradation to signal transduction. The ubiquitination pathway requires orchestration of a ubiquitin (Ub)-activating E1, Ub-conjugating E2, and E3 Ub ligase to modify substrates[1]. A distinguishing feature of the Homologous to E6AP C-terminus (HECT) E3 Ub ligases is their ability to directly influence the substrate's cellular fate through formation of distinct polymeric Ub (polyUb) signals that recruit different cellular response factors[1,4,112]. For example, the founding member of the HECT family, E6AP, is specific for lysine (Lys or K)48-linked polyUb[113,114] and can target substrates for proteasomal degradation[115,116]. Alternatively, yeast Rsp5, a homolog of human NEDD4, adds K63-linked polyUb onto its targets during endocytic processes[117,118]. Mutations that disrupt the functionality of HECT Ub ligases are frequently observed in cancers and neurodegenerative disorders, among other diseases, making them crucial research targets[119]. Significant efforts have elucidated several critical aspects of HECT-type ligation[46–48,120,121], however, a clear picture of how they encode polyUb specificity is an active area of research[42].

As an alternative approach to understanding the mechanism of Ub ligation in eukaryotic HECT E3 ligases (eHECTs), we turned to a family of related enzymes in bacteria. While the complete ubiquitination pathway is present only in eukaryotes, microbial pathogens secrete Ub-targeted effector proteins to dysregulate the host Ub system in ways that benefit invasion, persistence, and replication[122]. Several classes of these bacterial effector proteins can functionally mimic eukaryotic E3s and insert themselves into the host ubiquitination

pathway[72,123], including the HECT-like effector proteins SopA from *Salmonella enterica* Typhimurium and NleL from Enterohemorrhagic *Escherichia coli* (EHEC)[17,49]. Crystal structures of the bacterial HECT-like E3 Ub ligases (bHECTs) NleL and SopA revealed structurally distinct but topologically similar HECT domains, with an E2-binding N-lobe and catalytic C-lobe joined by a linker region[50]. Also similar to eHECTs, the bHECT catalytic HECT-like domain is located at the protein C-terminus with substrate-binding regions positioned upstream that mediate interactions with host factors[26,35,50]. While extensive work has demonstrated how eHECTs interact with Ub, E2, and E2~Ub during ligation, it remains largely unknown how bHECTs interact with Ub, or even E2~Ub in the process of catalyzing ubiquitination[46–48,103,113,120,121,124–133].

Like many of their eukaryotic counterparts, bHECTs also assemble specific types of polyUb signals. Interestingly, the bHECT NleL robustly generates K6-linked polyUb as a ~50:50 mixture with K48-linked polyUb, representing the most K6-specific ligase known to-date[17,57]. A clear understanding for the role of NleL and the K6-linked polyUb signals it generates is lacking, though several reports would indicate a connection with actin pedestals formed by EHEC[35,59]. Meanwhile, the only other reported bHECT, SopA, preferentially generates K48-linked polyUb and has been tied to the Ub-dependent degradation of its targeted host factors, TRIM56 and TRIM65[26,58,122]. How NleL and SopA are able to dictate their polyUb products, and whether any of these mechanisms also mimic those used by eHECTs, remains an open question. The generally accepted model of polyUb chain formation by HECT E3s involves simultaneous coordination of two Ub molecules: a donor Ub (Ub^D) that is transiently bound to the active site cysteine (Cys) of the HECT

C-lobe, and an acceptor Ub (Ub^A) that is optimally oriented so that the correct Lys residue performs nucleophilic attack[42,134]. Among eHECTs, this polyUb linkage specificity appears to be partially encoded in the very C-terminal residues of the C-lobe[47,103]. Still, a mechanism for how HECT E3 ligases catalyze specific polyUb signals largely remains unclear.

Here, to elucidate the mechanisms of bHECT ligation, we first validated additional examples from both human and plant pathogens. Crystal structures of three bHECTs – NleL, SopA, and VsHECT – bound to Ub^D at their active sites revealed key features of this catalytic intermediate. These structures, combined with NMR data, identified commonalities and differences between bHECT- and eHECT-mediated Ub ligation. Crystal packing of the NleL-Ub^D structure revealed the acceptor site for K48-linked polyUb ligation, providing a rare visualization of the HECT:Ub^A interface[1,42]. By mutating this Ub^A interface, K48-linked polyUb ligation by bHECTs could be redirected to K6-linked polyUb. Illustrating the functional mimicry of eHECT ligases, insights from the NleL:Ub^A interface informed mutational analyses of the eHECT HUWE1 that redirected its specificity toward increased K6-linked polyUb ligation. Thus, despite considerable differences in sequence and structure, bHECTs follow many of the same underlying principles of Ub ligation as their eukaryotic counterparts.

Results

Expansion of the bacterial HECT-like E3 Ub ligase family

Unlike other bacterial E3 ligase families that are widely distributed among human and plant

pathogens[14,135–137], only two examples of bHECT E3s were known[17,49]. To identify additional family members, we examined sequence and structural homology signatures of the bHECT fold (see Experimental Methods section) (**Fig. 3.1A**). These signatures included 1) an aromatic residue in the putative N-lobe E2 interaction site, 2) a potential C-lobe catalytic Cys residue ~30 amino acids from the protein C-terminus, and 3) a linker region bridging the N- and C-lobes (**Fig. 3.1A**)[17,42,50]. Though it was not used as a selection criterion, we found many bHECT candidates also encoded an N-terminal β-helix domain that is likely involved in substrate recognition[26]. bHECT candidates were found in both human and plant pathogen genomes, with relatively low amino acid conservation across the bHECT domain as well as individual regions (**Fig. 3.1B, 3.2A-C**). We selected candidates from *Proteus vulgaris* (PvHECT), *Verrucomicrobia* spp. (VsHECT), *Erwinia amylorova* (EaHECT), and *Proteus stewartii* (PsHECT) for testing E3 ligase activity of recombinantly purified protein (**Table 3.1**), amongst a larger list of potential, unvalidated bHECT candidates (**Table 3.2**). In a gel-based assay, PvHECT, PsHECT, and VsHECT, in addition to the known bHECTs NleL and SopA, all consumed monomeric Ub to produce free polyUb chains and/or auto-ubiquitination (**Fig. 3.1C**). Mutation of the predicted active site Cys ablated ligase activity in all cases (**Fig. 3.1A, C**). Time-dependent ligase activity was additionally observed, to varying degrees, for PsHECT, EaHECT, PvHECT, and VsHECT using the fluorescence polarization (FP) method UbiReal (**Fig. 3.2D**)[138,139]. Using AlphaFold multimer[140,141], we modeled VsHECT, PvHECT, PsHECT, and EaHECT in complex with the canonical E2 for HECTs, UBE2L3 (**Fig. 3.2E**). Reassuringly, as observed experimentally for NleL and SopA[50], AlphaFold placed F63 of UBE2L3 adjacent to the predicted E2-binding residue in the bHECT N-lobes (**Fig. 3.1A**, **Fig. 3.2E**).

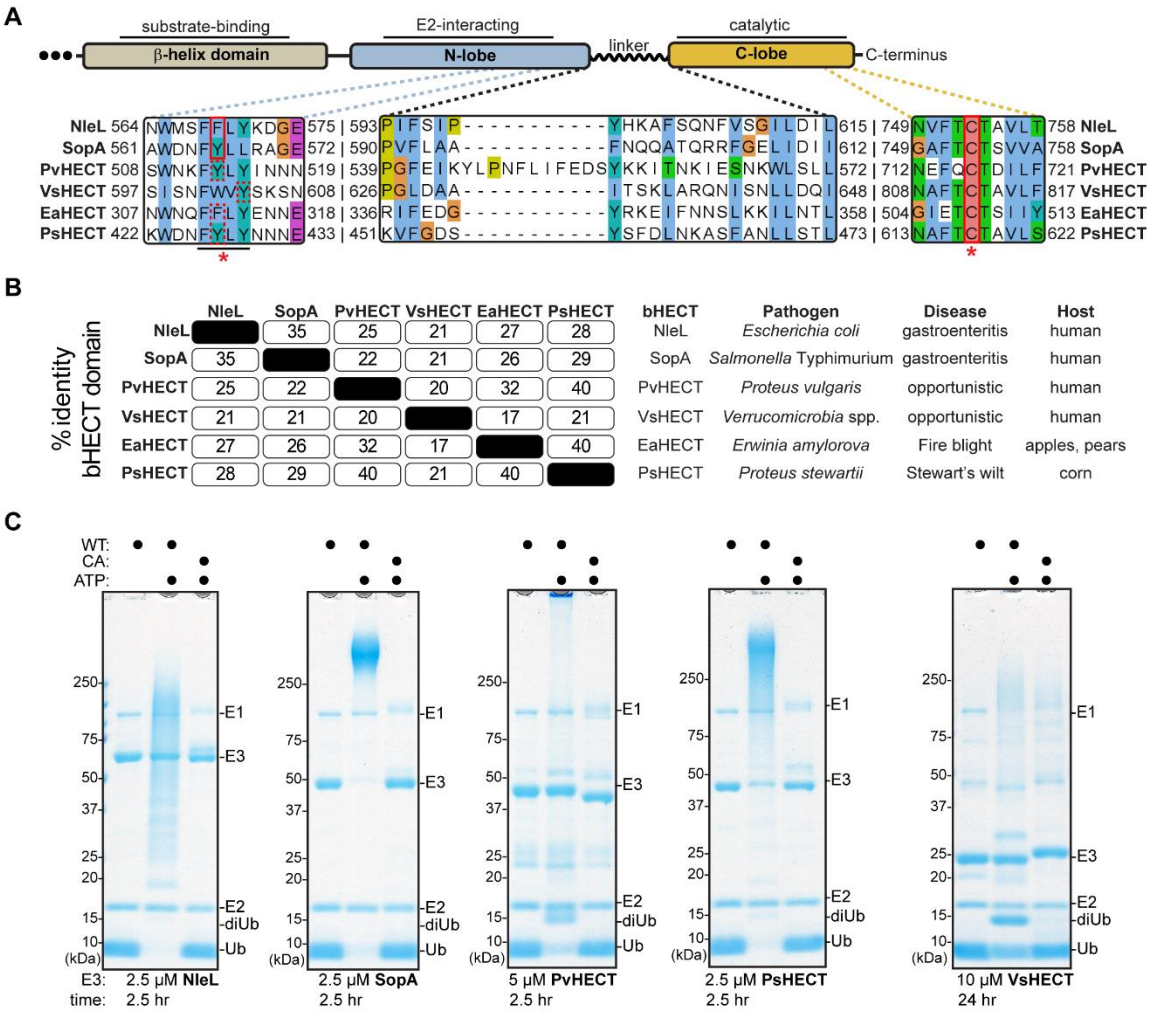

Figure 3.1 Expansion of the bacterial HECT-like E3 Ub ligase family (I/II)

A. bHECT domain architecture. Critical regions, including the N-lobe E2-interacting aromatic residue (dashed lines based on AlphaFold modeling), the C-lobe active site Cys, and the linker domain, are expanded to show sequence conservation. **B**. Percent sequence identity matrix for full HECT-like domains, along with species of origin, presenting disease, and host. **C**. Gel-based ligase assay for WT or the active site Cys-to-Ala mutant (CA) bHECTs.

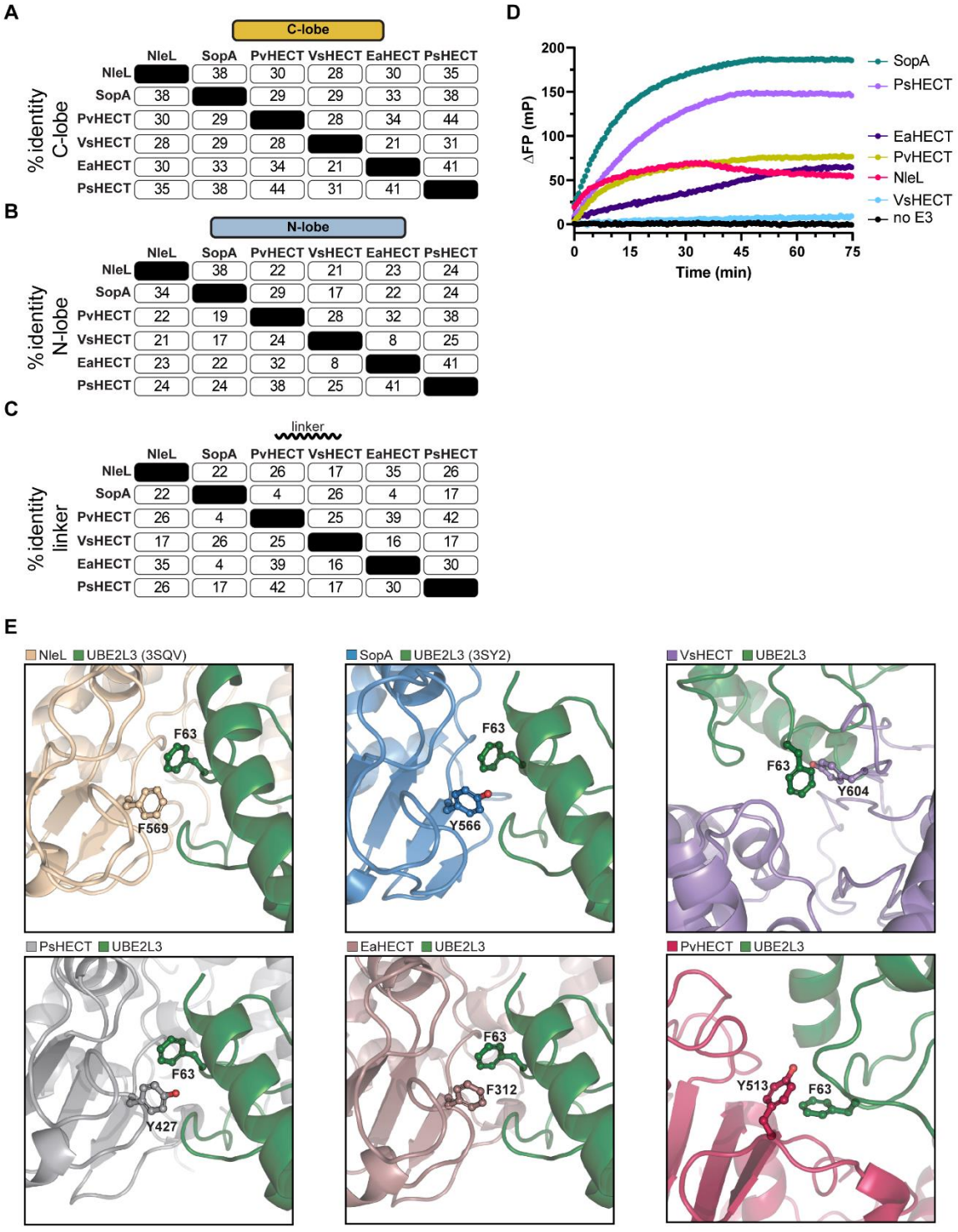
A
C-lobe
% identity C-lobe
NleL SopA PvHECT VsHECT EaHECT PsHECT
NleL 38 30 28 30 35
SopA 38 29 29 33 38
PvHECT 30 29 28 34 44
VsHECT 28 29 28 21 31
EaHECT 30 33 34 21 41
PsHECT 35 38 44 31 41
B
N-lobe
% identity N-lobe
NleL SopA PvHECT VsHECT EaHECT PsHECT
NleL 38 22 21 23 24
SopA 34 29 17 22 24
PvHECT 22 19 28 32 38
VsHECT 21 17 24 8 25
EaHECT 23 22 32 8 41
PsHECT 24 24 38 25 41
C
linker
% identity linker
NleL SopA PvHECT VsHECT EaHECT PsHECT
NleL 22 26 17 35 26
SopA 22 4 26 4 17
PvHECT 26 4 25 39 42
VsHECT 17 26 25 16 17
EaHECT 35 4 39 16 30
PsHECT 26 17 42 17 30
D
ΔFP (mP)
Time (min)
SopA
PsHECT
EaHECT
PvHECT
NleL
VsHECT
no E3
E
NleL UBE2L3 (3SQV)
F63
F569
SopA UBE2L3 (3SY2)
F63
Y566
VsHECT UBE2L3
F63
Y604
PsHECT UBE2L3
F63
Y427
EaHECT UBE2L3
F63
F312
PvHECT UBE2L3
Y513
F63

Figure 3.2 Expansion of the bacterial HECT-like E3 Ub ligase family (II/II)

A. Percent sequence identity matrix of bHECT C-lobe regions, **B**. N-lobe regions, and **C**. linker regions. **D**. Ub ligation monitored by fluorescence polarization (FP). Reactions were initiated with ATP at timepoint 0 min. Reactions are shown for the bHECTs NleL (4 µM), SopA (4 µM), PvHECT (4 µM), PsHECT (4 µM), EaHECT (12.5 µM), and VsHECT (4 µM). **E**. View of the E2:bHECT binding interface for NleL:UBE2L3 (PDB:3SQV), SopA:UBE2L3 (PDB: 3SY2), and AlphaFold multimer models of bHECTs VsHECT, PsHECT, EaHECT, and PvHECT with UBE2L3.

Crystal structures reveal mechanisms of donor Ub coordination by bHECTs

Notably, the only soluble expression construct of VsHECT that we could obtain was the minimal C-lobe domain, yet weak ligase activity was still observed despite the lack of an E2-binding N-lobe (**Fig. 3.1C, Fig. 3.2D**). Ligase activity was also observed with minimal C-lobe constructs of NleL and SopA, though kinetics were reduced compared to the full bHECT domains (**Fig. 3.3A**). To further show that the C-lobe was the minimal catalytic region, we tested reactivity against the Ub-Propargylamide (PA) activity-based probe, which has previously been used to profile eHECTs and other Ub regulators[22,124,142]. For all bHECTs tested, we observed strong reactivity consistent with a single modification event of the active site Cys (**Fig. 3.3B**). Notably, for eHECTs, reactivity with the Ub-PA probe is not observed in the absence of the N-lobe[124]. Thus, at least for bHECTs, the isolated C-lobe domain represents a minimal ligase module for studying Ub transfer events.

To obtain a better understanding of the bHECT Ub ligation pathway, we took advantage of the robust Ub-PA reactivity of the bHECT C-lobes and determined crystal structures for three complexes: NleL-Ub (2.50 Å), SopA-Ub (1.75 Å), and VsHECT-Ub (1.44 Å) (**Fig. 3.3C-E, 3.4A-C, Table 3.3**). Superposition of the bHECT-Ub^D structures revealed the similarity within each region of the fold (pairwise Cα RMSD between 1.6 and 3.2 Å) (**Fig. 3.3F**). Although they adopt a distinct α/β structure, eHECT C-lobes also demonstrate close structural homology to each other (pairwise Cα RMSD between 0.8 and 1.1 Å) (**Fig. 3.3G**). In contrast, while eHECT:Ub^D contacts are highly similar among resolved structures (pairwise Ub Cα RMSD between 0.7 and 5.7 Å)[47,48,120,124], the position of Ub^D on bHECT C-lobes is varied (pairwise Ub Cα RMSD between 8.0 and 15.4 Å) (**Fig. 3.3G-H**). When

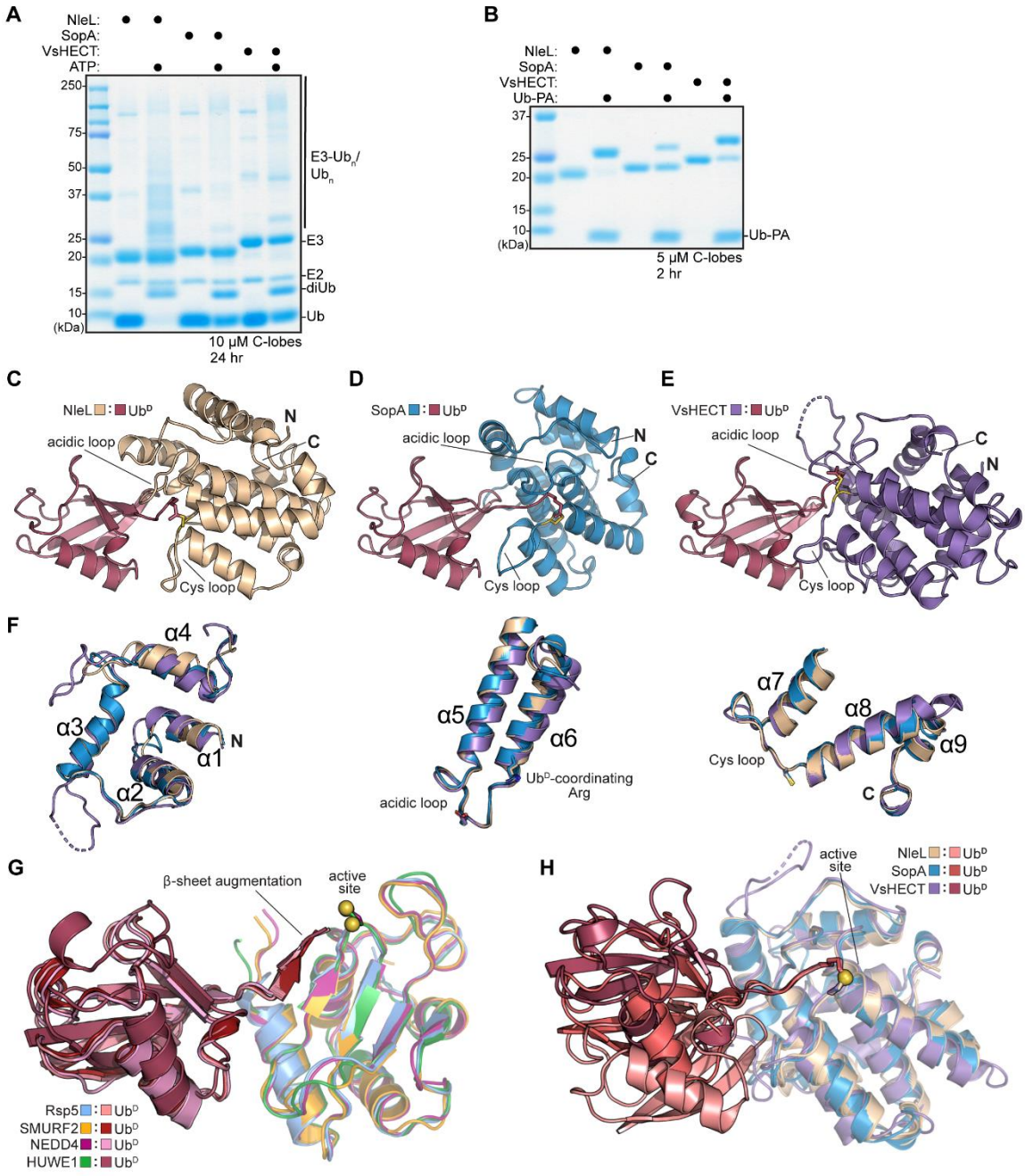
A
NleL:
SopA:
VsHECT:
ATP:
250
75
50
37
25
20
15
10
(kDa)
E3-Ub$_n$/
Ub$_n$
E3
E2
diUb
Ub
10 μM C-lobes
24 hr
B
NleL:
SopA:
VsHECT:
Ub-PA:
37
25
20
15
10
(kDa)
Ub-PA
5 μM C-lobes
2 hr
C
NleL : Ub^D
acidic loop
N
C
Cys loop
D
SopA : Ub^D
acidic loop
N
C
Cys loop
E
VsHECT : Ub^D
acidic loop
C
N
Cys loop
F
α4
α3
α1
N
α2
α5
α6
Ub^D-coordinating
Arg
acidic loop
α7
α8
α9
Cys loop
C
G
β-sheet augmentation
active
site
Rsp5 : Ub^D
SMURF2 : Ub^D
NEDD4 : Ub^D
HUWE1 : Ub^D
H
active
site
NleL : Ub^D
SopA : Ub^D
VsHECT : Ub^D

Figure 3.3 Structural and biochemical analysis of bHECT C-lobes (I/II)

A. Gel-based ligase assay of isolated bHECT C-lobes. **B**. Gel-based Ub-PA reactivity assay with the isolated bHECT C-lobes. **C**. 2.50 Å crystal structure of NleL-Ub^D. The PA linkage at the active site Cys (yellow) is shown, and the N- and C-termini are labeled. Views in C-E were generated by aligning on Ub^D. **D**. As in C, for the 1.75 Å SopA-Ub^D crystal structure. **E**. As in C, for the 1.44 Å VsHECT-Ub^D crystal structure. **F**. Overlay of the NleL, SopA, and VsHECT structures, aligned on the C-lobe and split into three sections to show conservation of each α-helical region. The α-helices are numbered from the N-terminus, with regions of interest (acidic loop, Cys loop, and critical residues) highlighted. **G**. Overlay of eHECT-Ub^D structures, aligned by the C-lobe for NEDD4-Ub^D (PDB: 4BBN), HUWE1-Ub^D (PDB: 6XZ1), Rsp5-Ub^D (PDB: 4LCD), and SMURF2-Ub^D (PDB: 6FX4) with the active site Cys (yellow) highlighted. **H**. Overlay of bHECT-Ub^D structures, aligned on their C-lobes, with the active site Cys (yellow) highlighted.

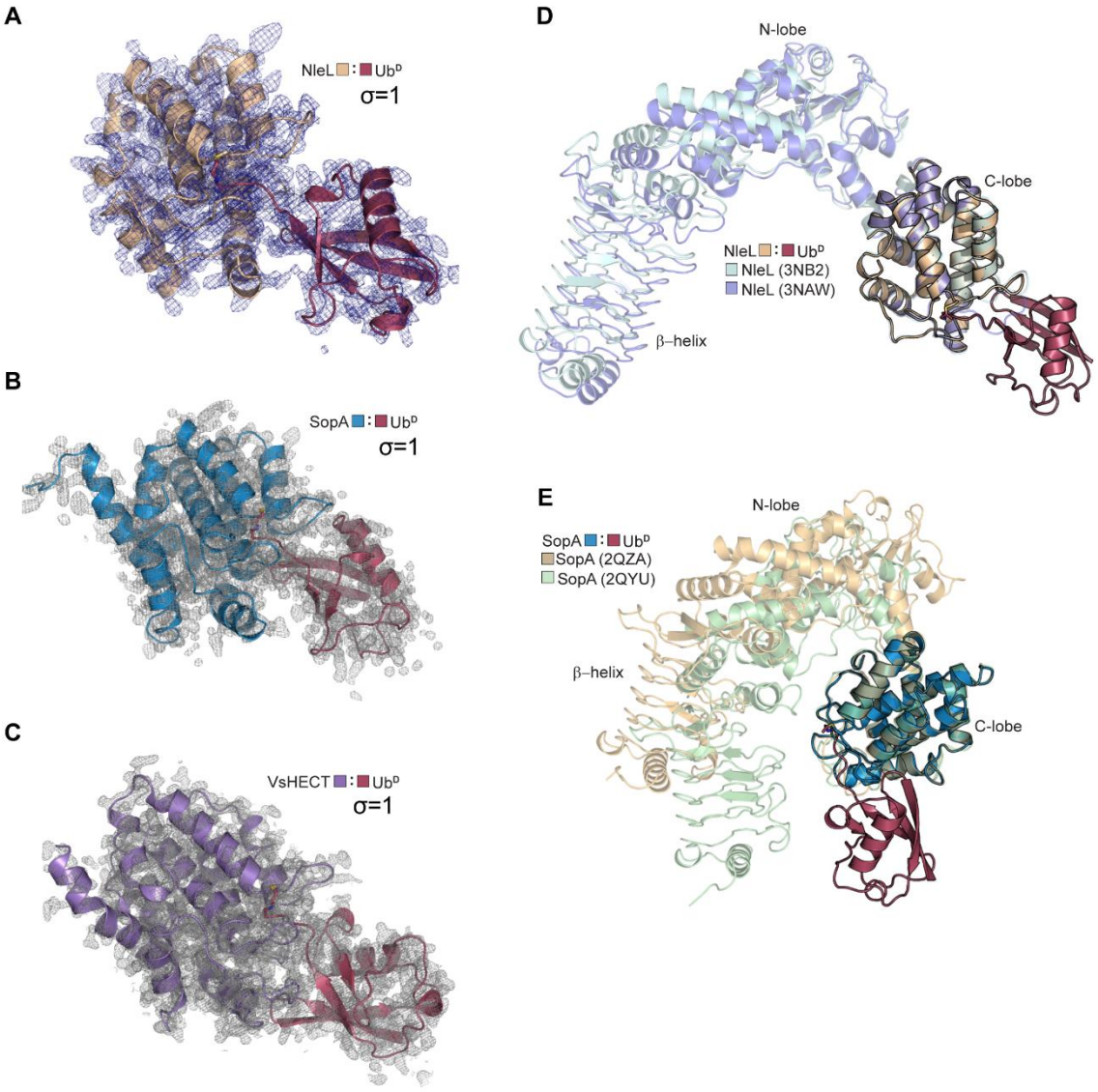

Figure 3.4 Structural and biochemical analysis of bHECT C-lobes (II/II)

A. Full 2|Fo-Fc| electron density for the NleL-Ub^D structure, shown at 1σ. **B**. Full 2|Fo-Fc| electron density for the SopA-Ub^D structure, shown at 1σ. **C**. Full 2|Fo-Fc| electron density for the VsHECT-Ub^D structure, shown at 1σ. **D**. Overlay of the NleL-Ub^D structure with two apo NleL structures (PDB: 3NB2 and 3NAW), aligned on their C-lobes. NleL β-helix, N-lobe, and C-lobe domains are labeled. **E**. Overlay of the SopA-Ub^D structure with two apo SopA structures (PDB: 2QZA and 2QYU), aligned on their C-lobes. SopA β-helix, N-lobe, and C-lobe domains are labeled.

superposed onto previous apo NleL or SopA structures that encompass the β-helix, N-lobe, and C-lobe domains, neither of the bound Ub^D molecules clash or form contacts outside of the C-lobe (**Fig. 3.4D-E**).

Donor Ub activation by bHECTs

Previous structural work for eHECTs bound to Ub^D revealed a conserved interaction referred to as β-sheet augmentation, whereby residues 73-75 of the Ub^D C-terminus form a parallel β-strand with the conserved β-sheet of eHECT C-lobes (**Fig. 3.3G, 3.5A**)[47,48,120]. Though they lack the β-sheet architecture, bHECT C-lobes also exhibit a strong coordination of the Ub^D C-terminal tail, primarily through extensive hydrogen bonding (**Fig. 3.6A**). This coordination relies upon a conserved bHECT Arg residue at the base of α-helix 6, which forms hydrogen bonds with the peptide backbone of Ub^D R74 (**Fig. 3.5B, 3.6B**). Mutation of this Arg residue severely diminishes bHECT ligase activity (**Fig. 3.5C-F**), and reactivity with Ub-PA (**Fig. 3.6C**). NleL and SopA mediate secondary contacts to the Ub^D C-terminus via hydrogen bonds from E710 and D707, respectively, and mutations at these sites also reduce ligase activity (**Fig. 3.5C, E, 3.6A**). Thus, similar to eHECTs and other human ligase complexes[143–145], bHECTs stretch and coordinate the C-terminal tail of Ub^D, priming it for nucleophilic attack by an incoming Lys.

Outside of the C-terminal tail, SopA and VsHECT make additional Ub^D contacts. SopA forms hydrogen bonds between H748 and E34 of Ub^D, as well as between H745 and T9 of Ub^D (**Fig. 3.6D**). A SopA H748A mutation showed a small decrease in ligase activity (**Fig. 3.5E**). VsHECT contacts both the I36 and L8 hydrophobic patches of Ub^D, mediated in

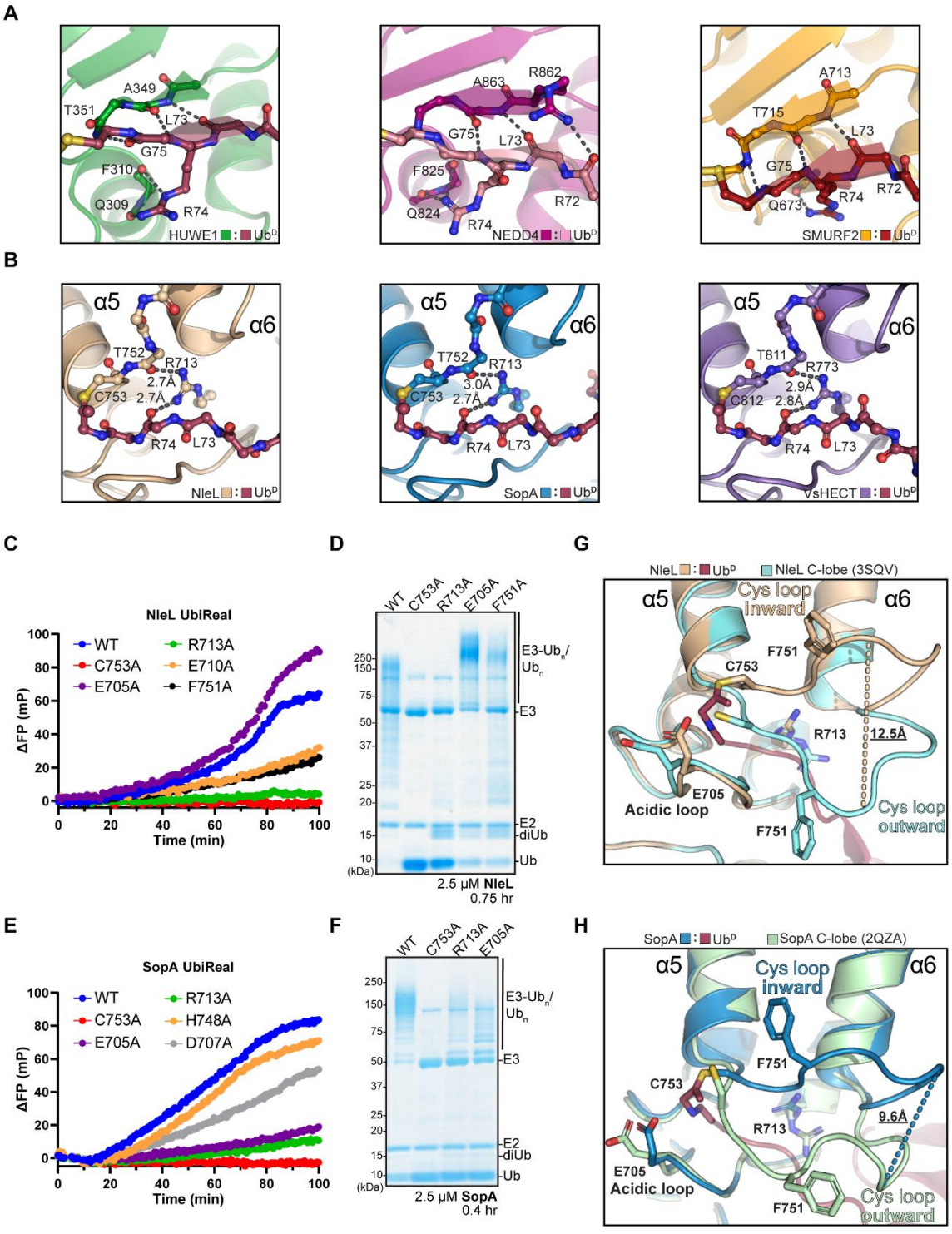
A
A349
T351
L73
G75
F310
Q309
R74
HUWE1 : Ub^D
A863
R862
G75
L73
F825
R72
Q824
R74
NEDD4 : Ub^D
A713
T715
L73
G75
R72
Q673
R74
SMURF2 : Ub^D
B
α5
α6
T752
R713
2.7Å
C753
2.7Å
R74
L73
NleL : Ub^D
3.0Å
SopA : Ub^D
T811
R773
2.9Å
C812
2.8Å
VsHECT : Ub^D
C
NleL UbiReal
WT
C753A
E705A
R713A
E710A
F751A
ΔFP (mP)
Time (min)
D
WT
C753A
R713A
E705A
F751A
E3-Ub_n/ Ub_n
E3
E2 diUb
Ub
(kDa)
2.5 μM NleL
0.75 hr
G
NleL : Ub^D
NleL C-lobe (3SQV)
Cys loop inward
F751
C753
R713
12.5Å
E705
Acidic loop
Cys loop outward
E
SopA UbiReal
WT
C753A
E705A
R713A
H748A
D707A
F
2.5 μM SopA
0.4 hr
H
SopA : Ub^D
SopA C-lobe (2QZA)
9.6Å

Figure 3.5 bHECT activation of donor Ub (I/II)

A. β-sheet augmentation of the Ub^D C-terminal tail in HUWE1-Ub^D (PDB: 6XZ1), NEDD4-Ub^D (PDB: 4BBN), and SMURF2-Ub^D (PDB: 6FX4). Hydrogen bonds are shown as black dashes. **B**. Ub^D C-terminal tail coordination by the conserved Arg residue at the base of α-helix 6 in NleL-Ub^D, SopA-Ub^D, and VsHECT-Ub^D. Hydrogen bonds are shown as black dashes. **C**. Ligase assay using the FP-based method UbiReal, for WT NleL and sequence- or structure-guided mutations. **D**. Gel-based ligase assay of WT NleL and sequence- or structure-guided mutations. **E**. As in C, for SopA constructs. **F**. As in D, for SopA constructs. **G**. Structural overlay highlighting the large movement of the Cys loop from the outward conformation observed in the apo NleL structure (PDB: 3NB2) to the inward conformation observed upon Ub^D binding. **H**. As in G, comparing the outward conformation observed in the apo SopA structure (PDB: 2QYU) to the inward conformation observed upon Ub^D binding.

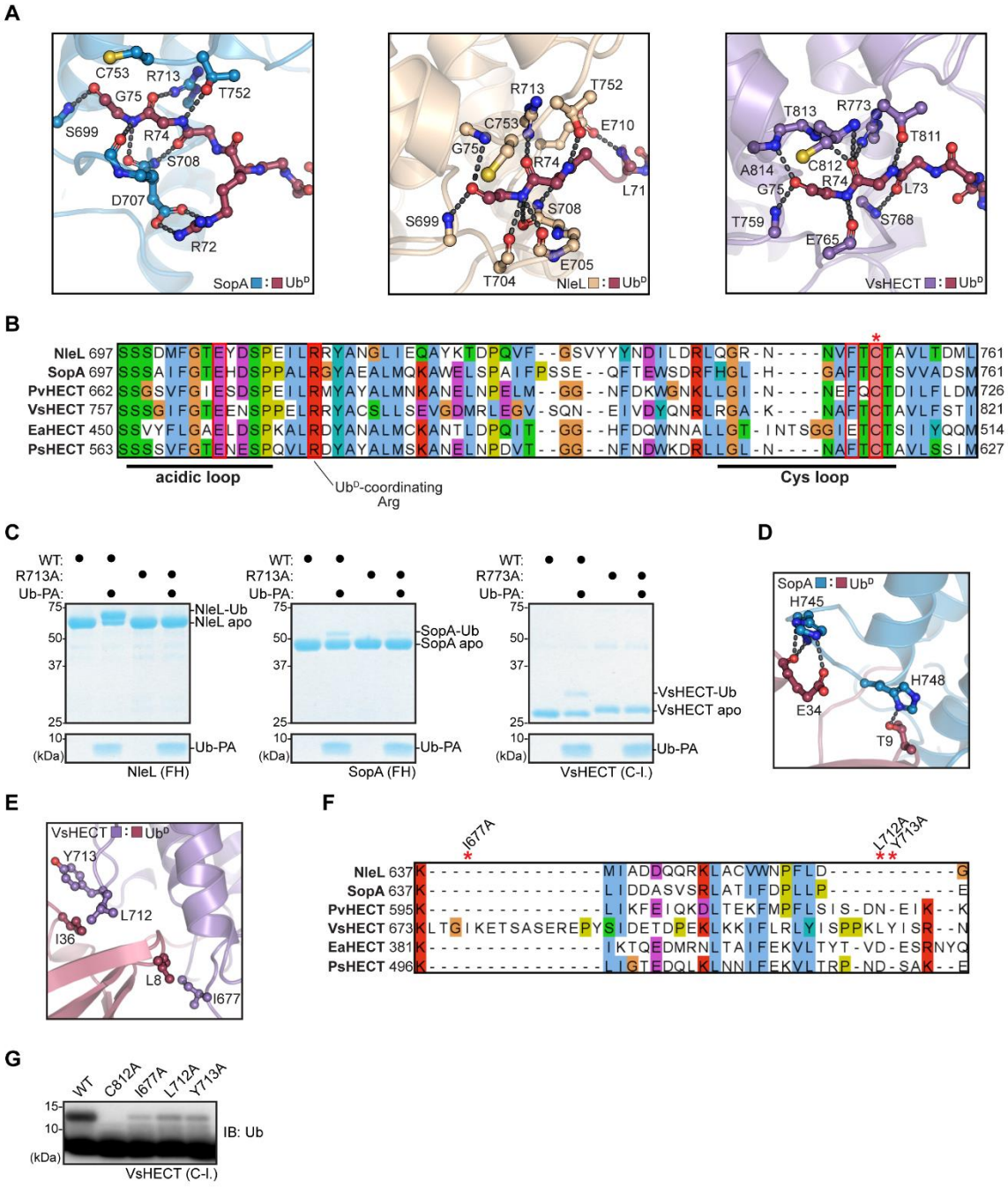
A
C753
R713
G75
T752
S699
R74
S708
D707
R72
SopA : Ub^D
R713
T752
C753
E710
G75
R74
L71
S699
S708
E705
T704
NleL : Ub^D
T813
R773
T811
A814
C812
R74
G75
L73
T759
S768
E765
VsHECT : Ub^D
B
NleL 697 SSSDMFGTEYDSPEILRRYANGLIEQAYKTDPQVF--GSVYYYNDILDRLQGR-N----NVFTCTAVLTDML 761
SopA 697 SSSAIFGTEHDSPPALRGYAEALMQKAWELSPAIFPSSE--QFTEWSDRFHGL-H----GAFTCTSVVADSM 761
PvHECT 662 SSGSVFGIESDSPEILRMYAYALMNKANELNPELM--GG--NFDKWGNKLLGI-N----NEFQCTDILFLDM 726
VsHECT 757 SSSGIFGTEENSPPELRRYACSLLSEVGDMRLEGV-SQN--EIVDYQNRLRGA-K----NAFTCTAVLFSTI 821
EaHECT 450 SSVYFLGAELDSPKALRDYANALMCKANTLDPQIT--GG--HFDQWNNALLGT-INTSGGIETCTSIIYQQM 514
PsHECT 563 SSSSVFGTENESPQVLRDYAYALMSKANELNPDVT--GG--NFNDWKDRLLGL-N----NAFTCTAVLSSIM 627
acidic loop
Ub^D-coordinating Arg
Cys loop
C
WT:
R713A:
Ub-PA:
75
50
37
25
10
(kDa)
NleL-Ub
NleL apo
Ub-PA
NleL (FH)
SopA-Ub
SopA apo
SopA (FH)
R773A:
VsHECT-Ub
VsHECT apo
VsHECT (C-I.)
D
SopA : Ub^D
H745
H748
E34
T9
E
VsHECT : Ub^D
Y713
L712
I36
L8
I677
F
I677A
L712A
Y713A
NleL 637K----------MIADDQQRKLACVWNPFLD----------G
SopA 637K----------LIDDASVSRLATIFDPLLP----------E
PvHECT 595K----------LIKFEIQKDLTEKFMPFLSIS-DN-EIK--K
VsHECT 673KLTGIKETSASEREPYSIDETDPEKLKKIFLRLYISPPKLYISR--N
EaHECT 381K----------IKTQEDMRNLTAIFEKVLTYT-VD-ESRNYQ
PsHECT 496K----------LIGTEDQLKLNNIFEKVLTRP-ND-SAK--E
G
WT
C812A
I677A
L712A
Y713A
15
10
(kDa)
IB: Ub
VsHECT (C-I.)

Figure 3.6 bHECT activation of donor Ub (II/II)

A. Structures of SopA-Ub^{D}, NleL-Ub^{D}, and VsHECT-Ub^{D}, focusing on the hydrogen bonding networks established between the C-lobe and Ub^{D}. Hydrogen bonds are shown with black dashes. **B**. Multiple sequence alignment (MSA) of the bHECTs, focused on the C-lobe. The sequences of the acidic loops and Cys loops are highlighted. Asterisks and red boxes are used to indicated the conserved Ub^{D}-coordinating Arg residue, the acidic loop Glu residue, the partially-conserved Cys loop Phe residue, and the conserved active site Cys. **C**. Gel-based Ub-PA reactivity assay with WT or the Ub^{D}-coordinating Arg-to-Ala mutant for the full HECT (FH) domain NleL, FH domain SopA, and C-lobe domain (C-l) of VsHECT. 5 μM of bHECTs were reacted with 10 μM Ub-PA for 2 hr at 22 °C. Reactions were quenched and resolved by SDS-PAGE with Coomassie staining. **D**. Structure of SopA-Ub^{D}, highlighting the unique interactions observed at the C-lobe:Ub^{D} interface. **E**. Structure of VsHECT-Ub^{D}, highlighting the unique interactions observed at the C-lobe:Ub^{D} interface. **F**. MSA of the bHECTs, highlighting the sequence insertion that partially mediates the unique Ub^{D} interactions observed in the VsHECT C-lobe shown in E. VsHECT residues I677, I712, and Y713 from E are marked with red asterisks. **G**. Gel-based Ub ligase assay for WT VsHECT and structure-guided mutants as monitored by formation of diUb. Reactions were quenched, resolved by SDS-PAGE, and visualized by anti-Ub Western blot.

part by a unique insertion near the beginning of the C-lobe (**Fig. 3.6E-F**). Mutation of residues contacting either patch greatly reduced the ability of VsHECT to synthesize diUb (**Fig. 3.6G**). Altogether, while contacts at or near the Ub^D C-terminus are conserved and functionally required, additional contacts outside of the active site make important contributions to bHECT ligase activity as well.

Across all three bHECT-Ub^D structures, the Ub^D C-terminal tail was sandwiched between two loops: a "Cys loop" with a conserved Phe that precedes the active site Cys, and an "acidic loop", which contains a conserved Glu residue previously proposed to play a catalytic role as a general base (**Fig. 3.3C-E, 3.5G-H, 3.6B**)[50]. Relative to the apo structures, the Cys loops of both NleL and SopA undergo a substantial rearrangement upon linkage to Ub^D (**Fig. 3.5G-H**). The Cys loops of apo bHECTs adopt an outward conformation, away from α-helices 5 and 6, while in all three Ub^D-bound structures, the Cys loops tuck inward. This 12.5 Å and 9.6 Å rearrangement in NleL and SopA, respectively, coincide with rearrangements of the Ub^D-coordinating Arg that position it to contact both the Ub^D C-terminus and the Cys loop backbone. The Glu residue of the acidic loop also adopts a conformation closer to the active site in the Ub^D-bound structures (**Fig. 3.5G-H**).

Considering their conformational changes upon Ub^D binding, we assessed the importance of the Cys loop and acidic loop on bHECT ligase function. Within the NleL Cys loop, an F751A mutation greatly reduced ligase activity, whereas an E705A mutation within the acidic loop actually yielded a higher final FP value (**Fig. 3.5C**). Using a gel-based readout,

NleL E705A produced a higher molecular weight polyUb smear relative to WT (**Fig. 3.5D**), which may explain the higher FP value. Interestingly, in the case of SopA, the equivalent E705A mutation dramatically reduced activity (**Fig. 3.5E-F**). Thus, Cys loop and acidic loop residues play important roles in bHECT ligase activity, but their precise functions were unclear from the bHECT-Ub^{D} structures alone.

Model of E2-bHECT transthiolation

Overlaying our NleL-Ub^{D} structure with a previously reported UBE2L3:NleL structure produced a sensible model for an E2:NleL~Ub intermediate that occurs immediately following transthiolation of Ub to the E3, and before E2 dissociation (**Fig. 3.7A**)[50]. In this model, the orientation of E2 and Ub resemble a "backbent" conformation, previously observed among certain isolated E2~Ub conjugates[146–150]. At the interface of the reported NleL:UBE2L3 structure, we noted poor electron density for UBE2L3 side chains in Loop 8, and a complete lack of electron density for the NleL Cys loop (**Fig. 3.8A**). In contrast, the NleL-Ub^{D} and NleL apo (as well as SopA-Ub^{D} and SopA apo) structures resolve the Cys loop in inward and outward conformations (**Fig. 3.5G-H, 3.8B-C**), suggesting higher mobility in the E2:NleL complex.

To verify our E2:NleL:Ub model in solution, we utilized NMR as a highly sensitive approach for studying transient protein interactions. We elected to study interactions with the well-characterized E2 UBE2D3, which is active with bHECTs[15,17] and exhibits a high degree of structural homology to UBE2L3 (**Fig. 3.8A**)[17]. We generated stable, monomeric UBE2D3-O-Ub conjugate by incorporating the UBE2D3 active site C85S mutation as well

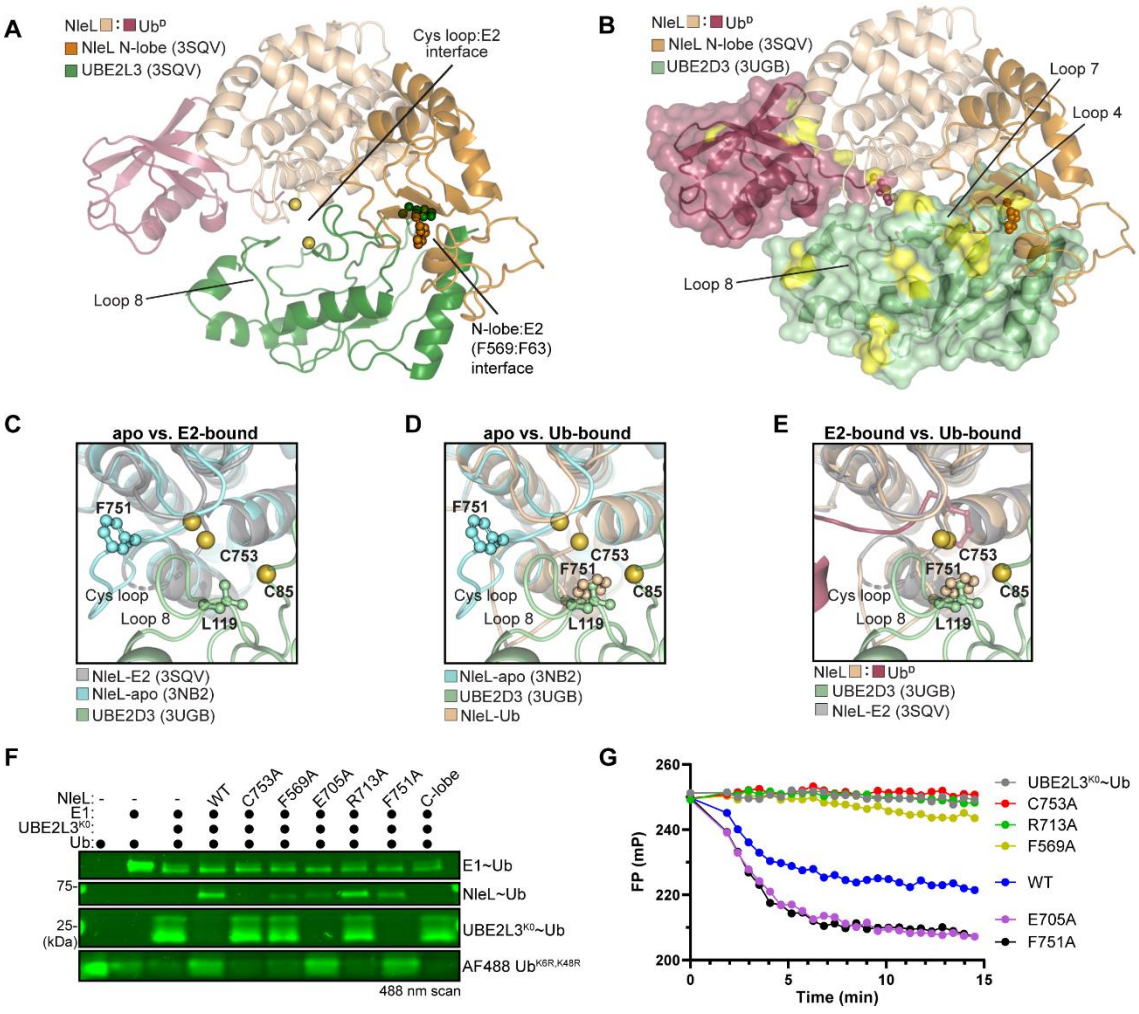
A
NleL : Ub^D
NleL N-lobe (3SQV)
UBE2L3 (3SQV)
Cys loop:E2 interface
Loop 8
N-lobe:E2 (F569:F63) interface
B
NleL : Ub^D
NleL N-lobe (3SQV)
UBE2D3 (3UGB)
Loop 7
Loop 4
Loop 8
C
apo vs. E2-bound
F751
C753
C85
Cys loop
Loop 8
L119
NleL-E2 (3SQV)
NleL-apo (3NB2)
UBE2D3 (3UGB)
D
apo vs. Ub-bound
F751
C753
F751
C85
Cys loop
Loop 8
L119
NleL-apo (3NB2)
UBE2D3 (3UGB)
NleL-Ub
E
E2-bound vs. Ub-bound
C753
F751
C85
Cys loop
Loop 8
L119
NleL : Ub^D
UBE2D3 (3UGB)
NleL-E2 (3SQV)
F
NleL: - - - WT C753A F569A E705A R713A F751A C-lobe
E1:
UBE2L3^K0:
Ub:
E1~Ub
75-
NleL~Ub
25-
(kDa)
UBE2L3^K0~Ub
AF488 Ub^K6R,K48R
488 nm scan
G
FP (mP)
260
240
220
200
0
5
10
15
Time (min)
UBE2L3^K0~Ub
C753A
R713A
F569A
WT
E705A
F751A

Figure 3.7 Model for E2-bHECT transthiolation (I/II)

A. View of NleL-Ub^{D} and NleL:UBE2L3 (PDB: 3SQV) overlaid structures, representing a model of the E2:NleL~Ub intermediate. The conserved Phe residues at the E2:N-lobe interface are shown in ball-and-sticks, and the active site Cys residues for both NleL and UBE2L3 and shown as yellow spheres. **B**. Structural model of the UBE2D3:NleL~Ub complex with the significant peak intensity changes from Fig. 3.8D-E colored in yellow. **C**. View of NleL Cys loop at the E2 interface comparing apo (PDB: 3NB2) and E2-bound (PDB: 3SQV) structures. Note that the Cys loop could not be modeled in the E2-bound NleL structure and is shown as dashes. The active site Cys residues for NleL and UBE2L3 are shown as yellow spheres. **D**. As in C, for the apo NleL (PDB: 3NB2) and NleL-Ub^{D} structures, highlighting the clash between the inward NleL-Ub^{D} Cys-loop Phe and residue L119 of UBE2D3 in the model. **E**. As in C, for the E2-bound (PDB: 3SQV) and NleL-Ub^{D} structures, highlighting the position of Ub^{D} at the interface of the E2:NleL~Ub^{D} model. **F**. Gel-based transthiolation assay using Lys-less $UBE2L3^{K0}$ and an N-terminally labeled Alexa 488 $Ub^{K6,K48R}$ substrate that prevents NleL from forming polyUb chains. EDTA was added after E2~Ub formation to prevent recycling of the Ub, and samples were quenched in non-reducing sample buffer after a 30-second reaction. Slices of Ub, E1~Ub, $UBE2L3^{K0}$~Ub, and NleL~Ub (WT or mutant) from the same gel are shown for clarity. **G**. E2~Ub discharge assay monitored by UbiReal. N-terminally labeled Alexa 488 $Ub^{K6,K48R}$ and $UBE2L3^{K0}$ were used to generate an E2~Ub conjugate, at which point EDTA was added and NleL-dependent discharge was monitored.

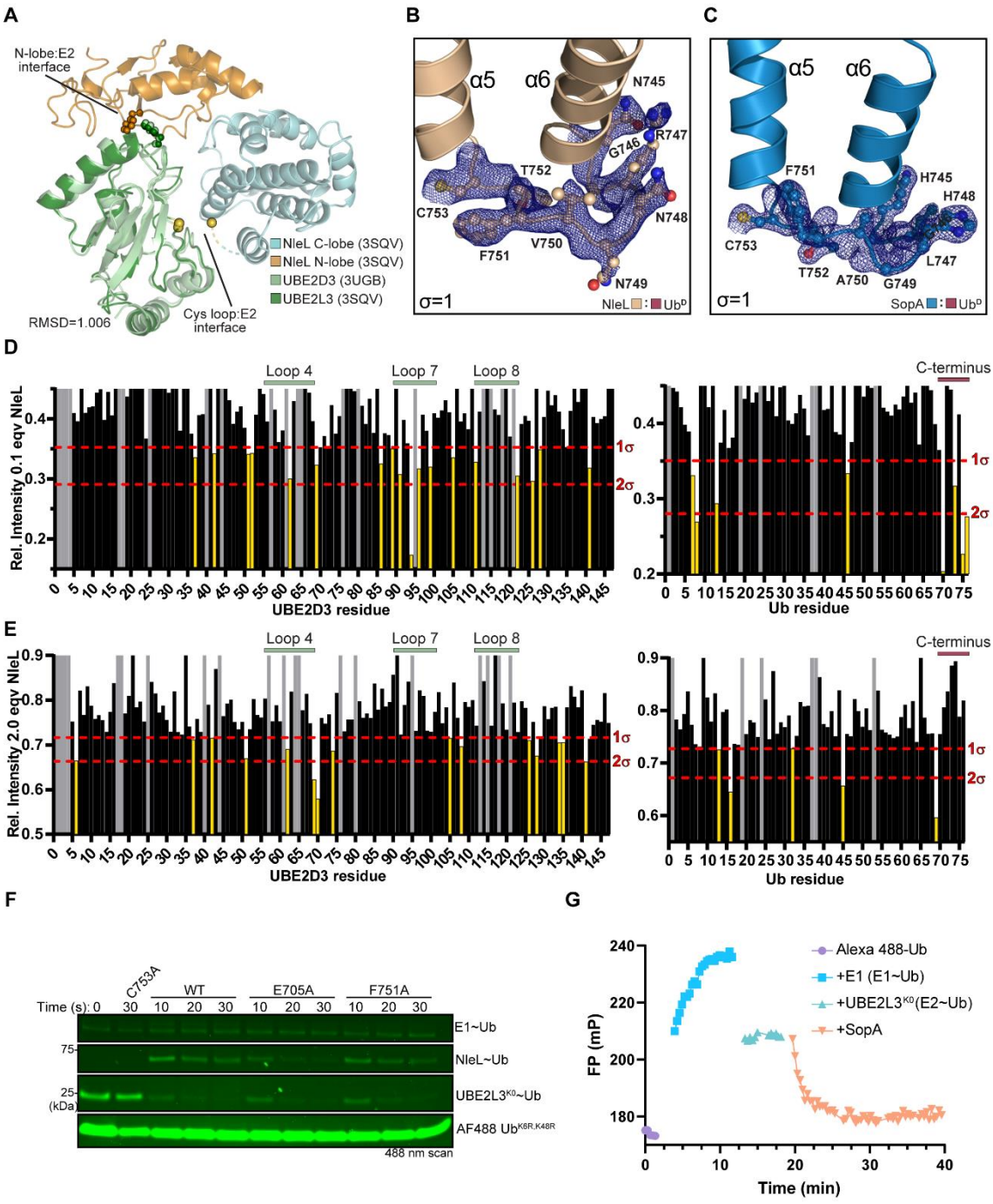
A
N-lobe:E2 interface
NleL C-lobe (3SQV)
NleL N-lobe (3SQV)
UBE2D3 (3UGB)
UBE2L3 (3SQV)
RMSD=1.006
Cys loop:E2 interface
B
α5
α6
N745
R747
G746
T752
C753
N748
F751
V750
N749
σ=1
NleL : Ubᴰ
C
α5
α6
F751
H745
H748
C753
T752
A750
G749
L747
σ=1
SopA : Ubᴰ
D
Loop 4
Loop 7
Loop 8
Rel. Intensity 0.1 eqv NleL
1σ
2σ
UBE2D3 residue
C-terminus
Ub residue
E
Loop 4
Loop 7
Loop 8
Rel. Intensity 2.0 eqv NleL
1σ
2σ
UBE2D3 residue
C-terminus
Ub residue
F
C753A
WT
E705A
F751A
Time (s): 0 30 10 20 30 10 20 30 10 20 30
E1~Ub
NleL~Ub
UBE2L3ᴷ⁰~Ub
AF488 Ubᴷᴳᴿ,ᴷ⁴⁸ᴿ
75-
25-
(kDa)
488 nm scan
G
Alexa 488-Ub
+E1 (E1~Ub)
+UBE2L3ᴷ⁰(E2~Ub)
+SopA
FP (mP)
Time (min)

Figure 3.8 Model for E2-bHECT transthiolation (II/II)

A. The NleL-Ub^{D} and NleL:UBE2L3 (PDB: 3SQV) overlay, representing a model of the E2:NleL~Ub intermediate, overlayed with a UBE2D3 structure (PDB: 3UGB) to highlight the similarity when using either E2. UBE2D3 was aligned onto UBE2L3 (Cα RMSD=1.006Å). The E2:Cys loop and E2:N-lobe interfaces are highlighted, with the conserved Phe residues mediating the interaction between E2 and NleL N-lobe shown as sticks, and the active site Cys residues for both NleL and UBE2L3/UBE2D3 shown as yellow spheres. **B**. 2|Fo-Fc| electron density for the entire Cys loop in the NleL-Ub^{D} structure at 1σ. Residues on the Cys loop are indicated, as well as the α-helix numbers. **C**. As in B, for the SopA-Ub^{D} structure. **D**. Histogram of relative peak intensities for UBE2D3 and Ub resonances from 1H,15N-TROSY spectra of 15N-labeled UBE2D3-O-Ub conjugate, following titration of 0.1 molar equivalencies (eqv) of NleL (residues 170-782) containing the catalytic C753A mutation. Peak intensities are relative to 15N-labeled UBE2D3-O-Ub conjugate alone. Grey bars indicate unassigned or Pro residues. Yellow bars indicate relative intensity changes greater than one standard deviation from the mean. The locations of UBE2D3 loops 4, 7, and 8, as well as the Ub C-terminus, are indicated with horizontal bars. **E**. Histogram of relative peak intensities for UBE2D3 and Ub resonances from 1H,15N-TROSY spectra of 15N-labeled UBE2D3-O-Ub conjugate, following titration of 2.0 molar equivalencies (eqv) of NleL C-lobe (residues 606-782) with the C753A mutation. Peak intensities are relative to 15N-labeled UBE2D3-O-Ub conjugate alone. Grey bars indicate unassigned or Pro residues. Yellow bars indicate relative intensity changes greater than one standard deviation from the mean. The locations of UBE2D3 loops 4, 7, and 8, as well as the Ub C-terminus, are indicated with horizontal bars. **F**. Gel-based transthiolation assay using $UBE2L3^{K0}$ and an N-terminally labeled Alexa 488 $Ub^{K6,K48R}$ substrate that prevents NleL from forming polyUb chains. EDTA was added after E2~Ub formation to prevent recycling of the Ub. Slices of Ub, E1~Ub, $UBE2L3^{K0}$~Ub, and NleL~Ub (WT or mutant) from the same gel are shown for clarity. Samples were quenched in non-reducing sample buffer after reacting with the $UBE2L3^{K0}$~Ub for the indicated times at 4 °C, resolved by SDS-PAGE, and scanned at 488 nm. **G**. Validation of the E2~Ub FP discharge assay. FP values of Alexa 488-labeled $Ub^{K6R, K48R}$ change relative to molecular weight as E1 is added to form E1~Ub, $UBE3L3^{K0}$ is added to form $UBE3L3^{K0}$~Ub, and SopA is added resulting in E2~Ub discharge to free Ub via a transient E3~Ub intermediate.

as the 'backside' S22R mutation[151]. $^{1}H,^{15}N$-TROSY spectra of ^{15}N-labeled UBE2D3-O-Ub upon titration of either the NleL C-lobe alone or the full HECT-like domain revealed the interaction to be in the intermediate exchange regime, resulting in selective peak broadening and intensity loss. Analysis of peak intensity changes allowed identification of specific E2~Ub residues involved in binding to NleL (**Fig. 3.8D-E**). These residues were mapped onto UBE2D3 and Ub within the NleL complex (**Fig. 3.7B**), highlighting consistencies with our model. The resonance corresponding to F62, the UBE2D3 residue in Loop 4 critical for interaction with the NleL N-lobe, broadened significantly with titration of both the full NleL HECT-like domain and the isolated C-lobe (**Fig. 3.7B, 3.8D-E**). In our model, the NleL C-lobe does approach UBE2D3 underneath Loop 4, and the aromatic nature of F62 might make it particularly sensitive to reporting on this interaction. In contrast, significant peak broadening was observed for Loop 7 (residues 90-95) of UBE2D3 only in the presence of the N-lobe, which can be explained in our model by contacts from an NleL loop downstream of the conserved F569. Significant peak broadening within the Ub C-terminal tail was also observed with titration of the full HECT-like domain, consistent with contacts to the NleL C-lobe prior to transthiolation (**Fig. 3.7B, 3.8D**).

Based upon our model for Ub transthiolation, the outward Cys loop conformation of the apo NleL structure faces away from the E2 interface (**Fig. 3.5G, 3.7C**). Upon Ub^{D} binding and Cys loop rearrangement to the inward conformation, the Cys loop, and F751 in particular, would clash with Loop 8 of UBE2D3 (**Fig. 3.7D**). However, the Ub^{D} itself doesn't appear to clash at the NleL Cys loop:E2 interface (**Fig. 3.7E**). These observations

suggest a model where the Cys loop rearrangement to the well-ordered inward conformation following Ub transthiolation may result in steric clashes that help to dissociate the C-lobe from the E2, though not necessarily affecting interactions with the N-lobe. This would be consistent with the two different C-lobe conformations that are observed between the apo and E2-bound NleL structures[17,50].

Since important residues in the Cys loop and acidic loop are located near the modeled E2:C-lobe interface, we sought to test whether their mutation impacted transthiolation from the E2 (e.g., discharging the E2~Ub bond to form E3~Ub or free Ub). We first generated an E2~Ub conjugate between Lys-less UBE2L3^{K0} (to prevent E2 ubiquitination), and a fluorescently-labeled Ub that contained K6R and K48R mutations (to prevent polyUb chain formation). NleL WT completely discharged the E2~Ub conjugate to generate E3~Ub or free Ub, while the catalytically inactive NleL C753A failed to do so (**Fig. 3.7F**). This indicated that E2~Ub discharge was dependent on transthiolation to the NleL active site Cys, and that any released Ub from the reaction was a result of discharge from the E3~Ub intermediate. An isolated C-lobe construct or incorporation of an F569A mutation within the N-lobe E2-binding site eliminated E2~Ub discharge. Consistent with a role in activating the Ub^{D} C-terminus (**Fig. 3.5B**), the NleL R713A mutant could still receive Ub from the E2 but was inefficient at discharging it. For both the Cys loop mutant F751A and the acidic loop mutant E705A, complete discharge of the E2~Ub conjugate was observed, primarily yielding free Ub. In contrast to NleL WT, the E3~Ub intermediate was only observed at very early timepoints (**Fig. 3.7F, 3.8F**). This indicated that E2~Ub transthiolation was not inhibited, and the resulting E3~Ub conjugate formed by these

mutants may be more labile toward hydrolysis. A modified FP-based UbiReal assay[138] corroborated these observations with better temporal resolution (**Fig. 3.8G**). Through monitoring fluorescent Ub incorporated into an E2~Ub conjugate, we observed that the E705A and F751A mutants produced lower FP values, matching results from the gel-based assays indicating a larger ratio of free Ub to E3~Ub intermediate as compared to WT (**Fig. 3.7G**).

NleL coordination of K48 acceptor Ub

Previous work has shown that some eHECT C-lobes can be swapped to alter polyUb

During our analysis of the NleL-Ub^D structure, we observed close crystal contacts between NleL-Ub^D active sites and Ub K48 from neighboring molecules, representing a potential acceptor Ub, Ub^A (**Fig. 3.9A-B, 3.10A**). NleL produces a mixture of K6- and K48-linked polyUb[17,57,152], but whether this specificity is retained within the crystallized C-lobe construct was not known. From a K-only panel of Ub mutants, in which all Lys residues but one are mutated to Arg, the NleL C-lobe construct preferentially generated K6- and K48-linked polyUb[20,35] (**Fig. 3.10B**). The specificity of the SopA C-lobe construct toward K48-linked polyUb, as previously established[26], also mimicked the full HECT-like domain[26] (**Fig. 3.10C**), indicating that bHECT C-lobes represent a minimal unit for polyUb specificity. Thus, in our structure of the NleL-Ub^D intermediate, we fortuitously captured a snapshot of K48-linked polyUb ligation.

In addition to K48 approaching the NleL active site, we observed several other notable contacts at the NleL:Ub^A interface. Residue F751 of the NleL Cys loop, positioned in the

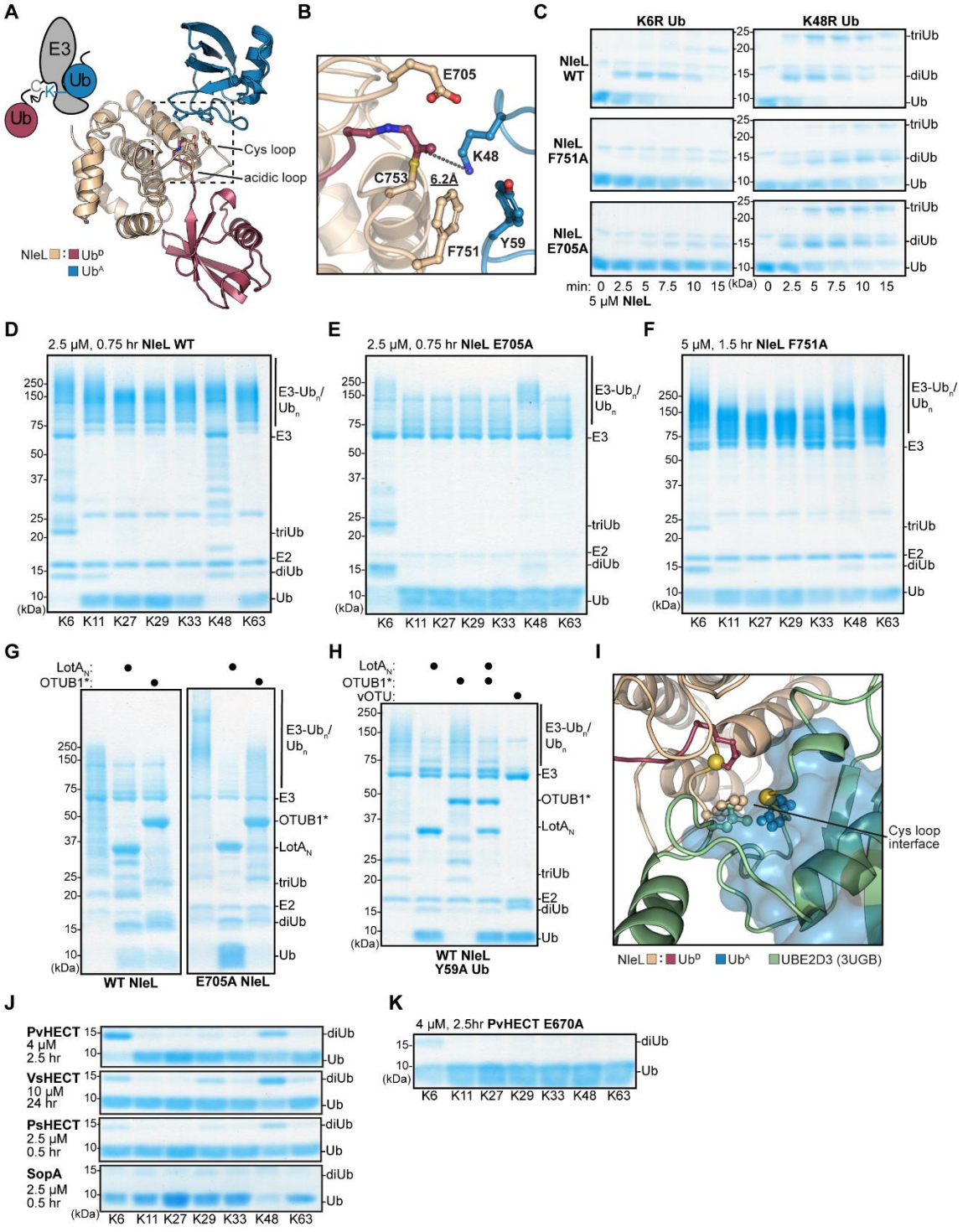
A
E3
Ub
Ub
Cys loop
acidic loop
NleL : Ub^D
Ub^A
B
E705
K48
C753
6.2Å
F751
Y59
C
K6R Ub
K48R Ub
NleL WT
NleL F751A
NleL E705A
triUb
diUb
Ub
min: 0 2.5 5 7.5 10 15 (kDa) 0 2.5 5 7.5 10 15
5 μM NleL
D
2.5 μM, 0.75 hr NleL WT
E
2.5 μM, 0.75 hr NleL E705A
F
5 μM, 1.5 hr NleL F751A
E3-Ub_n/Ub_n
E3
triUb
E2
diUb
Ub
(kDa)
K6 K11 K27 K29 K33 K48 K63
G
LotA_N:
OTUB1*:
E3-Ub_n/Ub_n
E3
OTUB1*
LotA_N
triUb
E2
diUb
Ub
WT NleL
E705A NleL
H
LotA_N:
OTUB1*:
vOTU:
WT NleL
Y59A Ub
I
Cys loop interface
NleL : Ub^D Ub^A UBE2D3 (3UGB)
J
PvHECT 4 μM 2.5 hr
VsHECT 10 μM 24 hr
PsHECT 2.5 μM 0.5 hr
SopA 2.5 μM 0.5 hr
diUb
Ub
K
4 μM, 2.5hr PvHECT E670A

Figure 3.9 bHECT coordination of K48 acceptor Ub (I/II)

A. View of the Ub^A:NleL-Ub^D interface observed through crystal symmetry, with key residues highlighted. **B**. Zoomed-in view of the Ub^A:NleL-Ub^D interface shown in A, with key residues highlighted. The distance between the ε-amino group of K48 and the Ub^D C-terminus is shown. **C**. Gel-based assay monitoring the consumption of K6R or K48R Ub by NleL WT, F751A, and E705A. **D**. Gel-based polyUb specificity assay for NleL WT using the panel of K-only Ub mutants, each containing only the single Lys indicated with all others mutated to Arg. **E**. As in D, for the NleL E705A mutant. **F**. As in D, for the NleL F751A mutant. **G**. UbiCRest assay monitoring the cleavage of polyUb generated by NleL WT or E705A using K6-specific $LotA_N$ and K48-specific OTUB1*. **H**. As in G, for polyUb generated by NleL WT with Ub Y59A. The nonspecific DUB vOTU is used as a positive control for comparison. **I**. Structural overlay showing overlap of the Ub^A- and UBE2D3-binding sites on the NleL C-lobe. **J**. As in D for PvHECT, VsHECT, PsHECT, and SopA. Only the monoUb and diUb region of the gels are shown for ease of comparison. **K**. As in D for the PvHECT E670A acidic loop mutant.

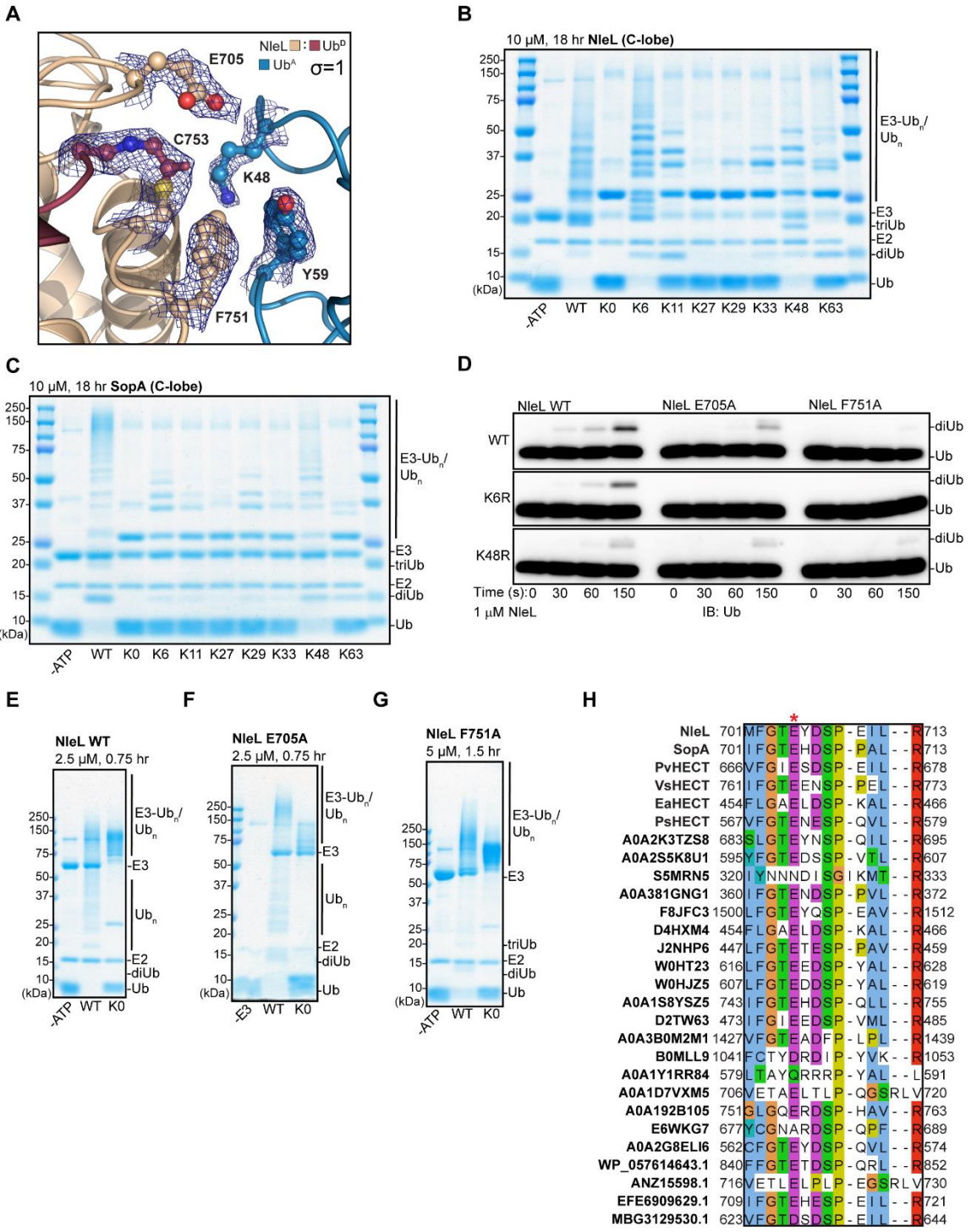
A
NleL: UbD
UbA
σ=1
E705
C753
K48
Y59
F751
B
10 μM, 18 hr NleL (C-lobe)
250
150
75
50
37
25
20
15
10
(kDa)
E3-Ubn/
Ubn
E3
triUb
E2
diUb
Ub
-ATP
WT
K0
K6
K11
K27
K29
K33
K48
K63
C
10 μM, 18 hr SopA (C-lobe)
D
NleL WT
NleL E705A
NleL F751A
WT
K6R
K48R
diUb
Ub
Time (s):0 30 60 150 0 30 60 150 0 30 60 150
1 μM NleL
IB: Ub
E
NleL WT
2.5 μM, 0.75 hr
F
NleL E705A
2.5 μM, 0.75 hr
G
NleL F751A
5 μM, 1.5 hr
H
NleL 701MFGTEYDSP-EIL--R713
SopA 701IFGTEHDSP-PAL--R713
PvHECT 666VFGIESDSP-EIL--R678
VsHECT 761IFGTEENSP-PEL--R773
EaHECT 454FLGAELDSP-KAL--R466
PsHECT 567VFGTENESP-QVL--R579
A0A2K3TZS8 683SLGTEYNSP-QIL--R695
A0A2S5K8U1 595YFGTEDSSP-VTL--R607
S5MRN5 320IYNNNDISGIKMT--R333
A0A381GNG1 360IFGTENDSP-PVL--R372
F8JFC3 1500LFGTEYQSP-EAV--R1512
D4HXM4 454FLGAELDSP-KAL--R466
J2NHP6 447LFGTETESP-PAV--R459
W0HT23 616LFGTEEDSP-YAL--R628
W0HJZ5 607LFGTEDDSP-YAL--R619
A0A1S8YSZ5 743IFGTEHDSP-QLL--R755
D2TW63 473IFGIEEDSP-VML--R485
A0A3B0M2M1 1427VFGTEADFP-LPL--R1439
B0MLL9 1041FCTYDRDIP-YVK--R1053
A0A1Y1RR84 579LTAYQRRRP-YAL--L591
A0A1D7VXM5 706VETAELTLP-QGSRLV720
A0A192B105 751GLGQERDSP-HAV--R763
E6WKG7 677YCGNARDSP-QPF--R689
A0A2G8ELI6 562CFGTEYDSP-QVL--R574
WP_057614643.1 840FFGTETDSP-QRL--R852
ANZ15598.1 716VETLELPLP-EGSRLV730
EFE6909629.1 709IFGTEHESP-EIL--R721
MBG3129530.1 623VFGTDSDSP-EIL--R644

Figure 3.10 bHECT coordination of K48 acceptor Ub (II/II)

A. 2|Fo-Fc| electron density for key interactions at the Ub^A:NleL-Ub^D interface, shown at 1σ. Acidic loop residue E705, Cys loop residues C753 and F751, and Ub^A residues K48 and Y59 are shown. **B**. Gel-based polyUb specificity assay for the NleL C-lobe, using the panel of K-only Ub mutants. Reactions were quenched and resolved by SDS-PAGE with Coomassie staining. **C**. As in B, for the SopA C-lobe. **D**. Gel-based ligase assay monitoring consumption of WT, K6R, or K48R Ub by NleL WT or mutants, as in Fig. 5D. Visualized by anti-Ub Western blot. **E**. Gel-based ligation assay for NleL WT, from the same assay as Fig. 5D, using WT or Lys-less (K0) Ub. Reactions were quenched and resolved by SDS-PAGE with Coomassie staining. **F**. Gel-based ligation assay for NleL E705A, from the same assay as Fig. 5E, using WT or K0 Ub. Reactions were quenched and resolved by SDS-PAGE with Coomassie staining. **G**. Gel-based ligation assay for NleL F751A, from the same assay as Fig. 5F, using WT or K0 Ub. Reactions were quenched and resolved by SDS-PAGE with Coomassie staining. **H**. Multiple sequence alignment of bHECTs NleL, SopA, PvHECT, VsHECT, EaHECT, and PsHECT with the unvalidated bHECT candidates from Table 3.2, showing the area of the acidic loop. A red asterisk is used to indicate the location of E705 in NleL.

inward conformation (**Fig. 3.5G**), forms a hydrophobic interface with Y59 of the Ub^A (**Fig. 3.9B**). Acidic loop residue E705, observed to approach the active site upon Ub^D conjugation (**Fig. 3.5G**), is also near the NleL:Ub^A interface (**Fig. 3.9B**). Since only the F751A mutant affected total ligase activity and neither mutant affected E2 transthiolation (**Fig. 3.5C-F, 3.7F-G** and **Fig. 3.8F**), we tested if these residues were involved in K48-specific polyUb ligation. While NleL WT consumed K6R or K48R Ub substrates at equal rates, producing K48- and K6-linked polyUb, respectively, both the F751A and E705A mutants greatly preferred the K48R substrate, and were very slow to produce any polyUb products with the K6R substrate (**Fig. 3.9C, 3.10D**). The F751A mutant was markedly slower than WT to produce polyUb with the K48R substrate, suggesting that this region of the NleL Cys loop may also play a role in K6-linked polyUb assembly. Remarkably, the E705A mutation severely abrogated the ability of NleL to generate K48-linked polyUb, rendering it largely specific for K6 polyUb (**Fig. 3.9D-E, 3.10D**). The F751A mutation also inhibited K48-linked polyUb ligation, though total Ub ligation was also impaired (**Fig. 3.9F**). However, some auto-ubiquitination activity was retained with the K48-only mutant, compared to a Lys-less Ub K0 mutant control (**Fig. 3.10E-G**).

PolyUb specificity with a native Ub substrate was validated using UbiCRest, an assay that uses linkage-specific deubiquitinating enzymes (DUBs) to determine the types of polyUb linkages present in a sample[104]. To diagnose bHECT specificity, we utilized the K6-specific $LotA_N$ from *Legionella pneumophila*[41,153], and the optimized human K48-specific OTUB1*[111]. PolyUb chains generated by WT NleL were cleaved equally well by both $LotA_N$ and OTUB1*, yielding similar amounts of released monoUb (**Fig. 3.9G**). However,

polyUb chains generated by NleL E705A were more robustly cleaved by $LotA_N$ (**Fig. 3.9G**). Consistent with a role in K48-linked polyUb ligation, a SopA E705A mutant showed a substantial defect in total ubiquitination, likely because it favors just the single polyUb linkage type (**Fig. 3.5E-F, 3.10C**). Testing the reciprocal side of the NleL:Ub^A interface, incorporation of a Ub Y59A mutation ablated the ability of WT NleL to produce K48-linked polyUb without affecting assembly of K6-linked polyUb (**Fig. 3.9H**). Interestingly, Y59 of Ub^A occupies a similar position as UBE2D3 L119 in the modeled UBE2D3:NleL~Ub complex, suggesting that the E2 must either dissociate from the N-lobe, or the C-lobe must rearrange to a new conformation in order to allow K48-linked polyUb ligation (**Fig. 3.9I**).

Since the polyUb specificity of NleL could be redirected with single point mutations, we examined if features of polyUb specificity were shared among bHECTs (**Fig. 3.1C**). Across the panel of bHECTs, there was an underlying trend to ligate K6- and K48-linked polyUb to varying extents (**Fig. 3.9J**). VsHECT and PsHECT appeared to prefer K48-linked polyUb ligation, though some other linkages were observed as well. Interestingly, PvHECT appeared to natively prefer K6 ligation, despite having the conserved Glu on the acidic loop and Phe on the Cys loop (**Fig. 3.9J, 3.6B**). Mutating the PvHECT acidic loop Glu residue, analogous to NleL E705, also inhibited formation of the residual K48 linkages, though overall ligase activity appeared to be impaired as well (**Fig. 3.9J-K**).

Rewiring bHECT polyUb specificity

Previous work has shown that some eHECT C-lobes can be swapped to alter polyUb

specificity[103]. Due to the conserved fold among bHECT C-lobes (**Fig. 3.3F**), and because bHECT polyUb specificity is fully encoded within the C-lobe (**Fig. 3.10B-C**), we hypothesized that replacing the C-lobe of SopA with that of NleL would rewire SopA's ligase activity (**Fig. 3.11A**). Using the K-only panel of Ub mutants, we observed that the SopA-NleL chimera (SNc) ligase was able to ligate both K6- and K48-linked polyUb, similar to NleL (**Fig. 3.11B**). Further, adding the E705A acidic loop mutation eliminated most K48 ligation, resulting in a SopA construct rewired for K6-linked polyUb (**Fig. 3.11B**).

Previous studies have demonstrated that the RING domains of host TRIM56 and TRIM65 are targets of SopA ubiquitination[26,58]. SopA and NleL both contain a β-helix domain upstream of their HECT-like domains, and this domain was shown to be the substrate-binding region in a crystal structure of the SopA:TRIM56 complex[26]. We used the SopA:TRIM56 structure, along with a previously published SopA structure and our SopA-Ub^D structure, to construct a model of SopA primed for Ub transfer onto TRIM56 (**Fig. 3.12A**). This model also appeared to be compatible with the C-lobe of NleL, representing the SNc bHECT chimera (**Fig. 3.11A**, **Fig. 3.12B**). Therefore, we hypothesized that the rewired SopA chimera could also modify TRIM56 with K6-linked polyUb. To test this, SopA WT or the rewired SNc E705A chimera were used in a ligation assay in the presence of the TRIM56 RING domain (residues 1-94), and then subjected to UbiCRest analysis with the linkage-specific DUBs $LotA_N$ and OTUB1*, or the nonspecific DUB vOTU (**Fig. 3.11C-D**)[104]. An additional reaction incorporated a Lys-less Ub mutant to produce multi-mono-ubiquitination of TRIM56, which would represent complete cleavage from the

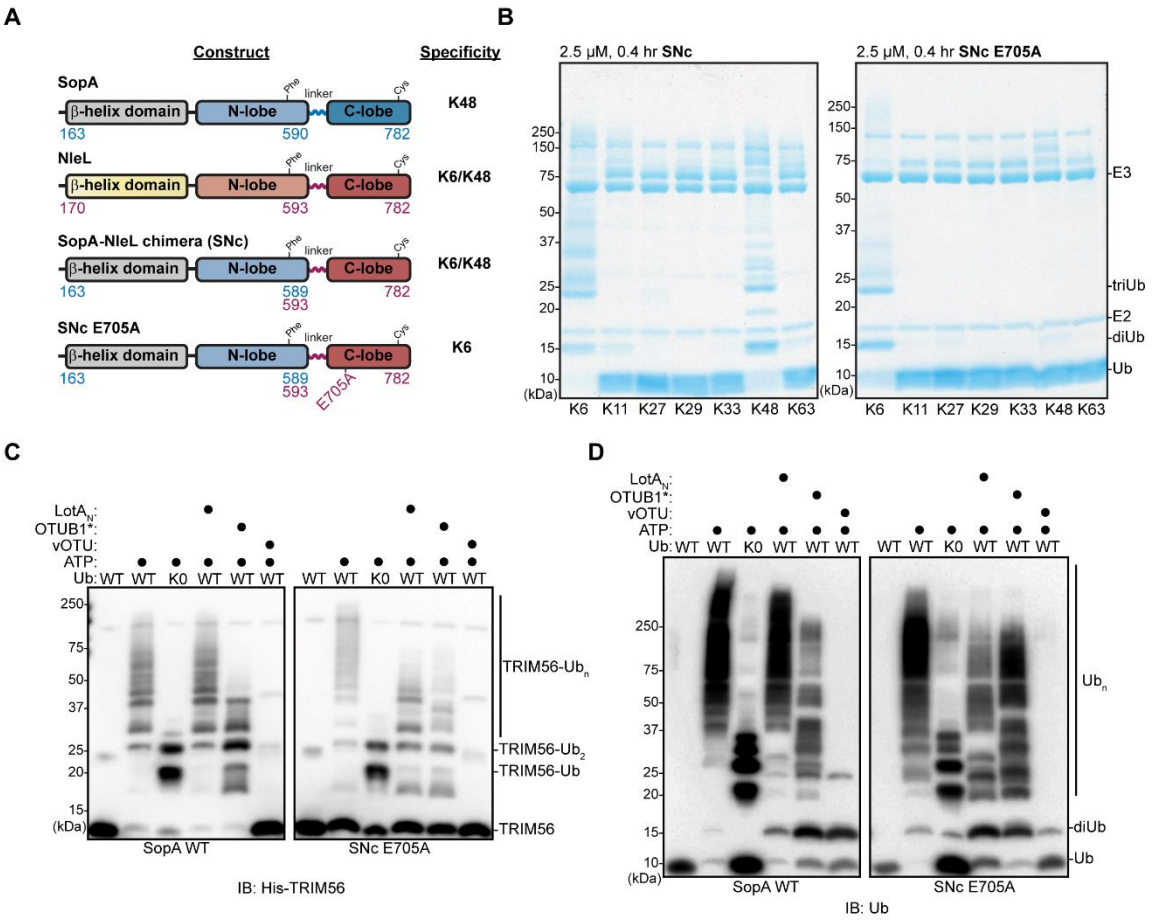

Figure 3.11 Rewiring bHECT polyUb specificity (I/II)

A. Schematics of SopA and NleL, and the rearrangements utilized to generate the SopA-NleL chimera (SNc) and SNc E705A constructs. Expected polyUb specificity of each construct is indicated. **B**. Gel-based polyUb specificity assay using the panel of K-only Ub mutants for the SNc chimera without (left) and with (right) the E705A acidic loop mutation. **C**. UbiCRest assay monitoring the cleavage of polyUb generated by SNc and SNc E705A with the TRIM56 substrate. Reactions with lysine-less (K0) Ub are used for comparison of mono-ubiquitinated TRIM56. Reactions were visualized by anti-TRIM56 Western blot. **D**. As in C, visualized by anti-Ub Western blot.

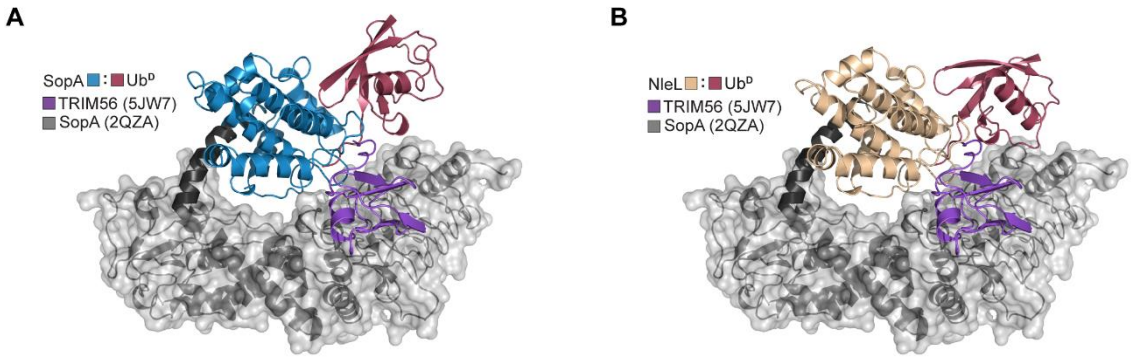

Figure 3.12 Rewiring bHECT polyUb specificity (II/II)

A. Structural overlay of the SopA-Ub^D, SopA:TRIM56 (PDB: 5JW7), and apo SopA (PDB: 2QZA) structures, modeling the SopA:TRIM56 ubiquitination complex. The model was generated by aligning the N-lobe portion of apo SopA with that of the SopA:TRIM56 structure, then aligning the SopA-Ub^D C-lobe to the C-lobe of apo SopA. The linker, C-lobe, Ub^D, and TRIM56 are shown as a cartoon representation, with the N-lobe and β-barrel domain shown as a surface representation. **B**. As in A, for the modeled SNc chimera. The model was generated as described in A, with the exception of aligning the NleL-Ub^D structure instead of SopA.

linkage-specific $LotA_N$ and OTUB1*. SopA robustly ubiquitinated TRIM56, as observed by Western blot against the TRIM56 substrate (**Fig. 3.11C**) and total Ub (**Fig. 3.11D**). The TRIM56 ubiquitination catalyzed by WT SopA was strongly collapsed by OTUB1* but not $LotA_N$ (**Fig. 3.11C-D**), consistent with SopA's established specificity for K48-linked polyUb (**Fig. 3.9J**). The SNc E705A chimera also ubiquitinated TRIM56, albeit somewhat less efficiently, suggesting that the bHECT C-lobe may play a minor role in substrate selection (**Fig. 3.11C-D**). However, the TRIM56 ubiquitination profile differed, as $LotA_N$ now showed increased cleavage of K6-linked polyUb (**Fig. 3.11C-D**). Some cleavage was also observed with OTUB1*, indicating that the chimera was not completely specific but still effective in rewiring SopA to append K6-linked polyUb onto the TRIM56 substrate.

HUWE1 acidic loop mutants show increased K6-linked polyUb ligation

The structural and biochemical work reported above illustrate clear roles for Cys loop

Though topologically different, the dual Cys loop and acidic loop architecture observed in bHECTs is also present in eHECTs (**Fig. 3.13A-B, 3.14A**). We hypothesized that a cryptic acidic loop may also be important for eHECT polyUb specificity. Aligning the Ub^D C-terminal tails across the HUWE1-Ub^D and the Ub^A:NleL-Ub^D structures placed the Ub^A in a plausible orientation for HUWE1-Ub^D ligation and highlighted the proximity to a putative acidic loop residue E4315 (**Fig. 3.14B**). As previous work indicated a reliance on the N-lobe for Ub recognition[124], we additionally searched outside the C-lobe for acidic loops, utilizing previously determined structures of the apo or Ub-bound HUWE1 HECT domain[124,126]. This revealed two additional potential acidic loops (**Fig. 3.13C, 3.14C**). In the HUWE1-Ub^D structure, which captures the "L"-conformation of the HECT domain, an

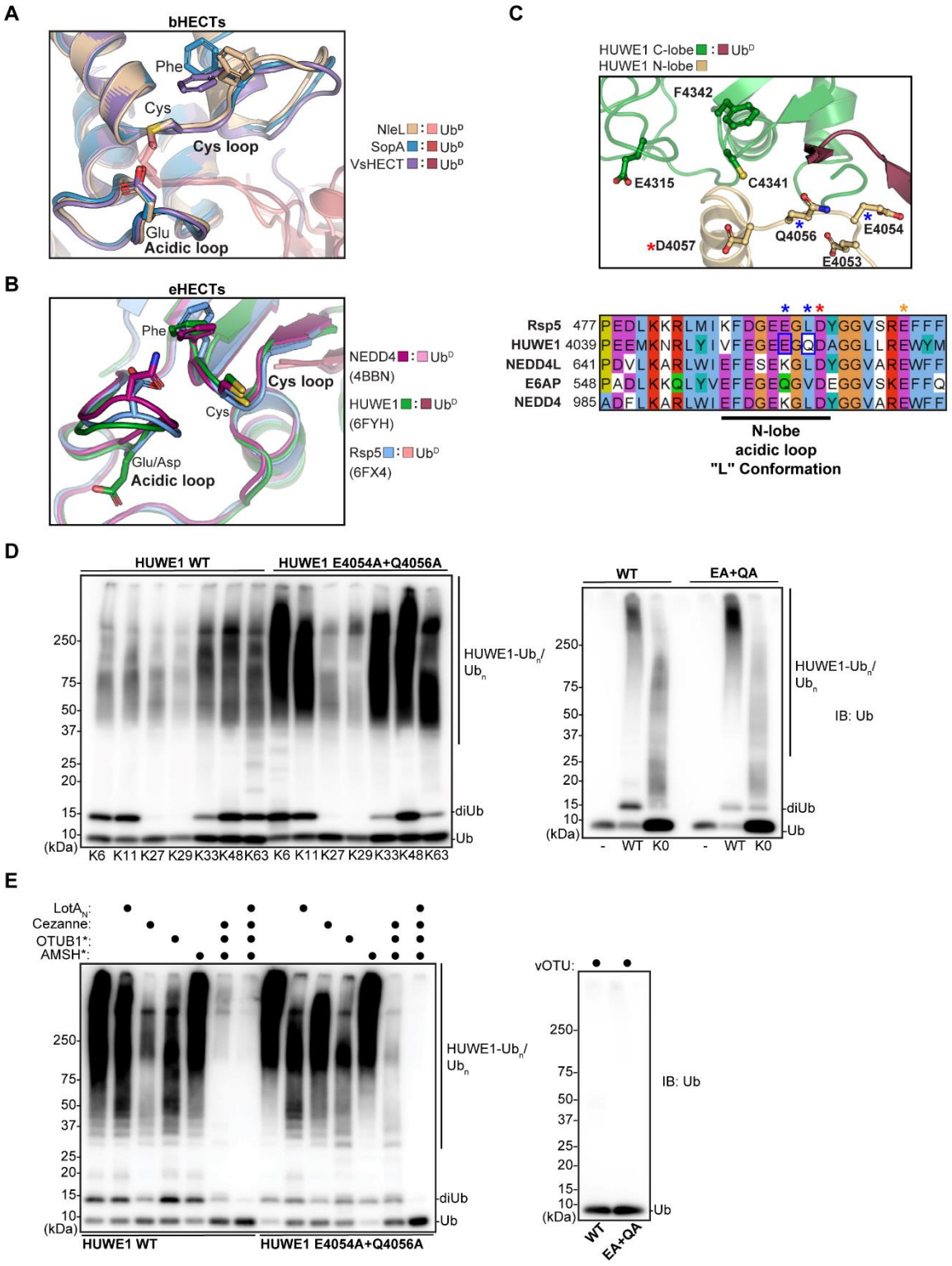
A
bHECTs
Phe
Cys
Cys loop
Glu
Acidic loop
NleL : Ub^D
SopA : Ub^D
VsHECT : Ub^D
B
eHECTs
Phe
Cys loop
Cys
Glu/Asp
Acidic loop
NEDD4 : Ub^D
(4BBN)
HUWE1 : Ub^D
(6FYH)
Rsp5 : Ub^D
(6FX4)
C
HUWE1 C-lobe : Ub^D
HUWE1 N-lobe
F4342
E4315
C4341
Q4056
E4054
D4057
E4053
Rsp5 477 PEDLKKRLMIKFDGEEGLDYGGVSREFFF
HUWE1 4039 PEEMKNRLYIVFEGEEGQDAGGLLREWYM
NEDD4L 641 PDVLKARLWIEFESEKGLDYGGVAREWFF
E6AP 548 PADLKKQLYVEFEGEQGVDEGGVSKEFFQ
NEDD4 985 ADFLKARLWIEFDGEKGLDYGGVAREWFF
N-lobe
acidic loop
"L" Conformation
D
HUWE1 WT
HUWE1 E4054A+Q4056A
250
75
50
37
25
20
15
10
(kDa)
K6 K11 K27 K29 K33 K48 K63 K6 K11 K27 K29 K33 K48 K63
HUWE1-Ub_n/Ub_n
diUb
Ub
WT
EA+QA
- WT K0 - WT K0
IB: Ub
E
LotA_N:
Cezanne:
OTUB1*:
AMSH*:
HUWE1 WT
HUWE1 E4054A+Q4056A
vOTU:
WT
EA+QA

Figure 3.13 HUWE1 acidic loop mutants show increased K6 polyUb ligation (I/II)

A. Overlay of the bHECT C-lobes, emphasizing the orientation of the Cys loop and acidic loop at the bHECT:Ub^D interface. **B**. Overlay of the eHECT C-lobes, emphasizing the orientation of the Cys loop and acidic loop at the eHECT:Ub^D interface for NEDD4 (PDB: 4BBN), HUWE1 (PDB: 6FYH), and Rsp5 (PDB: 4LCD). **C**. Structure of eHECT HUWE1-Ub^D (PDB: 6XZ1), focusing on the active site. Acidic loops in the C-lobe (green) and N-lobe (gold) are shown. Sequence conservation of the N-lobe acidic loop is shown with other eHECTs. The location of an Rsp5 acidic residue previously shown to be important for activity is indicated by a red star. The location of the eHECT E6AP Glu residue (not shown in the structure panel) mutated in Angelman's syndrome is indicated by an orange star. HUWE1 sites selected for mutational analysis are indicated with blue boxes and blue stars. **D**. PolyUb specificity assay for HUWE1 WT and the N-lobe acidic loop mutant E4054A+Q4056A, using the panel of K-only Ub mutants (left), WT Ub, or K0 Ub (right). Reactions were visualized by anti-Ub Western blot. **E**. UbiCRest assay monitoring the cleavage of polyUb generated by HUWE1 WT or E4054A+Q4056A, using K6-specific $LotA_N$, K11-specific Cezanne, K48-specific OTUB1*, K63-specific AMSH*, or nonspecific vOTU. Reactions were visualized by anti-Ub Western blot.

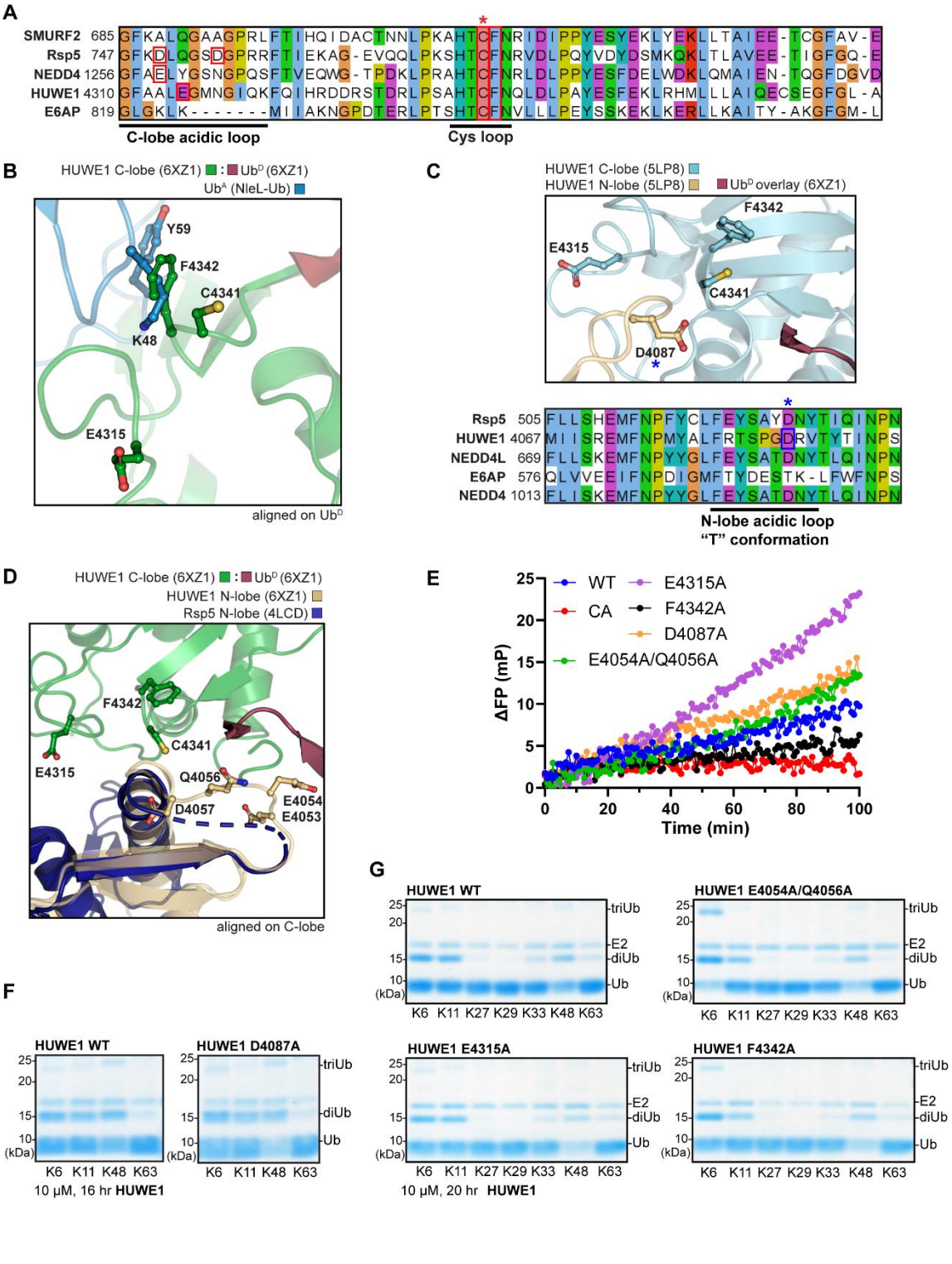
A
SMURF2 685 GFKALQGAAGPRLFTIHQIDACTNNLPKAHTCFNRIDIPPYESYEKLYEKLLTAIEE-TCGFAV-E
Rsp5 747 GFKDLQGSDGPRRFTIEKAG-EVQQLPKSHTCFNRVDLPQYVDYDSMKQKLTLAVEE-TIGFGQ-E
NEDD4 1256 GFAELYGSNGPQSFTVEQWG-TPDKLPRAHTCFNRLDLPPYESFDELWDKLQMAIEN-TQGFDGVD
HUWE1 4310 GFAALEGMNGIQKFQIHRDDRSTDRLPSAHTCFNQLDLPAYESFEKLRHMLLLAIQECSEGFGL-A
E6AP 819 GLGKLK-------MIIAKNGPDTERLPTSHTCFNVLLLPEYSSKEKLKERLLKAITY-AKGFGM-L
C-lobe acidic loop
Cys loop
B
HUWE1 C-lobe (6XZ1) : UbD (6XZ1)
UbA (NIeL-Ub)
Y59
F4342
C4341
K48
E4315
aligned on UbD
C
HUWE1 C-lobe (5LP8)
HUWE1 N-lobe (5LP8)
UbD overlay (6XZ1)
F4342
E4315
C4341
D4087
Rsp5 505 FLLSHEMFNPFYCLFEYSAYDNYTIQINPN
HUWE1 4067 MIISREMFNPMYALFRTSPGDRVTYTINPS
NEDD4L 669 FLLSKEMFNPYYGLFEYSATDNYTLQINPN
E6AP 576 QLVVEEIFNPDIGMFTYDESTK-LFWFNPS
NEDD4 1013 FLISKEMFNPYYGLFEYSATDNYTLQINPN
N-lobe acidic loop
"T" conformation
D
HUWE1 C-lobe (6XZ1) : UbD (6XZ1)
HUWE1 N-lobe (6XZ1)
Rsp5 N-lobe (4LCD)
F4342
C4341
E4315
Q4056
D4057
E4054
E4053
aligned on C-lobe
E
WT
CA
E4315A
F4342A
D4087A
E4054A/Q4056A
ΔFP (mP)
Time (min)
F
HUWE1 WT
HUWE1 D4087A
triUb
diUb
Ub
(kDa)
K6 K11 K48 K63
10 μM, 16 hr HUWE1
G
HUWE1 WT
HUWE1 E4054A/Q4056A
HUWE1 E4315A
HUWE1 F4342A
triUb
E2
diUb
Ub
(kDa)
K6 K11 K27 K29 K33 K48 K63
10 μM, 20 hr HUWE1

Figure 3.14 HUWE1 acidic loop mutants show increased K6 polyUb ligation (II/II)

A. MSA of selected eHECTs, highlighting the region of the C-lobe surrounding the active site. Asterisks and red boxes are used to indicate the conserved active site Cys and the conserved Cys-loop Phe. The sequences of the Cys loop and potential acidic loop are highlighted. Red boxes indicate potential acidic residues. **B**. Overlay of the HUWE1-Ub^D (PDB: 6XZ1) structure with Ub^A from the Ub^A:NleL-Ub^D structure, showing the Cys loop and C-lobe acidic loop of HUWE1, along with the Ub^A residues important for NleL K48-linked Ub ligation, Y59 and K48. **C**. Structure of apo HUWE1 (PDB: 5LP8), focusing on the active site, with the C-lobe shown in teal and the N-lobe shown in gold. The C-lobe acidic loop containing E4315 is shown, as well as a second acidic loop from the T-conformation of the N-lobe. Sequence conservation of the second N-lobe acidic loop is shown with other eHECTs, with the location of acidic residue selected for mutational analysis indicated with a blue star and blue box. **D**. View of the HUWE1-Ub^D structure (PDB: 6XZ1), overlayed with the N-lobe of Rsp5 (PDB: 4LCD). The acidic loop region lacking electron density in the Rsp5 structure is shown with the dashed line. Acidic loop and Cys loop residues for HUWE1 are shown. **E**. E3 ligase assay monitored by the FP-based method UbiReal, for WT HUWE1 and the sequence- or structure-guided mutants at 25 μM. Reactions were initiated with ATP at time point 0 min. **F**. Gel-based polyUb specificity assay for HUWE1 WT and the N-lobe acidic loop mutant D4087A, using a subset of K-only Ub mutants. Gel regions corresponding to monoUb, diUb, and triUb are shown for clarity. Reactions were quenched and resolved by SDS-PAGE with Coomassie staining. **G**. Gel-based polyUb specificity assay for HUWE1 WT, the N-lobe acidic loop mutant E4054A+Q4056A, the C-lobe acidic loop mutant E4315A, and the Cys loop mutant F4342A, using the panel of K-only Ub mutants. Gel regions corresponding to monoUb, diUb, and triUb are shown for clarity. Reactions were quenched and resolved by SDS-PAGE with Coomassie staining.

acidic loop from the N-lobe encoding E4054 and Q4056 is in close proximity to the active site (**Fig. 3.13C**). Interestingly, this loop matches by sequence and structural alignment to a structurally unresolved loop of Rsp5 that was previously demonstrated to have a critical catalytic function (**Fig. 3.14D**)[120]. In the apo HUWE1 structure, the C-lobe is shifted into a "T"-conformation that positions a different N-lobe acidic residue, D4087, near the active site (**Fig. 3.14C**).

We tested the effects of mutations in the putative HUWE1 acidic loops: E4315A, E4054A+Q4056A, and D4087A, on total activity in a UbiReal assay. We also tested the Cys-loop Phe residue of HUWE1, F4342, as the potentially structurally analogous residue of NleL which contributed to polyUb specificity (**Fig. 3.9F**). Except for the C-lobe acidic loop mutation, E4315A, none of the acidic mutants appreciably altered ligase activity by this assay (**Fig. 3.14E**). As observed in bHECTs, the HUWE1 Cys-loop mutant F4342A showed reduced overall ligase activity (**Fig. 3.14E**). Next, we assessed effects on polyUb specificity using the panel of K-only Ub mutants. Neither the C-lobe acidic mutant, E4315A, nor the T-conformation acidic mutant, D4087A, had appreciable effects on polyUb specificity (**Fig. 3.14F-G**). The Cys loop F4342A mutant had a minor impact on specificity, producing less K11-linked polyUb (**Fig. 3.14G**). Strikingly, however, the L-conformation acidic mutant, E4054A+Q4056A, produced more K6-linked polyUb and nearly consumed the available substrate (**Fig. 3.13D, 3.14G**). Using a UbiCRest assay, we observed increased production of K6-linked polyUb by the E4054A+Q4056A mutant, as $LotA_N$ showed more activity towards the polyUb smear both on its own or in combination with other linkage-specific DUBs (**Fig. 3.13E**). Thus, residues within the eHECT N-lobe

may contribute to ligase specificity, raising the possibility that distinct conformations of the HECT domain can influence the nature of the polyUb produced.

Discussion

Together with prior studies, our structural and biochemical data provide a more complete picture bHECT ligation. Combining our Ub-activated NleL structure with a previous E2-bound structure yielded a composite model for the initial E2-E3 transthiolation reaction that is supported by NMR and biochemical data. Held in place by contacts to the N-lobe, the E2~Ub conjugate is engaged by the bHECT C-lobe from the same direction as eHECTs, but opposite to eukaryotic RBR and RCR E3 ligases[46,50,154,155]. Ub transfer onto the E3 active site is coincident with a large conformational rearrangement of the Cys loop, including a conserved Phe residue, that may act in part to displace the activated C-lobe. Among the bHECT-Ub structures that we determined, contacts made to the Ub β-grasp domain are highly variable, resulting in large differences in how the activated Ub is oriented. In contrast, the Ub C-terminus is stabilized in an extended conformation by a conserved group of hydrogen bonds, many of which arise from a bHECT Arg residue that is required for priming the donor Ub. Flexibility within the linker domain allows movement of the activated C-lobe toward the substrate for Ub transfer. Alternatively, bHECTs can assemble linkage-specific polyUb chains through an acceptor Ub-binding site, which is captured in one of our structures through crystal packing. At the NleL active site lies a conserved acidic loop, the mutation of which also toggles NleL activity away from K48- and towards K6-linked polyUb. The same Cys loop rearrangement that displaced the E2 also creates part of the Ub^A binding site, wherein the conserved Phe contacts Y59 of the

incoming Ub, orienting K48 toward the active site. This interface is essential, as mutations on either side of the interface severely affected the ability of NleL to ligate K48-linked polyUb chains, with minimal or no effect on activity toward K6-linked polyUb. This structure provides a unique glimpse into K48-specific polyUb ligation by HECT-type ligases. Interestingly, reliance upon Ub Y59 may be a common strategy for K48 polyUb specificity, as the E2 enzymes UBE2K and UBE2R1 also require this contact[133,156,157], and it is observed at the ligation interface for the E3-E2 pair UBR2-UBR1[158]. Using chemical probes and cryo-EM, recent studies have also visualized mechanisms of HECT-type polyUb specificity for UBR5[159] and Ufd4[160].

Through expansion of the bHECT family, we gained a better appreciation of its sequence and functional diversity. While identification and validation of more bHECT examples will be crucial to fully understand their evolutionary origins, it is interesting that, at least for the subset investigated here (**Fig. 3.1, Table 3.1**), pathogens with diverse lifestyles appear to encode bHECTs. Their poor sequence homology (**Fig. 3.2A-C**), especially relative to the high conservation observed among human HECT domains, suggests that bHECTs have evolved separately, or at the very least have undergone rapid evolution. While it is unclear if there is a common ancestor, it is worth noting that a *nleL* gene was found within a prophage[53], which could suggest a potential mechanism of rapid dissemination.

Remarkably, we found that NleL is not alone in its ability to ligate atypical K6-linked polyUb, and in fact it appears to be the preferred product of PvHECT from the opportunistic pathogen *P. vulgaris*. *Proteus* species are commonly associated with urinary tract

infections, where they can form large extracellular clusters[161,162]. Interestingly, the related *P. mirabilis* also encodes a bHECT candidate (**Table 3.2**)[68,69]. EHEC similarly maintains an extracellular niche, the regulation of which has been tied to NleL ligase activity[35,59], suggesting that perhaps ligation of K6-linked polyUb plays a role for extracellular bacteria that is not required for pathogens with intracellular lifestyles, such as *Salmonella* Typhimurium, which encodes the K48-specific SopA. PsHECT also preferentially assembled K48-linked polyUb (**Fig. 3.9J**), and is from the plant pathogen *Pantoea stewartii*, which colonizes the intracellular regions of leaf tissue[163]. How polyUb specificity of bHECTs could be associated with the extracellular vs. intracellular lifestyle of the pathogen is unclear. Considering the critical role of the acidic loop residue E705 in polyUb specificity, investigation of bHECT candidates that natively lack this residue and the lifestyles of the associated pathogens may provide interesting clues into these relationships (**Fig. 3.10H**). These observations also raise an interesting contrast to recent work on other intracellular bacteria, such as *Legionella pneumophila*, which secrete DUBs that specifically remove K6-linked polyUb signals[41,153,164–167]. The signaling roles for K6-linked polyUb remain murky, particularly with respect to the host-pathogen interface. Our newfound ability to modulate the polyUb specificities of bHECTs will provide important tools for future studies on this ambiguous signal.

Despite their apparent differences in sequence and structure, many of the lessons learned from studying bHECTs could be translated to eHECTs. In particular, both bHECTs and eHECTs coordinate an extended C-terminal tail of Ub^{D}, which is accomplished by β-sheet augmentation in eHECTs[47,48,124], and primarily through a conserved Arg in the bHECTs.

Though the importance of these backbone interactions is difficult to test in eHECTs, we could show in bHECTs that mutation of the conserved Arg residue severely reduces ligase activity, presumably through an inability to orient the donor Ub for nucleophilic attack. We also observed that the Ub^D C-terminal tail is sandwiched between a Phe-containing Cys loop and an acidic loop for both eHECTs and bHECTs. Our structural work captured the importance of these loops in establishing an acceptor Ub-binding site, and while defining the basis of polyUb specificity among eHECTs has been a longstanding challenge, we could show that analogous loops in human HUWE1 also regulate polyUb specificity. Surprisingly, the HUWE1 acidic loop that influenced polyUb specificity to the largest extent was not encoded near the active site in the C-lobe, but was contributed from the N-lobe. This loop, by sequence and structure, corresponds to the location of an Asp residue critical for Rsp5 ligase activity[120]. Thus, for both SopA and Rsp5, which specifically ligate a single type of polyUb, mutation of the acidic loop ablates activity whereas for NleL and HUWE1, both of which encode multiple polyUb specificities, it instead alters the preferred product. This suggests the possibility that distinct acidic residues enable the formation of different polyUb products. In fact, many eHECTs encode conserved acidic residues near their C-termini, which are already known to partly mediate polyUb specificity in several cases[42,47,103,124].

The roles of acidic residues in Ub transfer are well documented[28,120,144,145,168]. Acidic residues near the active site may function to deprotonate the ε-amino group of an incoming Lys on the acceptor Ub or a substrate, or simply guide the target Lys into the E3 active site. Remarkably, this underlying principle of Ub ligation is even followed by the most

structurally distinct bacterial E3 ligases, including the Novel E3 Ligase (NEL) family found in *Salmonella* and *Shigella* species, as well as the SidC E3 ligase family from *Legionella* species[13,28,145,169,170]. Clearly, despite large differences in structure and evolutionary convergence of Ub ligase function, certain principles of Ub transfer still hold true. Just as our work on bHECT E3 ligases has demonstrated for polyUb specificity, studying the principles of bacterial E3 ligases may yet reveal further insights into the mechanisms governing eukaryotic Ub biology.

Acknowledgements: We thank David Komander (WEHI), Rachel Klevit (UW), and Thomas Mund (MRC LMB) for sharing expression plasmids. We thank members of our laboratories and the Seattle Ub Research Group for helpful discussions. Access to NMR facilities was generously granted by Rachel Klevit, who is supported by the National Institute of General Medical Sciences (NIGMS) (1R35GM144127). Use of the Stanford Synchrotron Radiation Lightsource, SLAC National Accelerator Laboratory, is supported by the US DOE under Contract No. DE-AC02-76SF00515. The SSRL Structural Molecular Biology Program is supported by the DOE and the NIH (P30GM133894). This work was supported by Oregon Health & Science University (JNP), the OHSU Program in Molecular and Cellular Biosciences (5T32GM071338-14 to TGF) and the NIGMS (R35GM142486 to JNP).

Experimental procedures

Bacterial HECT-like domain prediction

T-coffee[171] was used to generate a consensus sequence from a multiple sequence alignment

of the only two known HECT-like domains, NleL and SopA. With the consensus sequence of either the C-lobe alone, or the consensus sequence of the full HECT domain, the NCBI protein BLAST suite was used to search bacterial genomes for similar sequences. Sequences of bacterial proteins with HECT-like similarities were manually curated from BLAST by inspection for alignment to critical HECT-like features of NleL and SopA. Sequence features included an active site Cys residue, an E2-interacting aromatic residue, a linker region, and a HECT-like domain of similar size to NleL and SopA (~400 residues). Candidate sequences were next subjected to protein homology modeling using Phyre2[172]. Protein models of the candidate sequences were aligned with structures of NleL and SopA in PyMOL, and manually inspected for the bi-lobal structures characteristic of HECT and HECT-like domains. Candidates that met these criteria were synthesized (IDT), using codons optimized for *Escherichia coli* expression systems.

AlphaFold modeling

To build models of the E2:bHECT interface, we used AlphaFold multimer[140,141] through the ColabFold suite[173]. Sequences of the HECT domains of the bHECTs (**Table 3.1**) and the sequence for human UBE2L3 were provided to the ColabFold software which had been updated to use the PDB100, which searches the ColabFold-generated MSA with Foldseek[174] against the AlphaFold database. For detailed protocols, we direct the reader to the AlphaFold and ColabFold publications[140,141,173].

Cloning and mutagenesis

The *nleL* gene was cloned from *Escherichia coli* O157:H7 str. Sakai, the *sopA* gene was cloned from *Salmonella enterica* Typhimurium SL1344, and all other bHECT constructs (VsHECT, PvHECT, PsHECT, and EaHECT) were synthesized by IDT (**Table 3.1**). All

bHECT expression constructs were designed using Phyre2[172] and the available crystal structures of NleL[17] and SopA[49]. HUWE1 and E6AP were a kind gift from Thomas Mund (MRC Laboratory of Molecular Biology). All HECTs were cloned into the pOPIN-B vector which contains an 3C-cleavable N-terminal His-tag, except for EaHECT, which were cloned into the pOPIN-S vector which additionally has an N-terminal SUMO tag. Cloning and mutagenesis were performed using Phusion DNA Polymerase (New England BioLabs) and TOP10 *Escherichia coli* (MilliporeSigma).

Protein expression and purification

All pOPIN-B/S bHECT and eHECT constructs were expressed and purified similarly. Transformed Rosetta (DE3) *Escherichia coli* were grown in Luria broth containing 35 µg/mL chloramphenicol and 50 µg/mL kanamycin at 37 ºC until OD_{600} 0.6-0.8, induced with 300 µM IPTG, and left to express at 18 ºC for 18-20 hrs. Cells were harvested by centrifugation and resuspended in 25 mM Tris, 200 mM NaCl, 2 mM β-mercaptoethanol, pH 8.0 (Buffer A). Following a freeze-thaw cycle, cells were incubated for 30 min on ice with lysozyme, DNase, PMSF, and SigmaFAST protease inhibitor cocktail (MilliporeSigma), then lysed by sonication. Clarified lysates were applied to HisPur cobalt affinity resin (ThermoFisher), washed with Buffer A containing 500 mM NaCl and 5 mM imidazole, and eluted using Buffer A containing 300 mM imidazole. bHECT and eHECT proteins were concentrated using Amicon centrifugal filters (MilliporeSigma) and applied to a HiLoad Superdex 75 pg 16/600 size exclusion column (Cytiva) equilibrated in 25 mM Tris, 150 mM NaCl, 0.5 mM DTT, pH 8.0 at 4 ºC. Fractions were evaluated for purity by SDS-PAGE, collected, concentrated, and quantified by absorbance (280 nm) prior to flash freezing and storage at -80 ºC.

Untagged WT or mutant Ub constructs were expressed from the pET-17b vector. Transformed Rosetta (DE3) *Escherichia coli* were grown by auto-induction in a modified ZYM-5052 media[175] containing 35 µg/mL chloramphenicol and 100 µg/mL ampicillin at 37 ºC for 24-48 h. Cells were harvested by centrifugation, resuspended, and lysed as above. Clarified lysates were acidified by dropwise addition of 70% perchloric acid to a final concentration of 0.5%. The mixture was stirred on ice for 1 h prior to centrifugation. The clarified supernatant was dialyzed into 50 mM sodium acetate, pH 5.0 overnight. The protein was applied to a HiPrep SP FF 16/10 cation exchange column (Cytiva), washed with additional 50 mM sodium acetate, pH 5, and eluted over a linear gradient to a matched buffer containing 500 mM NaCl. Ub was finally purified by application to a HiLoad Superdex 75 pg 16/600 size exclusion column equilibrated in 25 mM Tris, 200 mM NaCl, pH 8.0. Purified Ub was quantified by absorbance (280 nm), or by a BCA standard curve for Ub Y59A (ThermoFisher), and flash frozen for storage at either -20 ºC or -80 ºC.

^{15}N-labeled proteins were grown in minimal MOPS medium supplemented with $^{15}NH_4Cl$. ^{15}N-Ub was expressed and purified as above for unlabeled Ub. Untagged ^{15}N-UBE2D3 C85S/S22R was expressed from pET17b using IPTG induction as described above, harvested, and resuspended in 50 mM MES, pH 6.0. Cells were lysed by sonication as described above, and UBE2D3 was purified by cation exchange chromatography on a HiPrep SP FF 16/10 column (Cytiva) using a 0-500 mM salt gradient in 50 mM MES, pH 6.0 at 4 ºC, followed by size exclusion using a HiLoad Superdex 75 pg 16/600 column. All ^{15}N-labeled proteins were exchanged into matched buffer containing 25 mM NaPi, 150 mM NaCl, 0.5 mM DTT, pH 7.4 prior to quantification and storage as described above.

The Ub-PA activity-based probes were prepared using intein chemistry[176], as described

previously in detail[153].

Ub-PA reactivity assays

Ub-PA reactivity assays were performed at a 1:2, bHECT:Ub-PA molar ratio using 5 μM bHECT and 10 μM Ub-PA in reaction buffer containing 25 mM Tris, 150 mM NaCl, 0.5 mM DTT, pH 8.0. Small-scale reactions were incubated at 37 ºC for 1 h. Samples were quenched with reducing Laemmli sample buffer and analyzed by SDS-PAGE.

Gel-based E3 ligase assays

E3 ligase assays were performed using 300 nM UBA1, 2 μM Lys-less UBE2L3, 50 μM Ub (WT, K-only, K-to-R, or Y59A), with HECT E3 ligases at concentrations indicated in the figure panel or figure legend, in the presence of 5 mM ATP, 0.5 mM DTT, and 10 mM $MgCl_2$. All gel-based ligase assays were performed at 37 ºC. Reaction times were scaled based on the specific activity of each HECT. At the time points indicated in the figure panel or figure legend, samples were quenched with reducing Laemmli sample buffer and analyzed by SDS-PAGE.

UbiCRest analysis

PolyUb chain assemblies using NleL, the SNc ligase, or mutants thereof, were prepared as described above. Reactions were quenched by addition of EDTA to 40 mM final concentration and DTT to 5 mM final concentration. DUBs were diluted into activation buffer containing 25 mM Tris, 150 mM NaCl, 10 mM DTT, pH 7.4 and incubated at 22 ºC for 10 min, as previously described[177]. DUBs were added at 5 μM final concentration to polyUb assemblies, mixed, and incubated at 37 ºC for 2 h prior to quenching in reducing Laemmli sample buffer and analysis by SDS-PAGE.

Western blot analysis

Reactions were resolved by SDS PAGE as described above. Next, gels were transferred onto PVDF membranes using the semi-dry Trans-Blot Turbo system (BioRad) using the mixed-molecular weight setting. Following transfer, membranes were blocked at room temperature for 1 hr with TBS-T (Tris-buffered Saline with 0.1% v/v Tween-20) containing 5% milk. After blocking, membranes were washed in TBS-T. Next, membranes were incubated with an anti-Ub antibody (MilliporeSigma, MAB1510-I; 1:1,000 dilution) or anti-His antibody (MilliporeSigma, 05-929; 1:1,000 dilution) at 4 ºC overnight with gentle rocking. Membranes were again washed in TBS-T, prior to incubation with the secondary antibody (MilliporeSigma, #12-349; 1:5,000 dilution) at room temperature for 1 hr. Finally, membranes were washed again in TBS-T and then briefly incubated with Clarity ECL reagent (BioRad) and visualized by chemiluminescence scan on a Sapphire Biomolecular Imager (Azure Biosystems).

Fluorescence-based E3 ligase (UbiReal) assays

UbiReal assays were performed as previously described[138,139]. Fluorescence polarization (FP) was recorded using a BMG LabTech ClarioStar plate reader with an excitation wavelength of 540 nm, an LP 566 nm dichroic mirror, and an emission wavelength of 590 nm. Reactions were performed at 22 ºC in low-binding Greiner 384-well small-volume HiBase microplates with 20 µL final reaction volumes.

Reactions contained 150 nM UBA1, 1 µM Lys-less UBE2L3, 37.5 µM WT (unlabeled) Ub, 10 mM $MgCl_2$, 0.5 mM DTT, and NleL, SopA, or HUWE1 (or mutants thereof), at 2 µM, 2 µM, or 25 µM, respectively. Each reaction also contained 100 nM Ub with an N-terminal TAMRA fluorophore. Each reaction, in the absence of ATP, was monitored for

several FP cycles, and these FP values were used as the minimum FP for the ΔFP calculation at each time point. Reactions were initiated with addition of ATP to 5 mM, and monitored over time by FP. Each reaction was performed with technical triplicates, and the average value is plotted at each time point.

Fluorescence-based E2~Ub discharge assays

E2~Ub discharge assays were performed using 100 nM K6R,K48R Ub modified with an N-terminal Alexa 488 fluorophore, 300 nM UBA1, 480 nM Lys-less UBE2L3, 5 mM ATP, 5 mM $MgCl_2$, and 1 mM TCEP. The mixture was allowed to react, with mixing, for 5 min at 22 ºC, followed by quenching with addition of EDTA to 50 mM.

For the FP-based experiment, FP was performed as described above, but monitored using an excitation wavelength of 482 nm, an LP 504 nm dichroic mirror, and an emission wavelength of 530 nm. The reaction mixture was added to the 384-well plate and monitored over time at 22 ºC. Cleavage of the E2~Ub conjugate was initiated (time point 0 min) by addition of NleL WT or mutant to 15 nM, or addition of buffer for the negative control. FP signal was monitored over time.

For the gel-based experiment, the reaction mixture was added to tubes containing NleL WT or mutant at 150 nM final concentration, and allowed to react at 22 ºC or 4 ºC (e.g., on ice) for the indicated amount of time. Samples were quenched with non-reducing Laemmli sample buffer, analyzed by SDS-PAGE, and visualized by fluorescence scan at 488 nm (Sapphire BioImager).

Protein crystallization and structure determination

NleL (606-782), SopA (603-782), and VsHECT (639-847) were prepared as described above and reacted with Ub-PA at a molar ratio of 1:2 bHECT:Ub-PA overnight at 4 ºC with rocking. Reactions were subsequently purified by anion exchange chromatography using a Resource Q column (Cytiva) with a 0 – 0.5 M NaCl gradient in 25mM Tris, 1 mM DTT, pH 8.5, followed by size exclusion on a HiLoad Superdex 75 pg 16/600 column (Cytiva) equilibrated with 25 mM Tris, 125 mM NaCl, 1 mM DTT, pH 7.4. NleL-Ub^D, SopA-Ub^D and VsHECT-Ub^D were concentrated to 15 mg/mL, 9 mg/mL, and 15 mg/mL, respectively. NleL-Ub^D crystallized in Ligand Friendly Screen (Molecular Dimensions) in sitting drop format with 20% PEG 3350, 0.2 M KSCN, 0.1 M bis-tris propane pH 7.5, 20% glycerol, and 10% ethylene glycol at 22 ºC in a 1 µL drop with 1:1 protein:precipitant ratio. SopA-Ub^D crystallized in hanging drop format with 22.5% PEG 8000, 0.2 M ammonium sulfate, 0.1 M sodium cacodylate pH 7.0, and 20% glycerol at 22 ºC in a 1 µL drop with 1:1 protein:precipitant ratio. VsHECT-Ub^D crystallized in hanging drop format with 20% PEG 2K MME, 0.1 M MES pH 6.0, and 20% ethylene glycol at 22 ºC in a 1 µL drop with 1:1 protein:precipitant ratio. Crystals for each bHECT-Ub^D were cryoprotected in mother liquor containing 25% glycerol prior to vitrification.

Diffraction data were collected at the Stanford Synchrotron Radiation Lightsource (SSRL), beamline 9-2. The data were integrated using XDS[178] and scaled using Aimless[179]. The NleL-Ub, SopA-Ub, and VsHECT-Ub structures were determined by molecular replacement with Phaser in CCP4i2, using search models consisting of NleL (PDB: 3NB2), SopA (PDB: 2QYU), or a model of VsHECT built using Phyre2[172], respectively, along with Ub (PDB: 1UBQ)[17,49,180–182]. Automated model building was performed using ARP/wARP[183], followed by iterative rounds of manual model building in COOT and

refinement in PHENIX[184,185]. All figures were generated using PyMOL (www.pymol.org).

NMR analysis of NleL:UBE2D3~Ub

The ^{15}N-UBE2D3-O-^{15}N-Ub conjugate was prepared using ^{15}N-Ub and ^{15}N-UBE2D3 C85S/S22R, as previously described[29]. NMR experiments were performed in 25 mM NaPi, 150 mM NaCl, 0.5 mM DTT, pH 7.4 with 10% D_2O on a 500 MHz Bruker AVANCE III at 25 °C. Data were processed using NMRPipe[186] and analyzed using NMRViewJ[187]. NMR spectra were recorded of 150 µM ^{15}N UBE2D3-O-Ub alone, or following the addition of 0.1 molar equivalents (15 µM final) of NleL C753A (170-782), or 2.0 molar equivalents (300 µM final) of NleL C753A (606-782). Surface structure representations of peak broadening following NleL titration were plotted using PyMOL.

Gene name	Organism	Uniprot ID	NCBI/GenBank	Construct
nleL	Enterohemorrhagic *Escherichia coli* O157:H7 str. Sakai	A0A0H3JDV8	WP_001301673.1	170-782 (FH) 606-782 (C-lobe)
sopA	*Salmonella enterica* Typhimurium str. SL1344	Q8ZNR3	WP_000703998.1	342-782 (FH) 603-782 (C-lobe)
vsHECT	*Verrucomicrobia species*	A0A2V2RSR1	PWU08673.1	639-847 (C-lobe)
pvHECT	*Proteus vulgaris*	A0A292CDM3	WP_192940890.1	292-745 (FH)
psHECT	*Pantoea stewartii*	H3RGA3	WP_006120546.1	210-646 (FH) 464-646 (C-lobe)
eaHECT	*Erwinia amylorova*	D4HXM4	WP_013036135.1	85-537 (FH)

Table 3.1 bHECT constructs used in this study

Organism	**UniProt ID**	**NCBI/GenBank**
Escherichia coli	A0A2K3TZS8	*See UniProt ID*
Pantoea sp. ICBG 1758	A0A2S5K8U1	*See UniProt ID*
Salmonella bongori N268-08	S5MRN5	*See UniProt ID*
Citrobacter freundii	A0A381GNG1	*See UniProt ID*
Hyphomicrobium sp. MC1	F8JFC3	*See UniProt ID*
Erwinia amylovora CFBP1430	D4HXM4	*See UniProt ID*
Pseudomonas sp. GM21	J2NHP6	*See UniProt ID*
Sodalis praecaptivus	W0HT23	*See UniProt ID*
Candidatus Sodalis pierantonius str. SOPE	W0HJZ5	*See UniProt ID*
Izhakiella australiensis	A0A1S8YSZ5	*See UniProt ID*
Arsenophonus nasoniae (son-killer infecting *Nasonia vitripennis*)	D2TW63	*See UniProt ID*
Arsenophonus endosymbiont of *Trialeurodes vaporariorum*	A0A3B0M2M1	*See UniProt ID*
Eubacterium siraeum DSM 15702	B0MLL9	*See UniProt ID*
Rothia nasimurium	A0A1Y1RR84	*See UniProt ID*
Streptomyces lydicus	A0A1D7VXM5	*See UniProt ID*
Pandoraea oxalativorans	A0A192B105	*See UniProt ID*
Pantoea sp. (strain At-9b)	E6WKG7	*See UniProt ID*
Erwinia sp. OLSSP12	A0A2G8ELI6	*See UniProt ID*
Yersinia frederiksenii	*See NCBI/GenBank ID*	WP_057614643.1
Streptomyces noursei ATCC 11455	*See NCBI/GenBank ID*	ANZ15598.1
Escherichia albertii	*See NCBI/GenBank ID*	EFE6909629.1
Proteus mirabilis	*See NCBI/GenBank ID*	MBG3129530.1

Table 3.2 Additional, unvalidated bHECT candidates

	NleL-Ub	SopA-Ub	VsHECT-Ub
Data collection			
Space group	I 1 2 1	P 21 21 21	P 1 21 1
Cell dimensions			
a, *b*, *c* (Å)	76.269, 61.023, 116.188	51.893, 63.644, 81.409	35.855, 157.276, 53.025
α, β, γ (°)	90, 99.2508, 90	90, 90, 90	90, 93.756, 90
Resolution (Å)	38.5-2.50 (2.59-2.50)*	36.06-1.75 (1.78-1.75)	39.32-1.44 (1.46-1.44)
R_{merge}	0.131 (0.718)	0.046 (0.665)	0.036 (0.597)
$I / \sigma I$	6.2 (1.6)	16.9 (2.00)	17.7 (1.9)
Completeness (%)	98.1 (96.8)	98.7 (98.1)	86.7 (41.7)
Redundancy	3.1 (3.0)	4.6 (4.5)	3.9 (3.5)
Refinement			
Resolution (Å)	38.5-2.50 (2.59-2.5)	36.06-1.75 (1.81-1.75)	32.57-1.44 (1.49-1.44)
No. reflections	37914	54714	91212
R_{work} / R_{free}	0.2036 / 0.2516	0.1765/0.1959	0.1699/0.1979
No. atoms			
Protein	4055	2161	4649
Ligand/ion	8	4	22
Water	132	218	540
B-factors			
Protein	40.11	28.67	22.83
Ligand/ion	36.03	29.45	16.92
Water	36.40	38.98	31.66
R.m.s. deviations			
Bond lengths (Å)	0.009	0.007	0.012
Bond angles (°)	1.06	0.85	1.25

Table 3.3 Data collection and refinement statistics for the crystal structures of NleL-Ub, SopA-Ub, and VsHECT-Ub

Chapter 4 – Bacterial pathogens evolve OTU deubiquitinase effectors to target diverse ubiquitin linkages that offer improved tools for the UbiCRest methodology

Warren, G.D., Kitao, T., Franklin, T.G., Nguyen, J.V., Geurink, P.P., Kubori, T., Nagai, H., and Pruneda, J.N. (2023). Mechanism of Lys6 poly-ubiquitin specificity by *the L. pneumophila* deubiquitinase LotA. *Molecular Cell* 83, 105-120.e5.

Schubert, A.F., Nguyen, J.V., Franklin, T.G., Geurink, P.P., Roberts, C.G., Sanderson, D.J., Miller, L.N., Ovaa, H., Hofmann, K., Pruneda, J.N., and Komander, D. (2020). Identification and characterization of diverse OTU deubiquitinases in bacteria. *EMBO Journal* 39, e105127. 10.15252/embj.2020105127.

Abbreviations: Ub, ubiquitin; monoUb, monoubiquitin; polyUb, polyubiquitin; Lys or K, lysine; Cys or C, cysteine; Met or M, methionine; HECT, Homologous to E6AP C-terminus; NleL, non-LEE(locus of enterocyte effacement) encoded ligase; DUB, deubiquitinase; USP, ubiquitin specific protease; OTU, ovarian tumor deubiquitinase; EHEC, enterohemorrhagic *Escherichia coli*; PDB, protein data bank.

Introduction

To establish a successful infection, pathogens are forced to adapt to and utilize their host's environment. Increasingly, it is becoming appreciated that pathogens target the Ub system of their host, which provides them access to the incredibly versatile polyUb code[72] (**Fig. 1.3**). Interestingly, though these effectors typically evolve convergently, they sometimes evolve, by sequence and/or structure, to mimic eukaryotic proteins of similar functionality. A good example of this phenomenon was investigated at length in Chapter 3, using the bacterial HECT-like E3 Ub ligases which demonstrated mimicry to the eukaryotic family of HECT E3 Ub ligases. While the investigation in Chapter 3 led to a plethora of tools for investigating K6-linked polyUb ligation, it still remains necessary to identify tools to study K6-linked polyUb from the deubiquitination side. The evolution of K6-linked polyUb specific ligases suggests the presence of this signal at the host-pathogen interface, and could hint at additional bacterial effectors, outside of E3 Ub ligases, dedicated to regulating this polyUb linkage-type. Towards this end, this Chapter describes a family of deubiquitinases in bacteria that evolved as mimics of the ovarian tumor (OTU) family of DUBs.

While we generally consider E3 Ub ligases to be specific for one or a few polyUb linkage-types, DUBs aren't required to have a polyUb linkage specificity, meaning some can generally cleave all forms of polyUb. This is frequently observed for the Ub specific protease (USP) family of DUBs[18,66]. As previously discussed in Chapter 1, seven different DUB families have been described in eukaryotes to date[66]. Another family of note, aside from the USP family, is the aforementioned OTU family. While USPs are often good

examples on nonspecific DUBs, the OTU family of DUBs exists at the other end of the spectrum where they can exhibit a strong preference for only a single polyUb linkage-type[18,66]. Depending on the polyUb linkage-type (**Fig. 1.1**, **1.3**), very different surfaces of the Ub are exposed. For instance, a K63-linked polyUb occludes several sites immediately around K63, but exposes several binding patches away from the linkage site, and these exposed binding patches look very different on, for example, a K48-linked polyUb.

In simple cases, the polyUb linkage specificity of DUBs revolves around the S1' site. Generally speaking, the S1 and S1' sites lie nearby the active site Cys of the DUB and mediate binding to two ubiquitins (a 'distal' Ub and a 'proximal' Ub) of a polyUb chain. These sites, in DUBs like USPs, are not selective for the particular orientations of Ub, allowing them to cleave each polyUb linkage type. In OTU DUBs, however, the S1' site can be highly selective and evolve to bind only one form of polyUb. One of the better examples of this is the OTU family member OTULIN, which cleaves M1-linked polyUb with high selectivity in innate immune signaling pathways[67,188,189]. Because eukaryotic OTU family members showcase some of the best examples of linkage-specific DUBs, and because the field has historically lacked a DUB specific for K6-linked polyUb, work in our lab has sought to identify OTU-mimicking DUBs in pathogenic bacteria, with the hopes of identifying novel, linkage-specific DUBs that could provide new research tools.

Just as we observed the polyUb linkage specificity by bacteria-evolved E3 Ub ligases, prior work has already revealed striking examples of polyUb linkage specificity for bacteria-evolved DUBs. Specific examples include K63-linked polyUb specificity by the DUB

SseL from *Salmonella Typhimurium*[12,21,39] and M1-linked polyUb specific RavD from *Legionella pneumophila*[23]. Another relevant bacterial DUB is ChlaOTU from *Chlamydia pneumonia*, which was the first bacterial OTU-type DUB to be identified by sequence similarity [190,191]. Notably, while ChlaOTU represents a DUB that has evolved to be recognizable as an OTU fold by sequence, other bacterial DUBs, like RavD, show no homology to any eukaryotic DUB, meaning pathogens are capable of evolving polyUb specificity outside of the eukaryotic models.

In this chapter, I present the polyUb specificity profiling of several recently described bacterial OTU family members, identified in a diverse set of human and plant pathogens (described in detail in ref.[22]). Work by our lab and others characterized an additional, and somewhat unusual, OTU DUB from *L. pneumophila* known as LotA[41,153,164,165]. LotA is unusual as it contains two separate OTU domains. PolyUb specificity analysis of the more N-terminal domain, $LotA_N$, reveals a DUB with exquisite specificity for K6-linked polyUb. Thorough testing of $LotA_N$ establishes it as a new tool for studying K6-linked polyUb, especially as a replacement for other DUBs in the powerful, previously-established UbiCRest methodology, which aims to utilize highly specific DUBs to diagnose the relative presence of different polyUb linkage types in complex samples.

Results

Profiling the chain specificity of the bacterial OTUs

Bioinformatic analyses (outside the scope of this dissertation but explained thoroughly in ref.[22]), revealed the presence of potential OTU domains in several pathogenic bacteria

OTU effector	**Bacteria**	**Disease**
EschOTU	*Escherichia albertii*	Gastroenteritis
Ceg7	*Legionella pneumophila*	Legionnaire's
BurkOTU	*Burkholderia ambifaria*	Opportunistic
ChlaOTU	*Chlamydia pneumoniae*	Pneumonia
RickOTU	*Rickettsia massiliae*	Spotted fever
wPipOTU	*Wolbachia pipientis wPip*	Endosymbiont
wMelOTU	*Wolbachia pipientis wMel*	Endosymbiont
Ceg23	*Legionella pneumophila*	Legionnaire's

Table 4.1 bOTU effectors

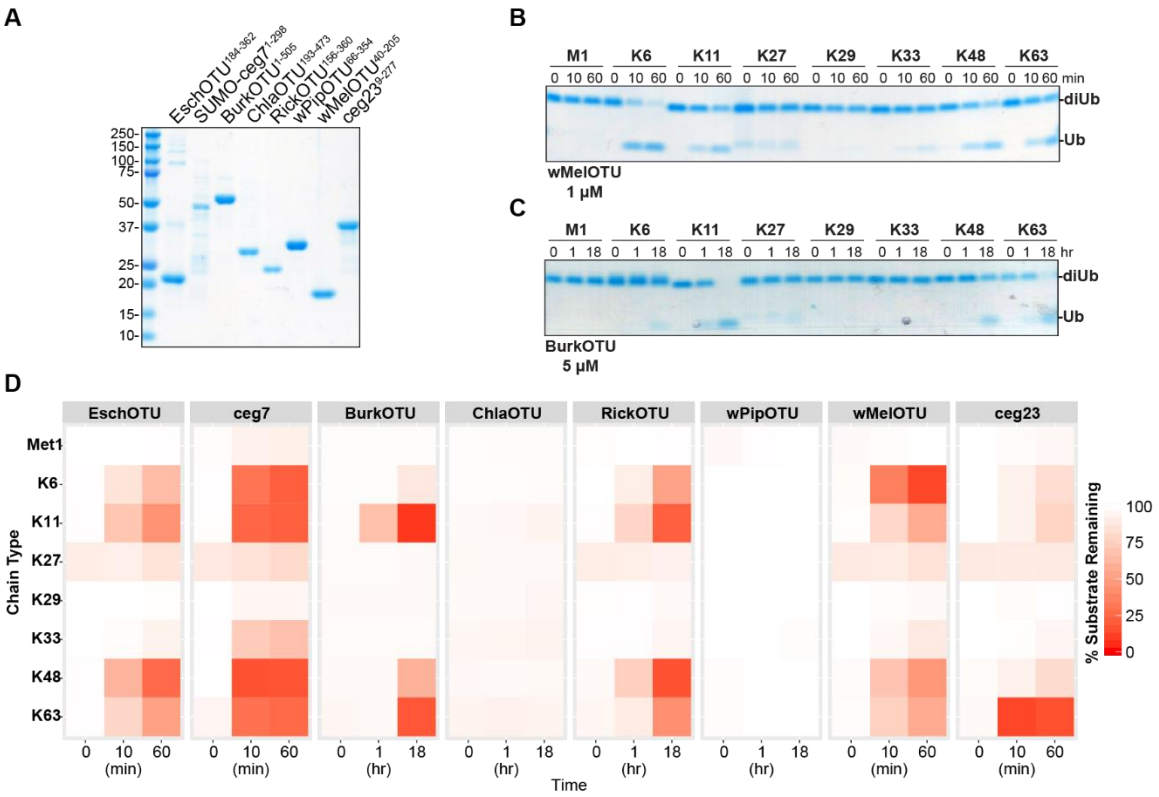

Figure 4.1 bOTUs target a diverse set of polyUb linkages

A. Coomassie-stained SDS–PAGE gel showing purified protein from the predicted bacterial OTU constructs. **B**. Ub chain specificity assay measuring wMelOTU activity toward the eight diUb linkages. Reaction samples were quenched at the indicated timepoints, resolved by SDS–PAGE, and visualized by Coomassie staining. **C**. Ub chain specificity assay measuring BurkOTU activity toward the eight diUb linkages. Reaction samples were quenched at the indicated timepoints, resolved by SDS–PAGE, and visualized by Coomassie staining. **D**. Heatmap representation of WT bacterial OTU activities toward the eight diUb linkages at the indicated timepoints.

(**Table 4.1**). Stable constructs of these bacterial OTU (bOTU) candidates were cloned and expressed (**Fig. 4.1A**). Next, the polyUb linkage-specificity of each bOTU was evaluated. As a proxy for each polyUb linkage-type, purified diUb for each of the eight linkage types were generated using polyUb linkage-specific E2s and E3s. The purified diUb substrates were incubated with each bOTU to monitor diUb cleavage via formation of free Ub and the disappearance of diUb, as resolved with SDS-PAGE. wMelOTU showed a reasonable preference for K6-linked polyUb, which was especially apparent at the 60 min timepoint where this linkage type was the only one to be fully cleaved (**Fig. 4.1B**). However, wMelOTU also showed appreciable cleavage of K11-, K48-, and K63-linked polyUb, indicating a somewhat promiscuous S1' site. A different bOTU, BurkOTU, showed an interesting dual-specificity for both K11- and K63-linked polyUb (**Fig. 4.1C**). Following analysis of each of the identified bOTUs, it was clear that many exhibited multiple polyUb specificities, largely for K6-, K11-, K48-, and K63-linked diUb (**Fig. 4.1D**). With the exception of ceg23, which heavily favored K63-linked diUb, none of the identified examples appeared to prefer a single polyUb linkage-type, as is occasionally observed in the eukaryotic OTUs. However, despite some shared polyUb specificity profiles, structural work on wMelOTU and EschOTU, and subsequent structure-guided sequence analysis, revealed variable regions within the S1 site that resulted in notably different interaction sites with substrate Ub[22].

A bacterial OTU from L. pneumophila advances the UbiCRest methodology.

During analysis of the bOTU family above[22] (**Table 4.1**), a separate group identified an additional OUT-family DUB from *L. pneumophila*, which actually harbored two distinct

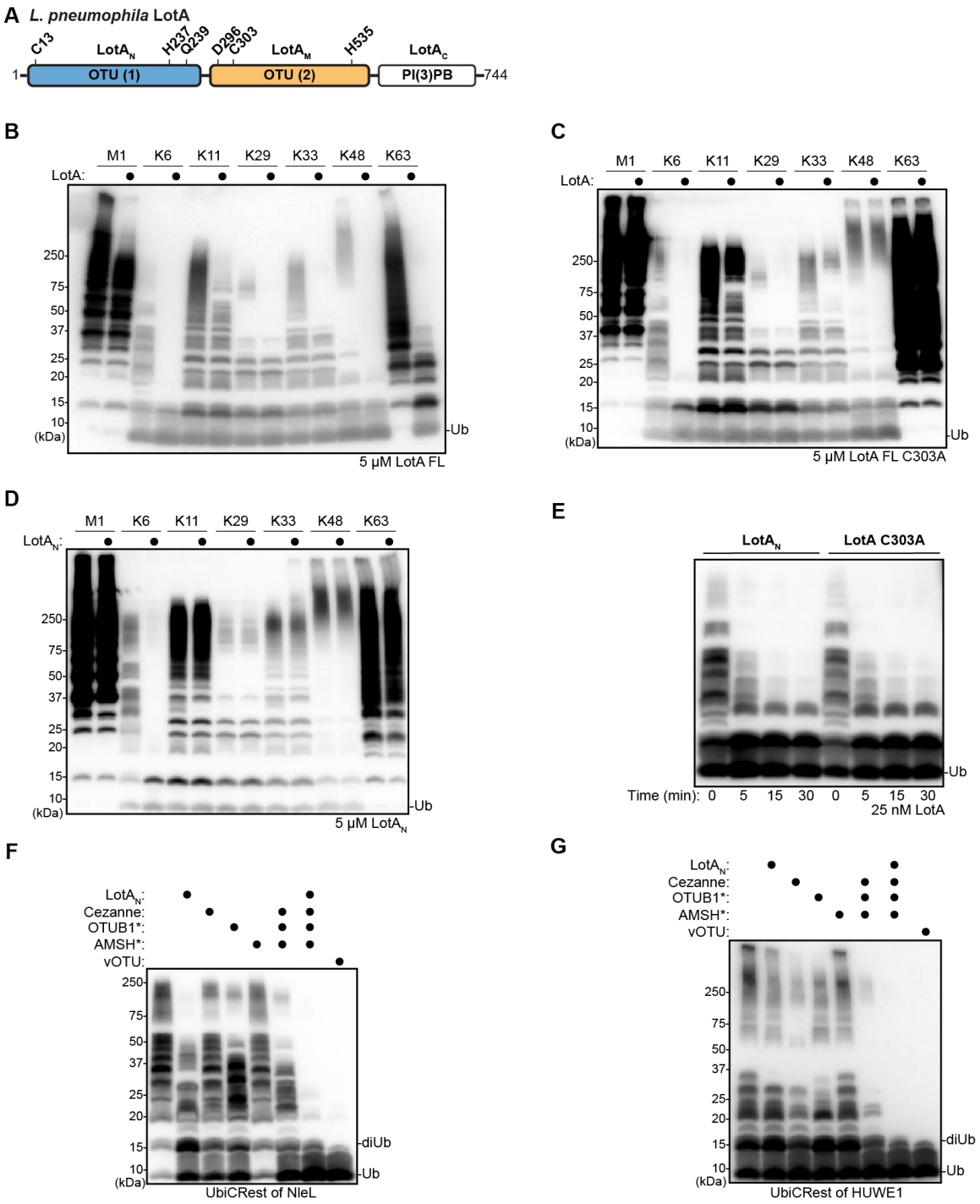
A L. pneumophila LotA
C13
LotA$_N$
H237
Q239
D296
C303
LotA$_M$
H535
LotA$_C$
1
OTU (1)
OTU (2)
PI(3)PB
744
B
M1 K6 K11 K29 K33 K48 K63
LotA:
250
75
50
37
25
20
15
10
(kDa)
Ub
5 μM LotA FL
C
M1 K6 K11 K29 K33 K48 K63
LotA:
250
75
50
37
25
20
15
10
(kDa)
Ub
5 μM LotA FL C303A
D
M1 K6 K11 K29 K33 K48 K63
LotA$_N$:
250
75
50
37
25
20
15
10
(kDa)
Ub
5 μM LotA$_N$
E
LotA$_N$
LotA C303A
Ub
Time (min): 0 5 15 30 0 5 15 30
25 nM LotA
F
LotA$_N$:
Cezanne:
OTUB1*:
AMSH*:
vOTU:
250
75
50
37
25
20
15
10
(kDa)
diUb
Ub
UbiCRest of NleL
G
LotA$_N$:
Cezanne:
OTUB1*:
AMSH*:
vOTU:
250
75
50
37
25
20
15
10
(kDa)
diUb
Ub
UbiCRest of HUWE1

Figure 4.2 $LotA_N$ targets K6-linked polyUb

A. Domain architecture of *L. pneuomophila* LotA, with catalytic triad residues annotated for each OTU domain. **B**. Homogeneous assemblies of seven polyUb linkage types were treated with a high concentration (5 μM) of full-length LotA for 2 h before the reactions were quenched and visualized by anti-Ub western blot. **C**. Homogeneous assemblies of seven polyUb linkage types were treated with a high concentration (5 mM) of full-length LotA C303A for 2 h before the reactions were quenched and visualized by anti-Ub western blot. **D**. Homogeneous assemblies of seven polyUb linkage types were treated with a high concentration (5 mM) of $LotA_N$ for 2 h before the reactions were quenched and visualized by anti-Ub western blot. **E**. A homogeneous assembly of K6-linked polyUb was treated with either $LotA_N$ or the full-length LotA C303A variant at 25 nM. Reaction samples were collected and visualized by anti-Ub western blot. **F**. UbiCRest analysis of an NleL ligase assembly with 1 mM K6-specific $LotA_N$, K11-specific Cezanne, K48-specific OTUB1*, K63-specific AMSH*, non-specific vOTU, or the indicated combinations. Reactions were visualized by anti-Ub western blot. Cleavage of NleL-assembled polyUb can be observed by a decrease in the ‘‘smear’’ or by a reappearance of monoUb. **G**. UbiCRest analysis of a HUWE1 ligase assembly with 1 mM K6-specific $LotA_N$, K11-specific Cezanne, K48-specific OTUB1*, K63-specific AMSH*, non-specific vOTU, or the indicated combinations. Reactions were visualized by anti-Ub western blot. Cleavage of HUWE1-assembled polyUb can be observed by a decrease in the smear or by a reappearance of monoUb.

OTU domains, the N-terminal OTU $LotA_N$ and the middle-domain OTU $LotA_M$, as well as a membrane localization PI(3)P-binding motif at the C-terminus (**Fig. 4.2A**)[41]. To thoroughly test the polyUb specificity of LotA, we generated homogenous polyUb of multiple chain-lengths, as previously described, which aids in testing the robustness of the specificity of DUBs[104]. Using the FL LotA against this polyUb panel, we observed cleavage of multiple chain-types (**Fig. 4.2B**). However, consistent with previous observations, introduction of an active site mutation (C303A) in the second OTU domain resulted in heavily reduced cleavage for all polyUb except K6-linked polyUb (**Fig. 4.2C**). Design of a new construct, $LotA_N$, which contained only the first OTU domain, also showed exquisite specificity for K6-linked polyUb (**Fig. 4.2D**), even at the relatively high concentration of 5 μM. The kinetics of K6-linked polyUb cleavage appeared to be the same for $LotA_N$ and FL LotA C303A, as demonstrated by a time-course between the two constructs (**Fig. 4.2E**).

These assays established $LotA_N$ as having a unique K6-linked polyUb specificity, and indicated the presence of an S1' site with high specificity for K6-linked polyUb. Indeed, structural work in our lab elucidated the structural determinants within the S1' site that enabled this coveted polyUb specificity[153]. One of the most useful methodologies for diagnosing polyUb linkage-types is through UbiCRest, which relies on treating complex, mixed polyUb samples with linkage-specific DUBs. Of course, this methodology relies on having highly specific DUBs, which, unfortunately, is a slight pitfall as not every linkage-type has an analogous DUB specific to its linkages. For example, the original UbiCRest methodology replied on the DUB OTUD3 to test for K6-linked polyUb, though this DUB

also cleaves several K11-linked polyUb[104]. Thus, the impressive K6-linked polyUb specificity of $LotA_N$ positions it as an excellent replacement for OTUD3 in the UbiCRest method. To test this, we assembled polyUb samples using a subset of the very few ligases reported to generate K6-linked polyUb: the bacterial HECT-like E3 Ub ligase NleL, and the eukaryotic HECT HUWE1. PolyUb assemblies using NleL, which ligates K6- and K48-linked polyUb at a ~50:50 mixture[57], were tested against $LotA_N$, as well as K11-linked polyUb preferring Cezanne, K48-linked polyUb specific OTUB1*, and K63-linked polyUb specific AMSH*. As expected for the known polyUb specificity of NleL, $LotA_N$ was able to cleave approximately half of polyUb assembly, and OTUB1* approximately the other half (**Fig 4.2F**). This was also evident when comparing the all-but-$LotA_N$ DUB treatment to the full DUB panel (**Fig. 4.2F** lanes 6 and 7, respectively). Using this approach for HUWE1, we were also able to corroborate the production of K6-linked polyUb by HUWE1[48] using the $LotA_N$-supplemented UbiCRest panel. The HUWE1 polyUb assembly could be visibly reduced by $LotA_N$ treatment, which was also evident when comparing the all-but-$LotA_N$ DUB treatment to the full DUB panel (**Fig. 4.2G**). In Chapter 3, we were also able to expand the use of $LotA_N$ as a UbiCRest tool for diagnosing K6-linked polyUb production by NleL and HUWE1 mutants that appeared to increase the production of K6-linked polyUb. Further in Chapter 3, the utility of $LotA_N$ extended to substrates of E3 Ub ligases, wherein we could observe the formation of K6-linked polyUb onto host proteins targeted by *Salmonella* Typhimurium. Collectively, these assays establish $LotA_N$ as a first-of-its-kind tool for cleaving K6-linked polyUb with exquisite specificity.

Discussion

With the exception of ceg23, which appeared to preferentially cleave K63-linked polyUb, the majority of bOTUs showed a multi-specific polyUb cleavage profile. This could indicate that the S1' site for these bOTUs may not be under selective pressure to cleave a specific-type of polyUb, but perhaps rather to cleave several types of polyUb. It will be interesting to investigate later if the diverse polyUb linkage specificities are related to the pathogenic lifecycle of each bOTU-encoding pathogen. Interestingly, structural analysis revealed that the S1 site exhibits notably different binding motifs among the bOTUs[22]. Additionally, a structure of one of the bOTUs, EschOTU, revealed a permutated fold relative to the eukaryotic OTU, which not only still functioned as a DUB (**Fig. 4.1**), but its topology could be applied in a mutated version of a viral OTU that still functioned, highlighting a fascinating evolutionary aspect of the OTU structural fold[22]. Thus, the insights gained from the discovery of the bOTU family, and their biochemical and structural characterization, revealed several fascinating aspects of OTU deubiquitinases.

Still, aside from wMelOTU, which did demonstrate surprising preference for K6-linked polyUb, the bacterial OTU domains were not as much of a treasure trove of linkage-specific DUBs that might have been expected. Interestingly, though not detected in the original methodology, another group identified the LotA effector which contained two OTU domains, and characterization here and elsewhere showed the N-terminal domain, $LotA_N$, is exquisitely specific for K6-linked polyUb[41]. In a fascinating structure of $LotA_N$ bound to K6-linked diUb, the S1' interaction site of $LotA_N$ contacted I36, E34, T9 and F4 of the proximal Ub, elegantly placing the K6-linked scissile bond across the active site Cys and revealing the unique specificity of $LotA_N$. Functionally, the role of K6-linked polyUb

specificity by $LotA_N$ during *L. pneumophila* infection is incompletely elucidated, but it is clear that the FL $LotA_N$ protein localizes to the *L. pneumophila* vacuole during infection, where each of its OTU domains are primed to cleave nearby polyUb and may function in part to prevent recruitment of and subsequent degradation by p97 activity[41,153]. It will be interesting to investigate if the two OTU domains act on the same host targets, or different targets, during infection by *L. pneumophila*. Finally, the revelation of a highly specific DUB in *L. pneumophila* and a K6/K48-polyUb specific ligase in EHEC (NleL), two pathogens with exceptionally different modes of infection, further sets the stage for an enigmatic role for K6-linked polyUb signaling at the host-pathogen interface. $LotA_N$ will undoubtedly play a key role in elucidating the biological functionality of this signal in the future.

Experimental procedures

Ub chain specificity profiling

K27-linked diUb was prepared chemically (van der Heden van Noort et al, 2017), M1-linked diUb was expressed and purified as a gene fusion, and the six other linkages were prepared enzymatically (Michel et al, 2018). Ub chain cleavage assays were performed as described (Pruneda & Komander, 2019). Bacterial OTUs were prepared at twice the desired concentration in 25 mM Tris, 150 mM NaCl, 10 mM DTT, pH 7.4 and incubated at room temperature for 15 min. diUb chains were prepared at 10 µM in 25 mM Tris, 150 mM NaCl, pH 7.4. The reaction was initiated by mixing 10 µl each of DUB and diUb, and allowed to proceed at 37°C for the indicated time periods. 5 µl reaction samples were quenched in SDS sample buffer, resolved by SDS–PAGE, and visualized by Coomassie

staining. Pixel intensities for the mono- and diUb bands were quantified using ImageJ (Schneider et al, 2012) and used to calculate the percent substrate remaining presented in the heatmap.

UbiCRest analysis

Linkage-specific polyUb chains were assembled according to published methods[192]. NleL and HUWE1 chain assemblies were performed at 37ºC for 2 h in 25 mM Tris, 150 mM NaCl, 10 mM MgCl2, 0.5 mM DTT, pH 7.4 using 375 nM UBE1, 1.5 mM Lys-less UBE2L3, 5 mM ATP, and either 3.75 mM NleL (aa 170-782) or 15 mM HUWE1 (aa 3993-4373). Prior to DUB treatment, all polyUb assembly reactions were quenched by addition of 50 mM EDTA and 5 mM DTT. DUBs were diluted to 10 mM in 25 mM Tris, 150 mM NaCl, 10 mM DTT, pH 7.4 and incubated at room temperature for 10 min. Equal volumes of polyUb assembly and DUB were mixed and incubated at 37ºC for 2 h, prior to quenching in Laemmli sample buffer containing 0.2 M DTT. Reactions were resolved by SDS PAGE prior to transfer onto PVDF membranes using a Trans-Blot Turbo system (BioRad). Membranes were blocked at room temperature for 30 mins with TBS-T (Tris-buffered Saline containing 0.1% Tween-20) containing 5% milk, then incubated with primary anti-Ub antibody (MilliporeSigma, MAB1510-I; 1:1,000 dilution) at 4ºC overnight. Membranes were washed in TBS-T and incubated with secondary antibody (MilliporeSigma, #12-349; 1:5,000 dilution) at room temperature for 1 hr before performing additional TBS-T washes and detection using Clarity ECL reagent (BioRad).

Chapter 5 – Discussion, the impact of the work, and future directions

Perspective

Ubiquitination is a powerful post-translational modification system that enables the cell to regulate an impressive amount of diverse cellular pathways (**Fig 1.3**). As thoroughly discussed in this dissertation, part of this nuanced and diverse regulatory ability of ubiquitination lies within the massive amounts of different polyUb signals that can be attached to substrates, and the different pathways each polyUb signal can initiate[1]. Ub is primarily attached onto Lys residues of substrates, and the seven native Lys residues (and N-terminus) of Ub enable the ability to attach Ub together via these seven native Lys residues means an incredible amount of homogenous and heterogeneous polyUb chains can be attached onto target substrates. For example, an E3 Ub ligase can attach a series of K48-linked tri- or tetra-polyUb onto the Lys residue of its substrate, and then begin linking K63-linked polyUb onto the existing K48 tetra-polyUb chain, generating 'branched' K48/K63-linked polyUb on its substrates, as is the case, at least from one study, for the HECT E3 Ub ligase WWP1[128]. This reasonably simplistic example, one step above the linkage of a homogenous K48-linked polyUb chain onto a substrate, represents just how complex the Ub code can become. Are there domains within Ub regulatory proteins that preferentially bind to branched substrates of two- or even three-polyUb linkage types? Compelling studies have shown that the branched K11/K48-linked polyUb signal is utilized by the anaphase promoting complex (APC/C) to instigate enhanced degradation, relative to the canonical homotypic K48-linked polyUb degradation signal, of its targets during cell proliferation[193–195].

How complex can the polyUb code become? What is the 'bottle-neck' within the system: is it limited by E3 Ub ligases to be cross-specific for multiple polyUb chain-types, by the ability of downstream polyUb-recognizing proteins to selectively bind to one complex polyUb assembly relative to another, or a related example? While it may be enticing to think, as has been thought historically, that the Ub system is primarily critical as the (K48-linked polyUb) signal for proteasomal degradation, it is worthwhile to note the seven native Lys residues have been fully conserved in eukaryotes, highlighting their importance.[196–198]

Yet, despite the overwhelming complexity of polyUb types that *could* exist within the cell, we still lack fundamental knowledge for the most simple, homotypic polyUb chain-types that we *know* exist within the cell (**Fig. 1.3**). K48-linked polyUb, recently K63-linked polyUb, and even more recently M1-linked polyUb, have been well-characterized because researchers have devoted vast amounts of blood, sweat, tears, graduate students, and grant money to identifying which set of E2s or E3s are able to generate that polyUb, which Ub-binding proteins can preferentially recognize that polyUb, and even which DUB can erase that signal. Critically, this dissertation has focused on just a single subset of polyUb and larger questions therein, which is the K6-linked polyUb signal.

K6-linked polyUb has been an understudied polyUb signal, primarily because of the rarity with which a Ub regulator shows a preference for this polyUb linkage-type. This dissertation and work in our lab have only just begun to elucidate the potential roles for this polyUb linkage-type. Compelling (but broad-in-scope) mass spectrometry studies have implicated the K6-linked polyUb signal as both degradative[6,7] and non-degradative[8]. Studies exploring mitophagy, or clearance of damaged mitochondria, also found a potential role for K6-linked polyUb, which was supported by the involvement of the DUB USP30

and RBR-type E3 Ub ligase Parkin in this pathway, both of which have demonstrated at least a partial K6-linked polyUb specificity[63,64]. Other studies on the DNA damage response found increased K6-linked polyUb upon UV-radiation[152,199], and while the ligase generating these signals is unclear, the RING-type E3 Ub ligase BRCA1, which plays critical roles in DNA damage repair, has also shown some preference from K6-linked polyUb[200,201]. Collectively, however, the lack of robust regulators and confounding roles for the K6-linked polyUb signal have prevented a clear elucidation of its cellular roles.

This dissertation used the pathogen-evolved bHECT NleL, which has demonstrated the most convincing K6-linked polyUb ligation of any ligase, as an inlet for studying this linkage-type, and resulted in the engineering of a K6-polyUb specific version of NleL. This dissertation also described the use of the pathogen evolved DUB LotA as a new tool for studying K6-linked polyUb. Finally, this dissertation also described the development of a new methodology, UbiReal, for monitoring ubiquitination in a high-throughput, and even linkage-specific, manner. A brief discussion of each work and its impact is included below.

The work on UbiReal

Chapter 2 and Appendix A of this dissertation described the UbiReal methodology. This assay had originally been developed with the intention of having an all-in-one assay that could be versatile enough to monitor the flow of Ub, from the initial E1~Ub formation step to the deubiquitination of polyUb by DUBs, but the assay also was also able to be used as a drug screen as well as for monitoring the interaction of different Ub regulators, i.e., E2-E3 pairs. In Chapter 3, in addition to using it to monitor ligation activity of NleL mutants,

we also adapted this methodology to monitor the transthiolation of UBE2L3~Ub to NleL~Ub and free Ub, enabling characterization of E3 mutants that may be involved in E2 interactions. The methodology was also published as a methods paper, which is provided in Appendix A.

As a methodology for monitoring all aspects of ubiquitination, future work on UbiReal is generally broad in scope. Since its publication, the methodology has been adapted for use as a high-throughput drug screen using the Ub-like (UBL) modifier UFM1[202], used to monitor polyUb formation by the E3 RFFL[203], and for monitoring the ligase activity of the E3 MARCH5 in the presence of different lipids[204]. As the assay is limited only by the availability of a fluorescently labeled substrate and downstream regulators, the assay could lend itself as a roadmap for generating similar assays of Ub-like modifiers, as our lab has since demonstrated with UFM1[202], but also for UBLs like SUMO, NEDD8, ISG15, and others[205]. Notably, considering that UbiReal could be used to validate drugs of the Ub pathway (**Fig. 2.2**) and an analogous assay could be used to screen for drugs of the UFM1 pathway[202], the utility of UbiReal as a drug screen may be as yet underutilized.

bHECTs

The majority of my dissertation work focused on characterizing the HECT-like E3 Ub ligases in bacteria. This fascinating family of ligases had previously only consisted of 2 examples, and this work expanded it to include more members from other human pathogens as well as plant pathogens. Along with foundational structural work that solved the apo and E2-bound structures of bHECTs SopA and NleL, we were able to construct a

full model for Ub ligation by bHECTs through using NMR to characterize the E2~Ub/bHECT intermediate, and X-ray crystallography to characterize the bHECT~Ub intermediate and the formation of polyUb. In phase 1 of this pathway, following binding of the E2 and transthiolation to the bHECT active site Cys, a large rearrangement of the C-lobe about the linker domain primes the bHECT~Ub intermediate for ligation (**Fig. 5.1**). This movement from the E2 may be partially mediated by the Cys loop of the bHECT, which, following Ub loading, adopts a highly-ordered inward conformation that clashes with the E2 interaction site on the C-lobe. The C-lobe of the bHECT~Ub utilizes several contacts between the Cys loop and C-terminal tail of Ub to form the interaction site, though many mutually exclusive contacts were observed between C-lobe and Ub among the NleL-Ub, SopA-Ub, and VsHECT-Ub structures. In phase 2, once in the primed position, the Cys loop and acidic loop can form an acceptor site, which we captured as a K48-linked polyUb specific acceptor site in this case, that places the K48 of the acceptor Ub towards the active site, and forming a K48-linked diUb product (**Fig. 5.1**). We also noted the E2-interaction site was occluded by the acceptor Ub binding, which could hold insight into the chain-building mechanism for bHECTs. Interestingly, the structure of SopA-Ub enabled us to make a structural model of substrate ligation using the structure of the SopA N-lobe bound to one of its host targets, TRIM56. Further, using insights gained from the Cys loop and acidic loop acceptor site in the NleL-Ub structure, we were able to augment the polyUb specificity of SopA towards K6-linked polyUb, and target TRIM56 with this polyUb linkage. Fascinatingly, the same insights allowed us to insert mutations into the eukaryotic HECT-type family member HUWE1, increasing its ligation of K6-linked polyUb.

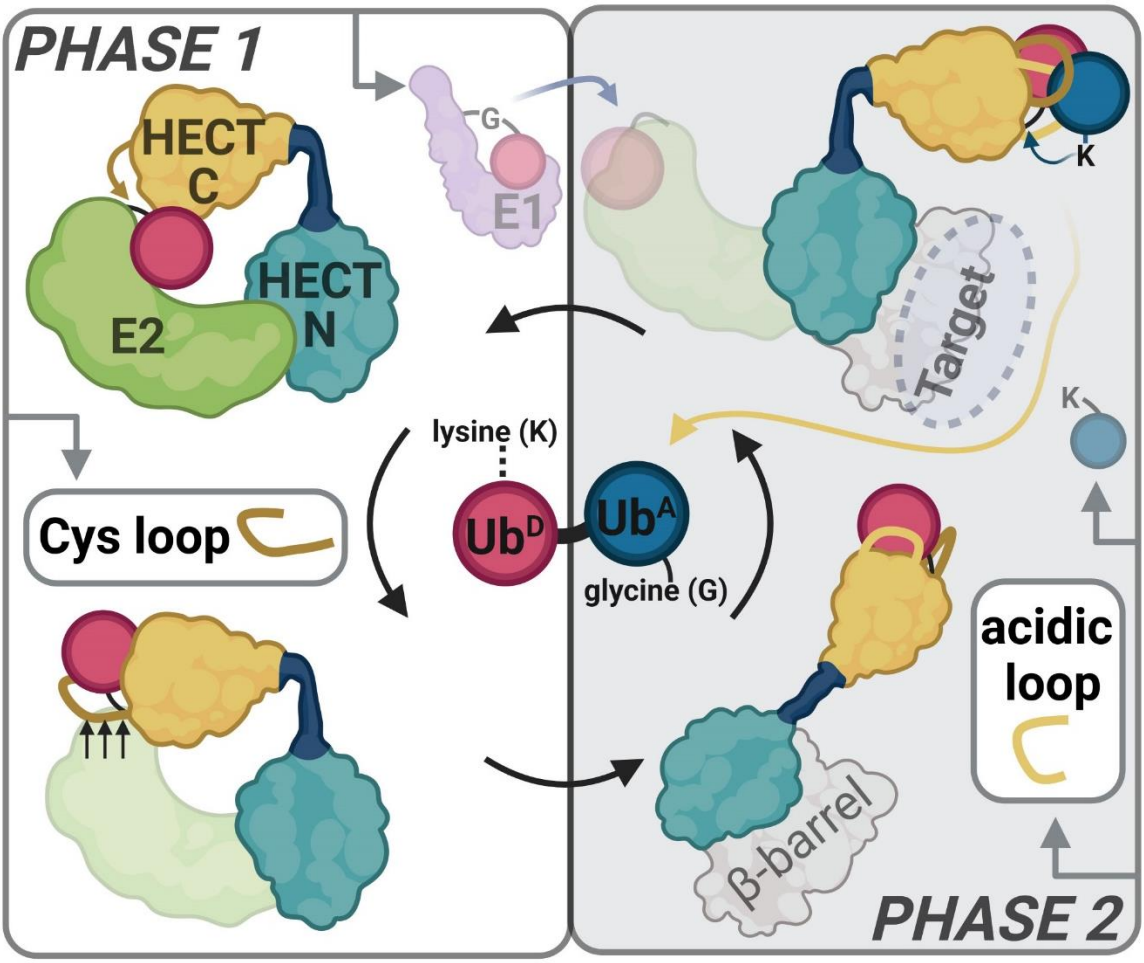

Figure 5.1 bHECT polyUb ligation mechanism

Overview of the mechanism of ligation by bHECTs.

Future work should foremost aim to reveal a function for the ligation of K6-linked polyUb by NleL, especially as it pertains to a successful EHEC infection and to the host targets. Other important investigations should explore how bHECTs, and E3 Ub ligases in general, coordinate donor Ub, acceptor Ub, polyUb chains and substrates during substrate polyubiquitination. As discussed in Chapter 3, it remains to be investigated if mutations in the acidic loop are structurally altering an acceptor site, or potentially altering the pKa of the catalytic interface and favoring nucleophilic attack by the K6 of Ub over the other Ub Lys residues. While insights from Chapter 3 enabled us to apply similar logic to HUWE1 and increase its ligation of K6-linked polyUb, the presence of different loops nearby the active site in different HUWE1 structures raises the potentiality that different structural conformations in the same E3 support different polyUb linkage specificities. However, as mentioned, it is possible we could be observing something more closely related to the alteration of pKa at the active site, and the resulting polyUb linkages types may be influenced by the native pKa of the different Ub Lys residues. Notably, it is interesting that more E3 Ub ligases do not show ligation of K6-linked polyUb, if it is the case that K6 of Ub is one of the more reactive Ub Lys residues. Regardless, a thorough investigation of the roles of pKa and different acidic loops at the active site in different conformations and their roles in polyUb linkage specificity is an important future direction. Excellent candidates for this future work may include very recently identified eukaryotic E3 Ub ligases that show surprising K6-linked polyUb specificity[206,207].

bOTUs

The polyUb chain specificity of the recently elucidated OTU family of DUBs in bacteria

provided a plethora of insights into polyUb targeting by pathogens. While the initial set of these OTUs revealed only a few examples of DUBs selective for one polyUb linkage-type, structural work and sequence analysis revealed the fascinating and ongoing evolution of insertion sites within the S1 site of the OTU domain that mediate part of the Ub-binding specificity. However, in terms of advancing the study of K6-linked polyUb, the most beneficial discovery was that of the K6-linked polyUb specificity of $LotA_N$. Structural work in our lab revealed the special K6-polyUb interaction site within the $LotA_N$ S1' site, that enabled the K6-polyUb linkage to be selectively targeted. Using assemblies of complex polyUb chains and E3 Ub ligases with K6 polyUb ligation specificity, we were able to demonstrate the utility of $LotA_N$ in the application of the UbiCRest methodology.

Further work should aim to identify the targets of $LotA_N$ during *L. pneumophila* infection, and ideally identify the potential K6-linked polyUb specific ligase that $LotA_N$ has evolved to regulate, be it of pathogen or host origin. In combination with other DUBs targeting K6-linked polyUb[167,208], a role for K6-linked polyUb at the host-pathogen interface is increasingly apparent, highlighting the need for future studies to explore the connection. With 1) new revelations for the direct targeting of intracellular bacteria by the Ub system[45], 2) investigations of the role of LotA in protecting the LCV from Ub targeting[153], and 3) new results identifying host E3s that ligate K6-linked polyUb at the host-pathogen interface[206,207], the role of Ub, and especially K6-linked polyUb, in host defense is of growing interest. Finally, since the publication of $LotA_N$, augmented constructs have been employed as a tool for performing pull-downs of K6-linked polyUb[206], highlighting that the work with LotA has indeed provided critical tools for future work exploring K6-linked

polyUb signaling, even aside from its demonstrated utility in UbiCRest[153].

In sum

Collectively, this dissertation has provided a novel K6-polyUb specific ligase and characterized a K6-polyUb specific DUB, which will enable the study of the biological functionality of this enigmatic signal. Along the way to these achievements, this thesis also provided thorough mechanistic insight into and expanded the family of the bacterial HECT-like E3 Ub ligases, and revealed the polyUb targeting specificities of a recently identified set of OTU deubiquitinases in bacteria. Along with the powerful UbiReal methodology, this dissertation has provided numerous tools to the field of Ub signaling, and sets the stage for further studies aimed at fully deciphering the Ub code.

References

1. Komander, D., and Rape, M. (2012). The Ubiquitin Code. Annu Rev Biochem *81*, 203–229. 10.1146/annurev-biochem-060310-170328.

2. Clague, M.J., Heride, C., and Urbé, S. (2015). The demographics of the ubiquitin system. Trends Cell Biol *25*, 417–426. 10.1016/j.tcb.2015.03.002.

3. Haakonsen, D.L., and Rape, M. (2019). Branching Out: Improved Signaling by Heterotypic Ubiquitin Chains. Trends Cell Biol *29*, 704–716. 10.1016/j.tcb.2019.06.003.

4. Akutsu, M., Dikic, I., and Bremm, A. (2016). Ubiquitin chain diversity at a glance. J Cell Sci *129*, 875–880. 10.1242/jcs.183954.

5. Swatek, K.N., and Komander, D. (2016). Ubiquitin modifications. Cell Res *26*, 399–422. 10.1038/cr.2016.39.

6. Kim, W., Bennett, E.J., Huttlin, E.L., Guo, A., Li, J., Possemato, A., Sowa, M.E., Rad, R., Rush, J., Comb, M.J., et al. (2011). Systematic and Quantitative Assessment of the Ubiquitin-Modified Proteome. Mol Cell *44*, 325–340. 10.1016/j.molcel.2011.08.025.

7. Rose, C.M., Isasa, M., Ordureau, A., Prado, M.A., Beausoleil, S.A., Jedrychowski, M.P., Finley, D.J., Harper, J.W., and Gygi, S.P. (2016). Highly Multiplexed Quantitative Mass Spectrometry Analysis of Ubiquitylomes. Cell Syst *3*, 395-403.e4. 10.1016/j.cels.2016.08.009.

8. Wagner, S.A., Beli, P., Weinert, B.T., Nielsen, M.L., Cox, J., Mann, M., and Choudhary, C. (2011). A Proteome-wide, Quantitative Survey of In Vivo Ubiquitylation Sites Reveals Widespread Regulatory Roles*. Mol Cell Proteomics *10*, M111.013284. 10.1074/mcp.m111.013284.

9. Okuda, J., Toyotome, T., Kataoka, N., Ohno, M., Abe, H., Shimura, Y., Seyedarabi, A., Pickersgill, R., and Sasakawa, C. (2005). Shigella effector IpaH9.8 binds to a splicing factor U2AF35 to modulate host immune responses. Biochem Bioph Res Co *333*, 531–539. 10.1016/j.bbrc.2005.05.145.

10. Wandel, M.P., Pathe, C., Werner, E.I., Ellison, C.J., Boyle, K.B., Malsburg, A. von der, Rohde, J., and Randow, F. (2017). GBPs Inhibit Motility of Shigella flexneri but Are Targeted for Degradation by the Bacterial Ubiquitin Ligase IpaH9.8. Cell Host Microbe *22*, 507-518.e5. 10.1016/j.chom.2017.09.007.

11. Li, P., Jiang, W., Yu, Q., Liu, W., Zhou, P., Li, J., Xu, J., Xu, B., Wang, F., and Shao, F. (2017). Ubiquitination and degradation of GBPs by a Shigella effector to suppress host defence. Nature *551*, 378–383. 10.1038/nature24467.

12. Rytkönen, A., Poh, J., Garmendia, J., Boyle, C., Thompson, A., Liu, M., Freemont, P., Hinton, J.C.D., and Holden, D.W. (2007). SseL, a Salmonella deubiquitinase required for macrophage killing and virulence. Proc National Acad Sci *104*, 3502–3507. 10.1073/pnas.0610095104.

13. Tanner, K., Brzovic, P., and Rohde, J.R. (2014). The bacterial pathogen-ubiquitin interface: lessons learned from Shigella: The bacterial pathogen-ubiquitin interface. Cell Microbiol *17*, 35–44. 10.1111/cmi.12390.

14. Rohde, J.R., Breitkreutz, A., Chenal, A., Sansonetti, P.J., and Parsot, C. (2007). Type III Secretion Effectors of the IpaH Family Are E3 Ubiquitin Ligases. Cell Host Microbe *1*, 77–83. 10.1016/j.chom.2007.02.002.

15. Zhang, Y., Higashide, W.M., McCormick, B.A., Chen, J., and Zhou, D. (2006). The inflammation-associated Salmonella SopA is a HECT-like E3 ubiquitin ligase. Mol Microbiol *62*, 786–793. 10.1111/j.1365-2958.2006.05407.x.

16. Hsu, F., Luo, X., Qiu, J., Teng, Y.-B., Jin, J., Smolka, M.B., Luo, Z.-Q., and Mao, Y. (2014). The Legionella effector SidC defines a unique family of ubiquitin ligases important for bacterial phagosomal remodeling. Proc National Acad Sci *111*, 10538–10543. 10.1073/pnas.1402605111.

17. Lin, D.Y., Diao, J., Zhou, D., and Chen, J. (2011). Biochemical and Structural Studies of a HECT-like Ubiquitin Ligase from Escherichia coli O157:H7. J Biol Chem *286*, 441–449. 10.1074/jbc.m110.167643.

18. Mevissen, T.E.T., and Komander, D. (2017). Mechanisms of Deubiquitinase Specificity and Regulation. Annu Rev Biochem *86*, 159–192. 10.1146/annurev-biochem-061516-044916.

19. Sheedlo, M.J., Qiu, J., Tan, Y., Paul, L.N., Luo, Z.-Q., and Das, C. (2015). Structural basis of substrate recognition by a bacterial deubiquitinase important for dynamics of phagosome ubiquitination. Proc National Acad Sci *112*, 15090–15095. 10.1073/pnas.1514568112.

20. Misaghi, S., Balsara, Z.R., Catic, A., Spooner, E., Ploegh, H.L., and Starnbach, M.N. (2006). Chlamydia trachomatis-derived deubiquitinating enzymes in mammalian cells during infection. Mol Microbiol *61*, 142–150. 10.1111/j.1365-2958.2006.05199.x.

21. Pruneda, J.N., Durkin, C.H., Geurink, P.P., Ovaa, H., Santhanam, B., Holden, D.W., and Komander, D. (2016). The Molecular Basis for Ubiquitin and Ubiquitin-like

Specificities in Bacterial Effector Proteases. Mol Cell *63*, 261–276. 10.1016/j.molcel.2016.06.015.

22. Schubert, A.F., Nguyen, J.V., Franklin, T.G., Geurink, P.P., Roberts, C.G., Sanderson, D.J., Miller, L.N., Ovaa, H., Hofmann, K., Pruneda, J.N., et al. (2020). Identification and characterization of diverse OTU deubiquitinases in bacteria. Embo J *39*, e105127. 10.15252/embj.2020105127.

23. Wan, M., Wang, X., Huang, C., Xu, D., Wang, Z., Zhou, Y., and Zhu, Y. (2019). A bacterial effector deubiquitinase specifically hydrolyses linear ubiquitin chains to inhibit host inflammatory signalling. Nat Microbiol *4*, 1282–1293. 10.1038/s41564-019-0454-1.

24. Sanada, T., Kim, M., Mimuro, H., Suzuki, M., Ogawa, M., Oyama, A., Ashida, H., Kobayashi, T., Koyama, T., Nagai, S., et al. (2012). The Shigella flexneri effector OspI deamidates UBC13 to dampen the inflammatory response. Nature *483*, 623–626. 10.1038/nature10894.

25. Zhang, L., Ding, X., Cui, J., Xu, H., Chen, J., Gong, Y.-N., Hu, L., Zhou, Y., Ge, J., Lu, Q., et al. (2012). Cysteine methylation disrupts ubiquitin-chain sensing in NF-κB activation. Nature *481*, 204–208. 10.1038/nature10690.

26. Fiskin, E., Bhogaraju, S., Herhaus, L., Kalayil, S., Hahn, M., and Dikic, I. (2017). Structural basis for the recognition and degradation of host TRIM proteins by Salmonella effector SopA. Nat Commun *8*, 14004. 10.1038/ncomms14004.

27. Wood, M.W., Jones, M.A., Watson, P.R., Siber, A.M., McCormick, B.A., Hedges, S., Rosqvist, R., Wallis, T.S., and Galyov, E.E. (2000). The secreted effector protein of Salmonella dublin, SopA, is translocated into eukaryotic cells and influences the induction of enteritis. Cell Microbiol *2*, 293–303. 10.1046/j.1462-5822.2000.00054.x.

28. Keszei, A.F.A., and Sicheri, F. (2017). Mechanism of catalysis, E2 recognition, and autoinhibition for the IpaH family of bacterial E3 ubiquitin ligases. Proc National Acad Sci *114*, 1311–1316. 10.1073/pnas.1611595114.

29. Levin, I., Eakin, C., Blanc, M.-P., Klevit, R.E., Miller, S.I., and Brzovic, P.S. (2010). Identification of an unconventional E3 binding surface on the UbcH5∼Ub conjugate recognized by a pathogenic bacterial E3 ligase. Proc. Natl. Acad. Sci. *107*, 2848–2853. 10.1073/pnas.0914821107.

30. Ashida, H., Kim, M., Schmidt-Supprian, M., Ma, A., Ogawa, M., and Sasakawa, C. (2010). A bacterial E3 ubiquitin ligase IpaH9.8 targets NEMO/IKKγ to dampen the host NF-κB-mediated inflammatory response. Nat Cell Biol *12*, 66–73. 10.1038/ncb2006.

31. Haraga, A., and Miller, S.I. (2006). A Salmonella type III secretion effector interacts with the mammalian serine/threonine protein kinase PKN1. Cell Microbiol *8*, 837–846. 10.1111/j.1462-5822.2005.00670.x.

32. Zheng, Z., Wei, C., Guan, K., Yuan, Y., Zhang, Y., Ma, S., Cao, Y., Wang, F., Zhong, H., and He, X. (2016). Bacterial E3 Ubiquitin Ligase IpaH4.5 of Shigella flexneri Targets TBK1 To Dampen the Host Antibacterial Response. J Immunol *196*, 1199–1208. 10.4049/jimmunol.1501045.

33. Ashida, H., Nakano, H., and Sasakawa, C. (2013). Shigella IpaH0722 E3 Ubiquitin Ligase Effector Targets TRAF2 to Inhibit PKC–NF-κB Activity in Invaded Epithelial Cells. Plos Pathog *9*, e1003409. 10.1371/journal.ppat.1003409.

34. Jong, M.F. de, Liu, Z., Chen, D., and Alto, N.M. (2016). Shigella flexneri suppresses NF-κB activation by inhibiting linear ubiquitin chain ligation. Nat Microbiol *1*, 16084. 10.1038/nmicrobiol.2016.84.

35. Sheng, X., You, Q., Zhu, H., Chang, Z., Li, Q., Wang, H., Wang, C., Wang, H., Hui, L., Du, C., et al. (2017). Bacterial effector NleL promotes enterohemorrhagic E. coli-induced attaching and effacing lesions by ubiquitylating and inactivating JNK. Plos Pathog *13*, e1006534. 10.1371/journal.ppat.1006534.

36. Gan, N., Nakayasu, E.S., Hollenbeck, P.J., and Luo, Z.-Q. (2019). Legionella pneumophila inhibits immune signalling via MavC-mediated transglutaminase-induced ubiquitination of UBE2N. Nat Microbiol *4*, 134–143. 10.1038/s41564-018-0282-8.

37. Gan, N., Guan, H., Huang, Y., Yu, T., Fu, J., Nakayasu, E.S., Puvar, K., Das, C., Wang, D., Ouyang, S., et al. (2020). Legionella pneumophila regulates the activity of UBE2N by deamidase-mediated deubiquitination. Embo J *39*, e102806. 10.15252/embj.2019102806.

38. Wang, Y., Zhan, Q., Wang, X., Li, P., Liu, S., Gao, G., and Gao, P. (2020). Insights into catalysis and regulation of non-canonical ubiquitination and deubiquitination by bacterial deamidase effectors. Nat Commun *11*, 2751. 10.1038/s41467-020-16587-w.

39. Mesquita, F.S., Thomas, M., Sachse, M., Santos, A.J.M., Figueira, R., and Holden, D.W. (2012). The Salmonella Deubiquitinase SseL Inhibits Selective Autophagy of Cytosolic Aggregates. Plos Pathog *8*, e1002743. 10.1371/journal.ppat.1002743.

40. Negrate, G.L., Krieg, A., Faustin, B., Loeffler, M., Godzik, A., Krajewski, S., and Reed, J.C. (2008). ChlaDub1 of Chlamydia trachomatis suppresses NF-κB activation and inhibits IκBα ubiquitination and degradation. Cell Microbiol *10*, 1879–1892. 10.1111/j.1462-5822.2008.01178.x.

41. Kubori, T., Kitao, T., Ando, H., and Nagai, H. (2018). LotA, a Legionella deubiquitinase, has dual catalytic activity and contributes to intracellular growth. Cell Microbiol *20*, e12840. 10.1111/cmi.12840.

42. Lorenz, S. (2018). Structural mechanisms of HECT-type ubiquitin ligases. Biol Chem *399*, 127–145. 10.1515/hsz-2017-0184.

43. Cotton, T.R., and Lechtenberg, B.C. (2020). Chain reactions: molecular mechanisms of RBR ubiquitin ligases. Biochem Soc T *48*, 1737–1750. 10.1042/bst20200237.

44. Pao, K.-C., Wood, N.T., Knebel, A., Rafie, K., Stanley, M., Mabbitt, P.D., Sundaramoorthy, R., Hofmann, K., Aalten, D.M.F. van, and Virdee, S. (2018). Activity-based E3 ligase profiling uncovers an E3 ligase with esterification activity. Nature *556*, 381–385. 10.1038/s41586-018-0026-1.

45. Otten, E.G., Werner, E., Crespillo-Casado, A., Boyle, K.B., Dharamdasani, V., Pathe, C., Santhanam, B., and Randow, F. (2021). Ubiquitylation of lipopolysaccharide by RNF213 during bacterial infection. Nature *594*, 111–116. 10.1038/s41586-021-03566-4.

46. Kamadurai, H.B., Souphron, J., Scott, D.C., Duda, D.M., Miller, D.J., Stringer, D., Piper, R.C., and Schulman, B.A. (2009). Insights into ubiquitin transfer cascades from a structure of a UbcH5B∼Ubiquitin-HECT(NEDD4L) complex. Mol Cell *36*, 1095–1102. 10.1016/j.molcel.2009.11.010.

47. Maspero, E., Valentini, E., Mari, S., Cecatiello, V., Soffientini, P., Pasqualato, S., and Polo, S. (2013). Structure of a ubiquitin-loaded HECT ligase reveals the molecular basis for catalytic priming. Nat Struct Mol Biol *20*, 696–701. 10.1038/nsmb.2566.

48. Jäckl, M., Stollmaier, C., Strohäker, T., Hyz, K., Maspero, E., Polo, S., and Wiesner, S. (2018). β-Sheet Augmentation Is a Conserved Mechanism of Priming HECT E3 Ligases for Ubiquitin Ligation. J Mol Biol *430*, 3218–3233. 10.1016/j.jmb.2018.06.044.

49. Diao, J., Zhang, Y., Huibregtse, J.M., Zhou, D., and Chen, J. (2008). Crystal structure of SopA, a Salmonella effector protein mimicking a eukaryotic ubiquitin ligase. Nat Struct Mol Biol *15*, 65–70. 10.1038/nsmb1346.

50. Lin, D.Y., Diao, J., and Chen, J. (2012). Crystal structures of two bacterial HECT-like E3 ligases in complex with a human E2 reveal atomic details of pathogen-host interactions. Proc National Acad Sci *109*, 1925–1930. 10.1073/pnas.1115025109.

51. Franklin, T.G., Brzovic, P.S., and Pruneda, J.N. (2023). Bacterial mimicry of eukaryotic HECT ubiquitin ligation. bioRxiv, 2023.06.05.543783. 10.1101/2023.06.05.543783.

52. Zhang, S., Santos, R.L., Tsolis, R.M., Stender, S., Hardt, W.-D., Bäumler, A.J., and Adams, L.G. (2002). The Salmonella enterica Serotype Typhimurium Effector Proteins SipA, SopA, SopB, SopD, and SopE2 Act in Concert To Induce Diarrhea in Calves. Infect Immun *70*, 3843–3855. 10.1128/iai.70.7.3843-3855.2002.

53. Layton, A.N., Brown, P.J., and Galyov, E.E. (2005). The Salmonella Translocated Effector SopA Is Targeted to the Mitochondria of Infected Cells. J Bacteriol *187*, 3565–3571. 10.1128/jb.187.10.3565-3571.2005.

54. Tobe, T., Beatson, S.A., Taniguchi, H., Abe, H., Bailey, C.M., Fivian, A., Younis, R., Matthews, S., Marches, O., Frankel, G., et al. (2006). An extensive repertoire of type III secretion effectors in Escherichia coli O157 and the role of lambdoid phages in their dissemination. Proc National Acad Sci *103*, 14941–14946. 10.1073/pnas.0604891103.

55. Zhang, Y., Higashide, W., Dai, S., Sherman, D.M., and Zhou, D. (2005). Recognition and Ubiquitination of Salmonella Type III Effector SopA by a Ubiquitin E3 Ligase, HsRMA1*. J Biol Chem *280*, 38682–38688. 10.1074/jbc.m506309200.

56. Nuber, U., and Scheffner, M. (1999). Identification of Determinants in E2 Ubiquitin-conjugating Enzymes Required for HECT E3 Ubiquitin-Protein Ligase Interaction. J. Biol. Chem. *274*, 7576–7582. 10.1074/jbc.274.11.7576.

57. Hospenthal, M.K., Freund, S.M.V., and Komander, D. (2013). Assembly, analysis and architecture of atypical ubiquitin chains. Nat Struct Mol Biol *20*, 555–565. 10.1038/nsmb.2547.

58. Kamanova, J., Sun, H., Lara-Tejero, M., and Galán, J.E. (2016). The Salmonella Effector Protein SopA Modulates Innate Immune Responses by Targeting TRIM E3 Ligase Family Members. Plos Pathog *12*, e1005552. 10.1371/journal.ppat.1005552.

59. Piscatelli, H., Kotkar, S.A., McBee, M.E., Muthupalani, S., Schauer, D.B., Mandrell, R.E., Leong, J.M., and Zhou, D. (2011). The EHEC Type III Effector NleL Is an E3 Ubiquitin Ligase That Modulates Pedestal Formation. Plos One *6*, e19331. 10.1371/journal.pone.0019331.

60. Sheng, X., You, Q., Zhu, H., Li, Q., Gao, H., Wang, H., You, C., Meng, Q., Nie, Y., Zhang, X., et al. (2020). Enterohemorrhagic E. coli effector NleL disrupts host NF-κB signaling by targeting multiple host proteins. J Mol Cell Biol. 10.1093/jmcb/mjaa003.

61. Zhu, B., Das, S., Mitra, S., Farris, T.R., and McBride, J.W. (2017). Ehrlichia chaffeensis TRP120 Moonlights as a HECT E3 Ligase Involved in Self- and Host Ubiquitination To Influence Protein Interactions and Stability for Intracellular Survival. Infect Immun *85*, e00290-17. 10.1128/iai.00290-17.

62. Cunningham, C.N., Baughman, J.M., Phu, L., Tea, J.S., Yu, C., Coons, M., Kirkpatrick, D.S., Bingol, B., and Corn, J.E. (2015). USP30 and parkin homeostatically regulate atypical ubiquitin chains on mitochondria. Nat. Cell Biol. *17*, 160–169. 10.1038/ncb3097.

63. Bingol, B., Tea, J.S., Phu, L., Reichelt, M., Bakalarski, C.E., Song, Q., Foreman, O., Kirkpatrick, D.S., and Sheng, M. (2014). The mitochondrial deubiquitinase USP30 opposes parkin-mediated mitophagy. Nature *510*, 370–375. 10.1038/nature13418.

64. Ordureau, A., Sarraf, S.A., Duda, D.M., Heo, J.-M., Jedrychowski, M.P., Sviderskiy, V.O., Olszewski, J.L., Koerber, J.T., Xie, T., Beausoleil, S.A., et al. (2014). Quantitative

Proteomics Reveal a Feedforward Mechanism for Mitochondrial PARKIN Translocation and Ubiquitin Chain Synthesis. Mol. Cell *56*, 360–375. 10.1016/j.molcel.2014.09.007.

65. Gersch, M., Gladkova, C., Schubert, A.F., Michel, M.A., Maslen, S., and Komander, D. (2017). Mechanism and regulation of the Lys6-selective deubiquitinase USP30. Nat. Struct. Mol. Biol. *24*, 920–930. 10.1038/nsmb.3475.

66. Clague, M.J., Urbé, S., and Komander, D. (2019). Breaking the chains: deubiquitylating enzyme specificity begets function. Nat. Rev. Mol. Cell Biol. *20*, 338–352. 10.1038/s41580-019-0099-1.

67. Keusekotten, K., Elliott, P.R., Glockner, L., Fiil, B.K., Damgaard, R.B., Kulathu, Y., Wauer, T., Hospenthal, M.K., Gyrd-Hansen, M., Krappmann, D., et al. (2013). OTULIN Antagonizes LUBAC Signaling by Specifically Hydrolyzing Met1-Linked Polyubiquitin. Cell *153*, 1312–1326. 10.1016/j.cell.2013.05.014.

68. Fiil, B.K., Damgaard, R.B., Wagner, S.A., Keusekotten, K., Fritsch, M., Bekker-Jensen, S., Mailand, N., Choudhary, C., Komander, D., and Gyrd-Hansen, M. (2013). OTULIN Restricts Met1-Linked Ubiquitination to Control Innate Immune Signaling. Mol. Cell *50*, 818–830. 10.1016/j.molcel.2013.06.004.

69. Mevissen, T.E.T., Kulathu, Y., Mulder, M.P.C., Geurink, P.P., Maslen, S.L., Gersch, M., Elliott, P.R., Burke, J.E., Tol, B.D.M. van, Akutsu, M., et al. (2016). Molecular basis of Lys11-polyubiquitin specificity in the deubiquitinase Cezanne. Nature *538*, 402–405. 10.1038/nature19836.

70. Lange, S.M., Armstrong, L.A., and Kulathu, Y. (2022). Deubiquitinases: From mechanisms to their inhibition by small molecules. Mol. Cell *82*, 15–29. 10.1016/j.molcel.2021.10.027.

71. Juang, Y.-C., Landry, M.-C., Sanches, M., Vittal, V., Leung, C.C.Y., Ceccarelli, D.F., Mateo, A.-R.F., Pruneda, J.N., Mao, D.Y.L., Szilard, R.K., et al. (2012). OTUB1 Co-opts Lys48-Linked Ubiquitin Recognition to Suppress E2 Enzyme Function. Mol Cell *45*, 384–397. 10.1016/j.molcel.2012.01.011.

72. Roberts, C.G., Franklin, T.G., and Pruneda, J.N. (2023). Ubiquitin-targeted bacterial effectors: rule breakers of the ubiquitin system. EMBO J. *42*, e114318. 10.15252/embj.2023114318.

73. Popovic, D., Vucic, D., and Dikic, I. (2014). Ubiquitination in disease pathogenesis and treatment. Nat Med *20*, 1242–1253. 10.1038/nm.3739.

74. Kirkin, V., and Dikic, I. (2011). Ubiquitin networks in cancer. Curr. Opin. Genet. Dev. *21*, 21–28. 10.1016/j.gde.2010.10.004.

75. Zheng, Q., Huang, T., Zhang, L., Zhou, Y., Luo, H., Xu, H., and Wang, X. (2016). Dysregulation of Ubiquitin-Proteasome System in Neurodegenerative Diseases. Front. Aging Neurosci. *8*, 303. 10.3389/fnagi.2016.00303.

76. Hu, H., and Sun, S.-C. (2016). Ubiquitin signaling in immune responses. Cell Res *26*, 457–483. 10.1038/cr.2016.40.

77. Huang, X., and Dixit, V.M. (2016). Drugging the undruggables: exploring the ubiquitin system for drug development. Cell Res. *26*, 484–498. 10.1038/cr.2016.31.

78. Hideshima, T., Richardson, P., Chauhan, D., Palombella, V.J., Elliott, P.J., Adams, J., and Anderson, K.C. (2001). The proteasome inhibitor PS-341 inhibits growth, induces apoptosis, and overcomes drug resistance in human multiple myeloma cells. Cancer Res. *61*, 3071–3076.

79. Vassilev, L.T., Vu, B.T., Graves, B., Carvajal, D., Podlaski, F., Filipovic, Z., Kong, N., Kammlott, U., Lukacs, C., Klein, C., et al. (2004). In Vivo Activation of the p53 Pathway by Small-Molecule Antagonists of MDM2. Science *303*, 844–848. 10.1126/science.1092472.

80. Gavory, G., O'Dowd, C.R., Helm, M.D., Flasz, J., Arkoudis, E., Dossang, A., Hughes, C., Cassidy, E., McClelland, K., Odrzywol, E., et al. (2018). Discovery and characterization of highly potent and selective allosteric USP7 inhibitors. Nat. Chem. Biol. *14*, 118–125. 10.1038/nchembio.2528.

81. Kategaya, L., Lello, P.D., Rougé, L., Pastor, R., Clark, K.R., Drummond, J., Kleinheinz, T., Lin, E., Upton, J.-P., Prakash, S., et al. (2017). USP7 small-molecule inhibitors interfere with ubiquitin binding. Nature *550*, 534–538. 10.1038/nature24006.

82. Lamberto, I., Liu, X., Seo, H.-S., Schauer, N.J., Iacob, R.E., Hu, W., Das, D., Mikhailova, T., Weisberg, E.L., Engen, J.R., et al. (2017). Structure-Guided Development of a Potent and Selective Non-covalent Active-Site Inhibitor of USP7. Cell Chem. Biol. *24*, 1490-1500.e11. 10.1016/j.chembiol.2017.09.003.

83. Pozhidaeva, A., Valles, G., Wang, F., Wu, J., Sterner, D.E., Nguyen, P., Weinstock, J., Kumar, K.G.S., Kanyo, J., Wright, D., et al. (2017). USP7-Specific Inhibitors Target and Modify the Enzyme's Active Site via Distinct Chemical Mechanisms. Cell Chem. Biol. *24*, 1501-1512.e5. 10.1016/j.chembiol.2017.09.004.

84. Turnbull, A.P., Ioannidis, S., Krajewski, W.W., Pinto-Fernandez, A., Heride, C., Martin, A.C.L., Tonkin, L.M., Townsend, E.C., Buker, S.M., Lancia, D.R., et al. (2017). Molecular basis of USP7 inhibition by selective small-molecule inhibitors. Nature *550*, 481–486. 10.1038/nature24451.

85. Coleman, K.G., and Crews, C.M. (2017). Proteolysis–Targeting Chimeras: Harnessing the Ubiquitin–Proteasome System to Induce Degradation of Specific Target Proteins. Annu. Rev. Cancer Biol. *2*, 1–18. 10.1146/annurev-cancerbio-030617-050430.

86. Macarrón, R., and Hertzberg, R.P. (2009). High Throughput Screening, Methods and Protocols, Second Edition. Methods Mol. Biol. *565*, 1–32. 10.1007/978-1-60327-258-2_1.

87. Dang, L.C., Melandri, F.D., and Stein, R.L. (1998). Kinetic and Mechanistic Studies on the Hydrolysis of Ubiquitin C-Terminal 7-Amido-4-Methylcoumarin by Deubiquitinating Enzymes. Biochemistry *37*, 1868–1879. 10.1021/bi9723360.

88. Hassiepen, U., Eidhoff, U., Meder, G., Bulber, J.-F., Hein, A., Bodendorf, U., Lorthiois, E., and Martoglio, B. (2007). A sensitive fluorescence intensity assay for deubiquitinating proteases using ubiquitin-rhodamine110-glycine as substrate. Anal. Biochem. *371*, 201–207. 10.1016/j.ab.2007.07.034.

89. Geurink, P.P., Oualid, F.E., Jonker, A., Hameed, D.S., and Ovaa, H. (2012). A General Chemical Ligation Approach Towards Isopeptide-Linked Ubiquitin and Ubiquitin-Like Assay Reagents. ChemBioChem *13*, 293–297. 10.1002/cbic.201100706.

90. Ye, Y., Akutsu, M., Reyes-Turcu, F., Enchev, R.I., Wilkinson, K.D., and Komander, D. (2011). Polyubiquitin binding and cross-reactivity in the USP domain deubiquitinase USP21. EMBO Rep. *12*, 350–357. 10.1038/embor.2011.17.

91. Foote, P.K., Krist, D.T., and Statsyuk, A.V. (2017). High-Throughput Screening of HECT E3 Ubiquitin Ligases Using UbFluor. Curr. Protoc. Chem. Biol. *9*, 174–195. 10.1002/cpch.24.

92. Krist, D.T., Park, S., Boneh, G.H., Rice, S.E., and Statsyuk, A.V. (2016). UbFluor: a mechanism-based probe for HECT E3 ligases. Chem. Sci. *7*, 5587–5595. 10.1039/c6sc01167e.

93. Park, S., Foote, P.K., Krist, D.T., Rice, S.E., and Statsyuk, A.V. (2017). UbMES and UbFluor: Novel probes for ring-between-ring (RBR) E3 ubiquitin ligase PARKIN. J. Biol. Chem. *292*, 16539–16553. 10.1074/jbc.m116.773200.

94. Sun, Y. (2005). Overview of Approaches for Screening for Ubiquitin Ligase Inhibitors. Methods Enzym. *399*, 654–663. 10.1016/s0076-6879(05)99043-5.

95. Cesare, V.D., Johnson, C., Barlow, V., Hastie, J., Knebel, A., and Trost, M. (2018). The MALDI-TOF E2/E3 Ligase Assay as Universal Tool for Drug Discovery in the Ubiquitin Pathway. Cell Chem. Biol. *25*, 1117-1127.e4. 10.1016/j.chembiol.2018.06.004.

96. Yang, Y., Kitagaki, J., Dai, R.-M., Tsai, Y.C., Lorick, K.L., Ludwig, R.L., Pierre, S.A., Jensen, J.P., Davydov, I.V., Oberoi, P., et al. (2007). Inhibitors of Ubiquitin-

Activating Enzyme (E1), a New Class of Potential Cancer Therapeutics. Cancer Res *67*, 9472–9481. 10.1158/0008-5472.can-07-0568.

97. von Delbrück, M., Kniss, A., Rogov, V.V., Pluska, L., Bagola, K., Löhr, F., Güntert, P., Sommer, T., and Dötsch, V. (2016). The CUE Domain of Cue1 Aligns Growing Ubiquitin Chains with Ubc7 for Rapid Elongation. Mol. Cell *62*, 918–928. 10.1016/j.molcel.2016.04.031.

98. Mot, A.C., Prell, E., Klecker, M., Naumann, C., Faden, F., Westermann, B., and Dissmeyer, N. (2018). Real-time detection of N-end rule-mediated ubiquitination via fluorescently labeled substrate probes. N. Phytol. *217*, 613–624. 10.1111/nph.14497.

99. Zhang, J.-H., Chung, T.D.Y., and Oldenburg, K.R. (1999). A Simple Statistical Parameter for Use in Evaluation and Validation of High Throughput Screening Assays. J. Biomol. Screen. *4*, 67–73. 10.1177/108705719900400206.

100. Buetow, L., Gabrielsen, M., and Huang, D.T. (2018). The Ubiquitin Proteasome System, Methods and Protocols. Methods Mol. Biol. *1844*, 19–31. 10.1007/978-1-4939-8706-1_2.

101. Pruneda, J.N., Littlefield, P.J., Soss, S.E., Nordquist, K.A., Chazin, W.J., Brzovic, P.S., and Klevit, R.E. (2012). Structure of an E3:E2~Ub Complex Reveals an Allosteric Mechanism Shared among RING/U-box Ligases. Mol Cell *47*, 933–942. 10.1016/j.molcel.2012.07.001.

102. Wenzel, D.M., Lissounov, A., Brzovic, P.S., and Klevit, R.E. (2011). UbcH7 reactivity profile reveals Parkin and HHARI to be RING/HECT hybrids. Nature *474*, 105–108. 10.1038/nature09966.

103. Kim, H.C., and Huibregtse, J.M. (2009). Polyubiquitination by HECT E3s and the Determinants of Chain Type Specificity. Mol Cell Biol *29*, 3307–3318. 10.1128/mcb.00240-09.

104. Hospenthal, M.K., Mevissen, T.E.T., and Komander, D. (2015). Deubiquitinase-based analysis of ubiquitin chain architecture using Ubiquitin Chain Restriction (UbiCRest). Nat. Protoc. *10*, 349–361. 10.1038/nprot.2015.018.

105. Renatus, M., Parrado, S.G., D'Arcy, A., Eidhoff, U., Gerhartz, B., Hassiepen, U., Pierrat, B., Riedl, R., Vinzenz, D., Worpenberg, S., et al. (2006). Structural Basis of Ubiquitin Recognition by the Deubiquitinating Protease USP2. Structure *14*, 1293–1302. 10.1016/j.str.2006.06.012.

106. An, H., and Statsyuk, A.V. (2013). Development of Activity-Based Probes for Ubiquitin and Ubiquitin-like Protein Signaling Pathways. J. Am. Chem. Soc. *135*, 16948–16962. 10.1021/ja4099643.

107. Bhattacharyya, S., Renn, J.P., Yu, H., Marko, J.F., and Matouschek, A. (2016). An assay for 26S proteasome activity based on fluorescence anisotropy measurements of dye-labeled protein substrates. Anal. Biochem. *509*, 50–59. 10.1016/j.ab.2016.05.026.

108. Pickart, C.M., and Raasi, S. (2005). Controlled Synthesis of Polyubiquitin Chains. Methods Enzym. *399*, 21–36. 10.1016/s0076-6879(05)99002-2.

109. Gladkova, C., Maslen, S.L., Skehel, J.M., and Komander, D. (2018). Mechanism of parkin activation by PINK1. Nature *559*, 410–414. 10.1038/s41586-018-0224-x.

110. Nordquist, K.A., Dimitrova, Y.N., Brzovic, P.S., Ridenour, W.B., Munro, K.A., Soss, S.E., Caprioli, R.M., Klevit, R.E., and Chazin, W.J. (2010). Structural and Functional Characterization of the Monomeric U-Box Domain from E4B. Biochemistry *49*, 347–355. 10.1021/bi901620v.

111. Michel, M.A., Elliott, P.R., Swatek, K.N., Simicek, M., Pruneda, J.N., Wagstaff, J.L., Freund, S.M.V., and Komander, D. (2015). Assembly and Specific Recognition of K29- and K33-Linked Polyubiquitin. Mol Cell *58*, 95–109. 10.1016/j.molcel.2015.01.042.

112. Radley, E., Long, J., Gough, K., and Layfield, R. (2019). The 'dark matter' of ubiquitin-mediated processes: opportunities and challenges in the identification of ubiquitin-binding domains. Biochem Soc T *47*, 1949–1962. 10.1042/bst20190869.

113. Wang, M., and Pickart, C.M. (2005). Different HECT domain ubiquitin ligases employ distinct mechanisms of polyubiquitin chain synthesis. Embo J *24*, 4324–4333. 10.1038/sj.emboj.7600895.

114. Kim, H.T., Kim, K.P., Lledias, F., Kisselev, A.F., Scaglione, K.M., Skowyra, D., Gygi, S.P., and Goldberg, A.L. (2007). Certain Pairs of Ubiquitin-conjugating Enzymes (E2s) and Ubiquitin-Protein Ligases (E3s) Synthesize Nondegradable Forked Ubiquitin Chains Containing All Possible Isopeptide Linkages. J. Biol. Chem. *282*, 17375–17386. 10.1074/jbc.m609659200.

115. Scheffner, M., Huibregtse, J.M., Vierstra, R.D., and Howley, P.M. (1993). The HPV-16 E6 and E6-AP complex functions as a ubiquitin-protein ligase in the ubiquitination of p53. Cell *75*, 495–505. 10.1016/0092-8674(93)90384-3.

116. Huibregtse, J.M., Scheffner, M., and Howley, P.M. (1991). A cellular protein mediates association of p53 with the E6 oncoprotein of human papillomavirus types 16 or 18. Embo J *10*, 4129–4135. 10.1002/j.1460-2075.1991.tb04990.x.

117. Franco, L.H., Nair, V.R., Scharn, C.R., Xavier, R.J., Torrealba, J.R., Shiloh, M.U., and Levine, B. (2017). The Ubiquitin Ligase Smurf1 Functions in Selective Autophagy of Mycobacterium tuberculosis and Anti-tuberculous Host Defense. Cell Host Microbe *21*, 59–72. 10.1016/j.chom.2016.11.002.

118. Zhu, L., Zhang, Q., Cordeiro, C.D., Banjade, S., Sardana, R., Mao, Y., and Emr, S.D. (2022). Adaptor linked K63 di-ubiquitin activates Nedd4/Rsp5 E3 ligase. Elife *11*, e77424. 10.7554/elife.77424.

119. Wang, Y., Argiles-Castillo, D., Kane, E.I., Zhou, A., and Spratt, D.E. (2020). HECT E3 ubiquitin ligases – emerging insights into their biological roles and disease relevance. J Cell Sci *133*, jcs228072. 10.1242/jcs.228072.

120. Kamadurai, H.B., Qiu, Y., Deng, A., Harrison, J.S., MacDonald, C., Actis, M., Rodrigues, P., Miller, D.J., Souphron, J., Lewis, S.M., et al. (2013). Mechanism of ubiquitin ligation and lysine prioritization by a HECT E3. Elife *2*, e00828. 10.7554/elife.00828.

121. Maspero, E., Mari, S., Valentini, E., Musacchio, A., Fish, A., Pasqualato, S., and Polo, S. (2011). Structure of the HECT:ubiquitin complex and its role in ubiquitin chain elongation. Embo Rep *12*, 342–349. 10.1038/embor.2011.21.

122. Franklin, T.G., and Pruneda, J.N. (2021). Bacteria make surgical strikes on host ubiquitin signaling. Plos Pathog *17*, e1009341. 10.1371/journal.ppat.1009341.

123. Maculins, T., Fiskin, E., Bhogaraju, S., and Dikic, I. (2016). Bacteria-host relationship: ubiquitin ligases as weapons of invasion. Cell Res *26*, 499–510. 10.1038/cr.2016.30.

124. Nair, R.M., Seenivasan, A., Liu, B., Chen, D., Lowe, E.D., and Lorenz, S. (2021). Reconstitution and Structural Analysis of a HECT Ligase-Ubiquitin Complex via an Activity-Based Probe. Acs Chem Biol *16*, 1615–1621. 10.1021/acschembio.1c00433.

125. Ries, L.K., Liess, A.K.L., Feiler, C.G., Spratt, D.E., Lowe, E.D., and Lorenz, S. (2020). Crystal structure of the catalytic C-lobe of the HECT-type ubiquitin ligase E6AP. Protein Sci *29*, 1550–1554. 10.1002/pro.3832.

126. Sander, B., Xu, W., Eilers, M., Popov, N., and Lorenz, S. (2017). A conformational switch regulates the ubiquitin ligase HUWE1. Elife *6*, e21036. 10.7554/elife.21036.

127. French, M.E., Kretzmann, B.R., and Hicke, L. (2009). Regulation of the RSP5 Ubiquitin Ligase by an Intrinsic Ubiquitin-binding Site. J Biol Chem *284*, 12071–12079. 10.1074/jbc.m901106200.

128. French, M.E., Klosowiak, J.L., Aslanian, A., Reed, S.I., Yates, J.R., and Hunter, T. (2017). Mechanism of ubiquitin chain synthesis employed by a HECT domain ubiquitin ligase. J Biol Chem *292*, 10398–10413. 10.1074/jbc.m117.789479.

129. Huang, L., Kinnucan, E., Wang, G., Beaudenon, S., Howley, P.M., Huibregtse, J.M., and Pavletich, N.P. (1999). Structure of an E6AP-UbcH7 Complex: Insights into

Ubiquitination by the E2-E3 Enzyme Cascade. Science *286*, 1321–1326. 10.1126/science.286.5443.1321.

130. Konno, H., Takeda, K., Muro, I., Kobayashi, F., Flechsig, H., Kodera, N., and Ando, T. (2022). Structural dynamics of E6AP E3 ligase HECT domain and involvement of flexible hinge loop in ubiquitin chain synthesis mechanism. 10.1101/2022.11.18.516873.

131. Wang, M., Cheng, D., Peng, J., and Pickart, C.M. (2006). Molecular determinants of polyubiquitin linkage selection by an HECT ubiquitin ligase. Embo J *25*, 1710–1719. 10.1038/sj.emboj.7601061.

132. Verdecia, M.A., Joazeiro, C.A.P., Wells, N.J., Ferrer, J.-L., Bowman, M.E., Hunter, T., and Noel, J.P. (2003). Conformational Flexibility Underlies Ubiquitin Ligation Mediated by the WWP1 HECT Domain E3 Ligase. Mol Cell *11*, 249–259. 10.1016/s1097-2765(02)00774-8.

133. Nakasone, M.A., Majorek, K.A., Gabrielsen, M., Sibbet, G.J., Smith, B.O., and Huang, D.T. (2022). Structure of UBE2K–Ub/E3/polyUb reveals mechanisms of K48-linked Ub chain extension. Nat Chem Biol *18*, 422–431. 10.1038/s41589-021-00952-x.

134. Deol, K.K., Lorenz, S., and Strieter, E.R. (2019). Enzymatic Logic of Ubiquitin Chain Assembly. Front Physiol *10*, 835. 10.3389/fphys.2019.00835.

135. Kubori, T., Hyakutake, A., and Nagai, H. (2008). Legionella translocates an E3 ubiquitin ligase that has multiple U-boxes with distinct functions. Mol Microbiol *67*, 1307–1319. 10.1111/j.1365-2958.2008.06124.x.

136. Janjusevic, R., Abramovitch, R.B., Martin, G.B., and Stebbins, C.E. (2006). A Bacterial Inhibitor of Host Programmed Cell Death Defenses Is an E3 Ubiquitin Ligase. Science *311*, 222–226. 10.1126/science.1120131.

137. Mukaihara, T., Tamura, N., and Iwabuchi, M. (2010). Genome-Wide Identification of a Large Repertoire of Ralstonia solanacearum Type III Effector Proteins by a New Functional Screen. Mol Plant-microbe Interactions *23*, 251–262. 10.1094/mpmi-23-3-0251.

138. Franklin, T.G., and Pruneda, J.N. (2019). A High-Throughput Assay for Monitoring Ubiquitination in Real Time. Front Chem *7*, 816. 10.3389/fchem.2019.00816.

139. Franklin, T.G., and Pruneda, J.N. (2022). Plant Proteostasis, Methods and Protocols. Methods Mol. Biol. *2581*, 3–12. 10.1007/978-1-0716-2784-6_1.

140. Jumper, J., Evans, R., Pritzel, A., Green, T., Figurnov, M., Ronneberger, O., Tunyasuvunakool, K., Bates, R., Žídek, A., Potapenko, A., et al. (2021). Highly accurate protein structure prediction with AlphaFold. Nature *596*, 583–589. 10.1038/s41586-021-03819-2.

141. Evans, R., O'Neill, M., Pritzel, A., Antropova, N., Senior, A., Green, T., Žídek, A., Bates, R., Blackwell, S., Yim, J., et al. (2022). Protein complex prediction with AlphaFold-Multimer. bioRxiv, 2021.10.04.463034. 10.1101/2021.10.04.463034.

142. Ekkebus, R., Kasteren, S.I. van, Kulathu, Y., Scholten, A., Berlin, I., Geurink, P.P., Jong, A. de, Goerdayal, S., Neefjes, J., Heck, A.J.R., et al. (2013). On Terminal Alkynes That Can React with Active-Site Cysteine Nucleophiles in Proteases. J Am Chem Soc *135*, 2867–2870. 10.1021/ja309802n.

143. Dou, H., Buetow, L., Sibbet, G.J., Cameron, K., and Huang, D.T. (2012). BIRC7–E2 ubiquitin conjugate structure reveals the mechanism of ubiquitin transfer by a RING dimer. Nat Struct Mol Biol *19*, 876–883. 10.1038/nsmb.2379.

144. Plechanovová, A., Jaffray, E.G., Tatham, M.H., Naismith, J.H., and Hay, R.T. (2012). Structure of a RING E3 ligase and ubiquitin-loaded E2 primed for catalysis. Nature *489*, 115–120. 10.1038/nature11376.

145. Stieglitz, B., Rana, R.R., Koliopoulos, M.G., Morris-Davies, A.C., Schaeffer, V., Christodoulou, E., Howell, S., Brown, N.R., Dikic, I., and Rittinger, K. (2013). Structural basis for ligase-specific conjugation of linear ubiquitin chains by HOIP. Nature *503*, 422–426. 10.1038/nature12638.

146. Page, R.C., Pruneda, J.N., Amick, J., Klevit, R.E., and Misra, S. (2012). Structural Insights into the Conformation and Oligomerization of E2∼Ubiquitin Conjugates. Biochemistry-us *51*, 4175–4187. 10.1021/bi300058m.

147. Sakata, E., Satoh, T., Yamamoto, S., Yamaguchi, Y., Yagi-Utsumi, M., Kurimoto, E., Tanaka, K., Wakatsuki, S., and Kato, K. (2010). Crystal Structure of UbcH5b∼Ubiquitin Intermediate: Insight into the Formation of the Self-Assembled E2∼Ub Conjugates. Structure *18*, 138–147. 10.1016/j.str.2009.11.007.

148. Serniwka, S.A., and Shaw, G.S. (2009). The Structure of the UbcH8−Ubiquitin Complex Shows a Unique Ubiquitin Interaction Site. Biochemistry-us *48*, 12169–12179. 10.1021/bi901686j.

149. Eddins, M.J., Carlile, C.M., Gomez, K.M., Pickart, C.M., and Wolberger, C. (2006). Mms2–Ubc13 covalently bound to ubiquitin reveals the structural basis of linkage-specific polyubiquitin chain formation. Nat Struct Mol Biol *13*, 915–920. 10.1038/nsmb1148.

150. Pruneda, J.N., Stoll, K.E., Bolton, L.J., Brzovic, P.S., and Klevit, R.E. (2011). Ubiquitin in Motion: Structural Studies of the Ubiquitin-Conjugating Enzyme∼Ubiquitin Conjugate. Biochemistry-us *50*, 1624–1633. 10.1021/bi101913m.

151. Brzovic, P.S., Lissounov, A., Christensen, D.E., Hoyt, D.W., and Klevit, R.E. (2006). A UbcH5/Ubiquitin Noncovalent Complex Is Required for Processive BRCA1-Directed Ubiquitination. Mol Cell *21*, 873–880. 10.1016/j.molcel.2006.02.008.

152. Michel, M.A., Swatek, K.N., Hospenthal, M.K., and Komander, D. (2017). Ubiquitin Linkage-Specific Affimers Reveal Insights into K6-Linked Ubiquitin Signaling. Mol Cell *68*, 233-246.e5. 10.1016/j.molcel.2017.08.020.

153. Warren, G.D., Kitao, T., Franklin, T.G., Nguyen, J.V., Geurink, P.P., Kubori, T., Nagai, H., and Pruneda, J.N. (2023). Mechanism of Lys6 poly-ubiquitin specificity by the L. pneumophila deubiquitinase LotA. Mol Cell *83*, 105-120.e5. 10.1016/j.molcel.2022.11.022.

154. Lechtenberg, B.C., Rajput, A., Sanishvili, R., Dobaczewska, M.K., Ware, C.F., Mace, P.D., and Riedl, S.J. (2016). Structure of a HOIP/E2~ubiquitin complex reveals RBR E3 ligase mechanism and regulation. Nature *529*, 546–550. 10.1038/nature16511.

155. Mabbitt, P.D., Loreto, A., Déry, M.-A., Fletcher, A.J., Stanley, M., Pao, K.-C., Wood, N.T., Coleman, M.P., and Virdee, S. (2020). Structural basis for RING-Cys-Relay E3 ligase activity and its role in axon integrity. Nat Chem Biol *16*, 1227–1236. 10.1038/s41589-020-0598-6.

156. Chong, R.A., Wu, K., Spratt, D.E., Yang, Y., Lee, C., Nayak, J., Xu, M., Elkholi, R., Tappin, I., Li, J., et al. (2014). Pivotal role for the ubiquitin Y59-E51 loop in lysine 48 polyubiquitination. Proc National Acad Sci *111*, 8434–8439. 10.1073/pnas.1407849111.

157. Pickart, C.M., Haldeman, M.T., Kasperek, E.M., and Chen, Z. (1992). Iodination of tyrosine 59 of ubiquitin selectively blocks ubiquitin's acceptor activity in diubiquitin synthesis catalyzed by E2(25K). J Biol Chem *267*, 14418–14423. 10.1016/s0021-9258(19)49728-7.

158. Pan, M., Zheng, Q., Wang, T., Liang, L., Mao, J., Zuo, C., Ding, R., Ai, H., Xie, Y., Si, D., et al. (2021). Structural insights into Ubr1-mediated N-degron polyubiquitination. Nature *600*, 334–338. 10.1038/s41586-021-04097-8.

159. Hehl, L.A., Horn-Ghetko, D., Prabu, J.R., Vollrath, R., Vu, D.T., Berrocal, D.A.P., Mulder, M.P.C., Noort, G.J. van der H. van, and Schulman, B.A. (2023). Structural snapshots along K48-linked ubiquitin chain formation by the HECT E3 UBR5. Nat. Chem. Biol., 1–11. 10.1038/s41589-023-01414-2.

160. Mao, J., Ai, H., Wu, X., Zheng, Q., Cai, H., Liang, L., Tong, Z., Pan, M., and Liu, L. (2023). Structural Visualization of HECT-E3 Ufd4 accepting and transferring Ubiquitin to Form K29/K48-branched Polyubiquitination on N-degron. bioRxiv, 2023.05.23.542033. 10.1101/2023.05.23.542033.

161. Edén, C.S., Larsson, P., and Lomberg, H. (1980). Attachment of Proteus mirabilis to human urinary sediment epithelial cells in vitro is different from that of Escherichia coli. Infect. Immun. *27*, 804–807. 10.1128/iai.27.3.804-807.1980.

162. Schaffer, J.N., Norsworthy, A.N., Sun, T.-T., and Pearson, M.M. (2016). Proteus mirabilis fimbriae- and urease-dependent clusters assemble in an extracellular niche to initiate bladder stone formation. Proc National Acad Sci *113*, 4494–4499. 10.1073/pnas.1601720113.

163. Roper, M.C. (2011). Pantoea stewartii subsp. stewartii: lessons learned from a xylem-dwelling pathogen of sweet corn. Mol. Plant Pathol. *12*, 628–637. 10.1111/j.1364-3703.2010.00698.x.

164. Kang, S., Kim, G., Choi, M., Jeong, M., Noort, G.J. van der H. van, Roh, S.-H., and Shin, D. (2023). Structural insights into ubiquitin chain cleavage by Legionella ovarian tumor deubiquitinases. Life Sci Alliance *6*, e202201876. 10.26508/lsa.202201876.

165. Luo, J., Ruan, X., Huang, Z., Li, Z., Ye, L., Wu, Y., Zhen, X., and Ouyang, S. (2022). Structural basis for the dual catalytic activity of the Legionella pneumophila ovarian tumor (OTU) domain deubiquitinase LotA. J Biol Chem *298*, 102414. 10.1016/j.jbc.2022.102414.

166. Boll, V., Hermanns, T., Uthoff, M., Erven, I., Hörner, E.-M., Kozjak-Pavlovic, V., Baumann, U., and Hofmann, K. (2023). Unexpected functional and structural diversity in deubiquitinases of the Chlamydia-like bacterium Simkania negevensis. 10.21203/rs.3.rs-2647839/v1.

167. Erven, I., Abraham, E., Hermanns, T., Baumann, U., and Hofmann, K. (2022). A widely distributed family of eukaryotic and bacterial deubiquitinases related to herpesviral large tegument proteins. Nat Commun *13*, 7643. 10.1038/s41467-022-35244-y.

168. Yunus, A.A., and Lima, C.D. (2006). Lysine activation and functional analysis of E2-mediated conjugation in the SUMO pathway. Nat Struct Mol Biol *13*, 491–499. 10.1038/nsmb1104.

169. Wasilko, D.J., Huang, Q., and Mao, Y. (2018). Insights into the ubiquitin transfer cascade catalyzed by the Legionella effector SidC. Elife *7*, e36154. 10.7554/elife.36154.

170. Zhu, Y., Li, H., Hu, L., Wang, J., Zhou, Y., Pang, Z., Liu, L., and Shao, F. (2008). Structure of a Shigella effector reveals a new class of ubiquitin ligases. Nat Struct Mol Biol *15*, 1302–1308. 10.1038/nsmb.1517.

171. Notredame, C., Higgins, D.G., and Heringa, J. (2000). T-coffee: a novel method for fast and accurate multiple sequence alignment11Edited by J. Thornton. J Mol Biol *302*, 205–217. 10.1006/jmbi.2000.4042.

172. Kelley, L.A., Mezulis, S., Yates, C.M., Wass, M.N., and Sternberg, M.J.E. (2015). The Phyre2 web portal for protein modeling, prediction and analysis. Nat Protoc *10*, 845–858. 10.1038/nprot.2015.053.

173. Mirdita, M., Schütze, K., Moriwaki, Y., Heo, L., Ovchinnikov, S., and Steinegger, M. (2022). ColabFold: making protein folding accessible to all. Nat. Methods *19*, 679–682. 10.1038/s41592-022-01488-1.

174. Kempen, M. van, Kim, S.S., Tumescheit, C., Mirdita, M., Lee, J., Gilchrist, C.L.M., Söding, J., and Steinegger, M. (2023). Fast and accurate protein structure search with Foldseek. Nat. Biotechnol., 1–4. 10.1038/s41587-023-01773-0.

175. Studier, F.W. (2005). Protein production by auto-induction in high-density shaking cultures. Protein Expres Purif *41*, 207–234. 10.1016/j.pep.2005.01.016.

176. Wilkinson, K.D., Gan-Erdene, T., and Kolli, N. (2005). Derivitization of the C-Terminus of Ubiquitin and Ubiquitin-like Proteins Using Intein Chemistry: Methods and Uses. Methods Enzymol *399*, 37–51. 10.1016/s0076-6879(05)99003-4.

177. Pruneda, J.N., and Komander, D. (2019). Evaluating enzyme activities and structures of DUBs. Methods Enzymol *618*, 321–341. 10.1016/bs.mie.2019.01.001.

178. Kabsch, W. (2010). XDS. Acta Crystallogr Sect D Biological Crystallogr *66*, 125–132. 10.1107/s0907444909047337.

179. Evans, P.R., and Murshudov, G.N. (2013). How good are my data and what is the resolution? Acta Crystallogr Sect D Biological Crystallogr *69*, 1204–1214. 10.1107/s0907444913000061.

180. McCoy, A.J., Grosse-Kunstleve, R.W., Adams, P.D., Winn, M.D., Storoni, L.C., and Read, R.J. (2007). Phaser crystallographic software. J Appl Crystallogr *40*, 658–674. 10.1107/s0021889807021206.

181. Potterton, L., Agirre, J., Ballard, C., Cowtan, K., Dodson, E., Evans, P.R., Jenkins, H.T., Keegan, R., Krissinel, E., Stevenson, K., et al. (2018). CCP4i2: the new graphical user interface to the CCP4 program suite. Acta Crystallogr Sect D Struct Biology *74*, 68–84. 10.1107/s2059798317016035.

182. Vijay-Kumar, S., Bugg, C.E., and Cook, W.J. (1987). Structure of ubiquitin refined at 1.8Å resolution. J Mol Biol *194*, 531–544. 10.1016/0022-2836(87)90679-6.

183. Langer, G., Cohen, S.X., Lamzin, V.S., and Perrakis, A. (2008). Automated macromolecular model building for X-ray crystallography using ARP/wARP version 7. Nat Protoc *3*, 1171–1179. 10.1038/nprot.2008.91.

184. Emsley, P., Lohkamp, B., Scott, W.G., and Cowtan, K. (2010). Features and development of Coot. Acta Crystallogr Sect D *66*, 486–501. 10.1107/s0907444910007493.

185. Adams, P.D., Afonine, P.V., Bunkóczi, G., Chen, V.B., Davis, I.W., Echols, N., Headd, J.J., Hung, L.-W., Kapral, G.J., Grosse-Kunstleve, R.W., et al. (2010). PHENIX: a comprehensive Python-based system for macromolecular structure solution. Acta Crystallogr Sect D Biological Crystallogr *66*, 213–221. 10.1107/s0907444909052925.

186. Delaglio, F., Grzesiek, S., Vuister, G.W., Zhu, G., Pfeifer, J., and Bax, A. (1995). NMRPipe: A multidimensional spectral processing system based on UNIX pipes. J Biomol Nmr *6*, 277–293. 10.1007/bf00197809.

187. Johnson, B.A., and Blevins, R.A. (1994). NMR View: A computer program for the visualization and analysis of NMR data. J Biomol Nmr *4*, 603–614. 10.1007/bf00404272.

188. Damgaard, R.B., Walker, J.A., Marco-Casanova, P., Morgan, N.V., Titheradge, H.L., Elliott, P.R., McHale, D., Maher, E.R., McKenzie, A.N.J., and Komander, D. (2016). The Deubiquitinase OTULIN Is an Essential Negative Regulator of Inflammation and Autoimmunity. Cell *166*, 1215-1230.e20. 10.1016/j.cell.2016.07.019.

189. Damgaard, R.B., Nachbur, U., Yabal, M., Wong, W.W.-L., Fiil, B.K., Kastirr, M., Rieser, E., Rickard, J.A., Bankovacki, A., Peschel, C., et al. (2012). The Ubiquitin Ligase XIAP Recruits LUBAC for NOD2 Signaling in Inflammation and Innate Immunity. Mol Cell *46*, 746–758. 10.1016/j.molcel.2012.04.014.

190. Makarova, K.S., Aravind, L., and Koonin, E.V. (2000). A novel superfamily of predicted cysteine proteases from eukaryotes, viruses and Chlamydia pneumoniae. Trends Biochem. Sci. *25*, 50–52. 10.1016/s0968-0004(99)01530-3.

191. Furtado, A.R., Essid, M., Perrinet, S., Balañá, M.E., Yoder, N., Dehoux, P., and Subtil, A. (2013). ChlaOTU targets ubiquitin and NDP52. Cell. Microbiol. *15*, 2064–2079. 10.1111/cmi.12171.

192. Michel, M.A., Komander, D., and Elliott, P.R. (2018). The Ubiquitin Proteasome System, Methods and Protocols. Methods Mol. Biol. *1844*, 73–84. 10.1007/978-1-4939-8706-1_6.

193. Wu, T., Merbl, Y., Huo, Y., Gallop, J.L., Tzur, A., and Kirschner, M.W. (2010). UBE2S drives elongation of K11-linked ubiquitin chains by the Anaphase-Promoting Complex. Proc. Natl. Acad. Sci. *107*, 1355–1360. 10.1073/pnas.0912802107.

194. Meyer, H.-J., and Rape, M. (2014). Enhanced Protein Degradation by Branched Ubiquitin Chains. Cell *157*, 910–921. 10.1016/j.cell.2014.03.037.

195. French, M.E., Koehler, C.F., and Hunter, T. (2021). Emerging functions of branched ubiquitin chains. Cell Discov *7*, 6. 10.1038/s41421-020-00237-y.

196. Ozkaynak, E., Finley, D., Solomon, M.J., and Varshavsky, A. (1987). The yeast ubiquitin genes: a family of natural gene fusions. EMBO J. *6*, 1429–1439. 10.1002/j.1460-2075.1987.tb02384.x.

197. Zuin, A., Isasa, M., and Crosas, B. (2014). Ubiquitin Signaling: Extreme Conservation as a Source of Diversity. Cells *3*, 690–701. 10.3390/cells3030690.

198. Sharp, P.M., and Li, W.-H. (1987). Ubiquitin genes as a paradigm of concerted evolution of tandem repeats. J. Mol. Evol. *25*, 58–64. 10.1007/bf02100041.

199. Elia, A.E.H., Boardman, A.P., Wang, D.C., Huttlin, E.L., Everley, R.A., Dephoure, N., Zhou, C., Koren, I., Gygi, S.P., and Elledge, S.J. (2015). Quantitative Proteomic Atlas of Ubiquitination and Acetylation in the DNA Damage Response. Mol. Cell *59*, 867–881. 10.1016/j.molcel.2015.05.006.

200. Wu-Baer, F., Lagrazon, K., Yuan, W., and Baer, R. (2003). The BRCA1/BARD1 Heterodimer Assembles Polyubiquitin Chains through an Unconventional Linkage Involving Lysine Residue K6 of Ubiquitin*. J. Biol. Chem. *278*, 34743–34746. 10.1074/jbc.c300249200.

201. Irminger-Finger, I., and Jefford, C.E. (2006). Is there more to BARD1 than BRCA1? Nat. Rev. Cancer *6*, 382–391. 10.1038/nrc1878.

202. Pan, X., Alvarez, A.N., Ma, M., Lu, S., Crawford, M.W., Briere, L.C., Kanca, O., Yamamoto, S., Sweetser, D.A., Wilson, J.L., et al. (2023). Allelic strengths of encephalopathy-associated UBA5 variants correlate between in vivo and in vitro assays. eLife. 10.7554/elife.89891.

203. Taniguchi, S., Ono, Y., Doi, Y., Taniguchi, S., Matsuura, Y., Iwasaki, A., Hirata, N., Fukuda, R., Inoue, K., Yamaguchi, M., et al. (2023). Identification of α-Tocopherol succinate as an RFFL-substrate interaction inhibitor inducing peripheral CFTR stabilization and apoptosis. Biochem. Pharmacol. *215*, 115730. 10.1016/j.bcp.2023.115730.

204. Merklinger, L., Bauer, J., Pedersen, P.A., Damgaard, R.B., and Morth, J.P. (2022). Phospholipids alter activity and stability of mitochondrial membrane-bound ubiquitin ligase MARCH5. Life Sci. Alliance *5*, e202101309. 10.26508/lsa.202101309.

205. Taherbhoy, A.M., Schulman, B.A., and Kaiser, S.E. (2012). Ubiquitin-like modifiers. Essays Biochem. *52*, 51–63. 10.1042/bse0520051.

206. Rahmanto, A.S., Blum, C.J., Scalera, C., Heidelberger, J.B., Mesitov, M., Horn-Ghetko, D., Gräf, J.F., Mikicic, I., Hobrecht, R., Orekhova, A., et al. (2023). K6-linked

ubiquitylation marks formaldehyde-induced RNA-protein crosslinks for resolution. Mol. Cell. 10.1016/j.molcel.2023.10.011.

207. Yang, B., Pei, J., Lu, C., Wang, Y., Shen, M., Qin, X., Huang, Y., Yang, X., Zhao, X., Ma, S., et al. (2023). RNF144A promotes antiviral responses by modulating STING ubiquitination. EMBO Rep., e57528. 10.15252/embr.202357528.

208. Boll, V., Hermanns, T., Uthoff, M., Erven, I., Hörner, E.-M., Kozjak-Pavlovic, V., Baumann, U., and Hofmann, K. (2023). Functional and structural diversity in deubiquitinases of the Chlamydia-like bacterium Simkania negevensis. Nat. Commun. *14*, 7335. 10.1038/s41467-023-43144-y.

209. Vierstra, R.D. (2009). The ubiquitin–26S proteasome system at the nexus of plant biology. Nat Rev Mol Cell Bio *10*, 385–397. 10.1038/nrm2688.

210. Oualid, F.E., Merkx, R., Ekkebus, R., Hameed, D.S., Smit, J.J., Jong, A. de, Hilkmann, H., Sixma, T.K., and Ovaa, H. (2010). Chemical Synthesis of Ubiquitin, Ubiquitin-Based Probes, and Diubiquitin. Angewandte Chemie Int Ed Engl *49*, 10149–10153. 10.1002/anie.201005995.

Appendix A - Observing real-time ubiquitination in high-throughput with fluorescence polarization

Franklin, T.G. and Pruneda, J.N. (2022). *Plant Proteostasis, Methods and Protocols*. Methods Mol. Biol. 2581, 3–12. 10.1007/978-1-0716-2784-6_1.

Author Contributions: TF and JP conceptualized the approach. TF performed all experiments. TF and JP analyzed the data and wrote the manuscript.

Abbreviations: Ub, ubiquitin; FP, fluorescence polarization; DUB, deubiquitinase; HTS, high-throughput screen; T-Ub, TAMRA-Ub; F-Ub, Fluorescein-Ub.

A1.1 Introduction

Ubiquitination is a versatile post-translational modification that is used to regulate virtually every cellular pathway in eukaryotes using both degradative and non-degradative processes[1]. Approximately 5% of the human transcriptome encodes ubiquitin (Ub)-regulating proteins, and the dysregulation of even individual proteins in this intricate system can lead to disease states like cancer, neurodegenerative diseases, and autoimmunity in humans[2,73]. In plants, an estimated 6% of the transcriptome is dedicated to the Ub proteasome system (UPS), which crucially regulates plant responses to hormones, stressors, and infectious pathogens[209]. The vast number of Ub regulators in humans includes Ub-activating E1s (2), Ub-conjugating E2s (~35), Ub-ligating E3s (>600), deubiquitinases (DUBs, ~100), as well as proteins with Ub-binding domains (UBDs, >100), many of which are incompletely characterized[1,2]. For comparison, the model plant Arabidopsis thaliana expresses 2 E1s, at least 37 E2s, >1400 E3s, and ~64 DUBs, with a considerable amount more E3s involved in the UPS relative to humans[209]. In a typical ubiquitination event, an ATP-dependent reaction allows the formation of an activated E1~Ub complex, in which the Ub C-terminus is covalently attached to the E1 active site cysteine through a high energy, thioester linkage. Binding of an E2 enables Ub transfer and formation of an activated E2~Ub complex. Next, an E3 ligase will facilitate Ub transfer onto a substrate protein. In the case of E3 ligases from the Really Interesting New Gene (RING) family, Ub is transferred directly from the E2 to a substrate, whereas E3 ligases from the Homologous to the E6AP C-terminus (HECT) and RING-between-RING (RBR) families form one final E3~Ub intermediate before modifying a substrate.

The consequences of Ub dysregulation in humans and plants with respect to the vast

number of Ub regulatory proteins make it pertinent to understand how E1s, E2s, E3s, DUBs, and UBDs interact with each other to generate and fine-tune Ub signals. Similarly, therapeutic manipulation of those interactions and ubiquitination events will offer important advances in disease intervention for humans and in improved agricultural strategies for plants[73,209]. While many robust assays already exist for monitoring Ub regulation, most are either highly specialized to one network of interactions or are specific to deubiquitination events. Therefore, we sought to develop a versatile assay that could be used in real time to visualize the whole E1-E2-E3-DUB cascade — as well as the effects of inhibitors (or activators) on those regulators — in a high-throughput format.

Using fluorescence polarization (FP), which effectively monitors changes in protein size by virtue of tumbling rate, we developed the "UbiReal" assay that discerns the flow of Ub through the entire E1-E2-E3-DUB signaling cascade. A Ub labelled at the N-terminus with a TAMRA fluorophore (T-Ub) generates a small FP signal because of its small size, but a larger FP signal upon addition of the E1 and subsequent ATP-dependent formation of the E1~Ub complex (**Fig. A1. 1**). Next, addition of an E2 results in transfer of the T-Ub from the E1 to produce the relatively smaller E2~Ub conjugate, causing a resultant decrease in FP signal (**Fig. A1. 1**). Addition of a HECT-type E3, followed by excess unlabeled Ub, produces large increases in FP signal as the E3 generates polyUb signals and/or adds Ub onto itself (a process known as auto-ubiquitination) (**Fig. A1. 1**). Finally, addition of a DUB reduces the FP signal over time as the E3-generated polyUb signals are hydrolyzed. We have validated this real-time assay in a high-throughput, 384-well format to characterize an E1 inhibitor, monitor amino acid selectivity of E2s, determine specificity of E2 and E3 pairs, and observe the Ub chain-type specificity of both E3s and DUBs[138].

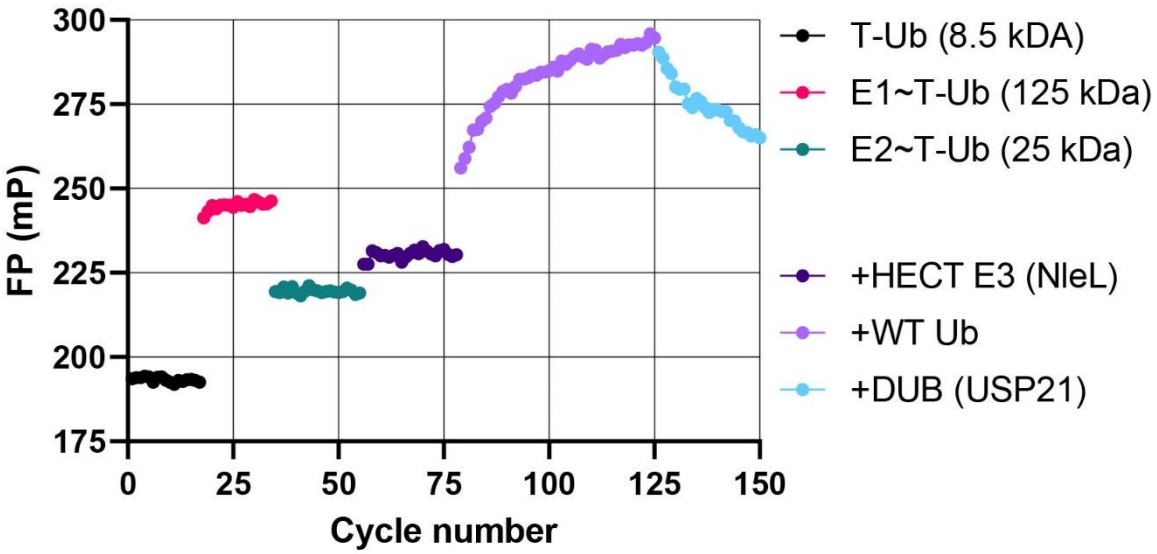

Figure A1. 1 Method overview

E1-E2-E3 ubiquitin conjugation and DUB hydrolysis using UbiReal. T-Ub (black) was monitored before addition of E1 to generate E1~T-Ub (red) (5 mM ATP and 10 mM MgCl2 were already present in the buffer). Next, the E2 UBE2D3 at 300 nM was added to produce E2~T-Ub (green). The E3 NleL at 700 nM was then added to produce NleL~T-Ub (dark blue) (with the possibility of ubiquitin chain formation). Next, unlabeled Ub was added at 25 µM and monitored for several cycles, showing NleL-conjugated poly-ubiquitin substrates which amplified the T-Ub signal (purple). Finally, the non-specific DUB USP21 at 250 nM was added and monitored for several cycles to begin cleaving the poly-ubiquitin signals back into mono-ubiquitin (cyan). The separation in FP signal between each complex presents a potential point at which to explore inhibition/activation by chemical or protein modulators. Other applications include investigating functional mutations of E1s, E2s, E3s, and DUBs, or interactions therein. Raw FP signal is shown. Data represent a single experiment.

Here, we provide a detailed description of these and additional applications of UbiReal, demonstrating its utility as a tool for basic and applied Ub research.

A1.2 Materials

A1.2.1 Ub enzymes

The recombinant enzymes that are required (i.e., E1, E2, etc.) will depend on the specific application and focus of research. These proteins can be produced in-house or many commonly used proteins can be purchased through companies such as R&D Systems. A kit of common UbiReal reagents will be available from R&D Systems in the near future.

A1.2.2 Fluorescent probes

Any Ub with a fluorophore on its N-terminus and an intact C-terminus should function in UbiReal. All experiments herein utilized Ub labelled at the N-terminus with a TAMRA fluorophore (T-Ub)[210] (available from UBPBio). We have also observed equal success using N-terminally labeled fluorescein Ub[138] (available from R&D Systems). Studies that require an available N-terminus, such as the formation of linear polyUb, should consider an alternative labeling site such as modification of a S20C Ub variant.

A1.2.3 Protein concentrations and buffer conditions

Unless otherwise specified, enzyme concentrations for each assay are as follows: 100 nM T-Ub, 125 nM E1, 2 μM E2 (UBE2D3 or UBE2L3), 2 μM E3 (NleL, SopA, or NEDD4L) (see Note 1).

All experiments were performed in buffer containing 25 mM sodium phosphate (pH 7.4), 150 mM sodium chloride, 0.5 mM dithiothreitol (DTT), 10 mM magnesium chloride, with any augmentations and the specific time of 5 mM ATP addition noted.

A1.2.4 Plate reader and assay parameters

All experiments were performed using a BMG LabTech CLARIOstar plate reader set to a controlled temperature of 20 °C. Data were collected every 30-60 seconds with 20 flashes per well. The instrument was set to read the T-Ub TAMRA fluorophore using an excitation wavelength of 540 nm, an emission wavelength of 590 nm, and an LP 566 nm dichroic mirror. All experiments utilized Greiner 384-well small-volume HiBase microplates using total volumes of approximately 20 µL per sample well.

A1.3 Methods

In this chapter, we provide detailed protocols for selected applications of the UbiReal methodology. Section A1.3.1 details how to use UbiReal for studying functional mutations of E3 Ub ligases. Section A1.3.2 describes how the UbiCRest methodology[104] can be applied to UbiReal to determine chain specificities of E3 Ub ligases. Finally, Section A1.3.3 explains a proof-of-concept application of UbiReal as a screen for ubiquitination inhibitors by quantifying inhibition of the E1~Ub complex by PYR-41[96].

A1.3.1 Monitoring activity of E3 Ub ligases

1) Prepare a 2X master mix (10 µL × number of samples) containing E1, E2, T-Ub, and 37.5 µM unlabeled wild-type (WT) Ub substrate (see Note 2) in the described buffer lacking ATP. After preparation, allow the master mix to come to room temperature (keeping it in a dark place) for approximately 5-10 mins (see Notes 3 and 4).

2) Prepare the E3 samples, as well as a ‘no E3' negative control, at 2X the desired final concentration in buffer containing 10 mM ATP and similarly allow these samples to come to room temperature.

3) Add 10 µL of the 2X master mix from Step 1 to sample wells of a 384-well plate and insert the plate into the plate reader. Begin the FP time-course experiment and record the baseline FP signal of each sample for 5-10 cycles.

4) Pause the FP experiment on the plate reader. Remove the plate from the plate reader and add 10 µL of the E3 samples (or the 'no E3' control) from Step 2 to each sample well, mix, and quickly resume the FP experiment in the plate reader (see Note 5). Monitor the experiment for 1-2 hrs, or until no further change in FP signal is observed (see Note 6).

5) Analyze and plot the data to compare the kinetics of the E3s (**Fig. A1. 2**) (see Section A1.3.4).

A1.3.2 Applying UbiReal to UbiCRest to determine Ub linkage types

1) Prepare a 1X master mix (15 µL × number samples) of E1, E2, E3, T-Ub, and 37.5 µM unlabeled WT Ub in the described buffer. Save a portion of the master mix without ATP added, at least 15 µL per DUB to be used later. Finally, add ATP to the remaining master mix.

2) Let the reaction proceed in the dark at 37 °C for 1-2 hrs, or more depending on the kinetics of the E2 and E3.

3) Quench the Ub conjugation reaction by adding a solution of high molarity EDTA and DTT to a final concentration of 30 mM and 5 mM, respectively.

4) Prepare the DUBs at 4X the final desired concentration in buffer supplemented with 10 mM DTT (5 µL × number of samples treated by that DUB).

5) Distribute 15 µL of each 1X master mix (including both the +ATP and the 'no ATP'

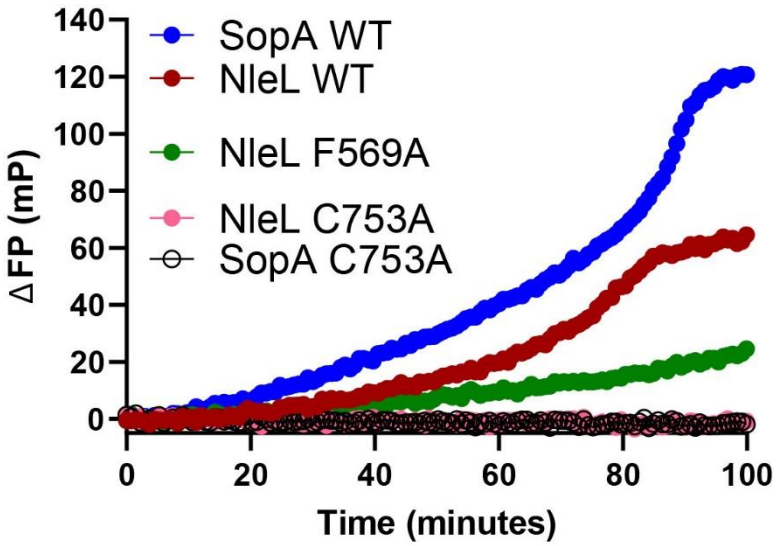

Figure A1. 2 Application to E3 Ub ligases

Ubiquitin conjugation assay using the HECT-type E3 ubiquitin ligases NleL and SopA, and some of their functionally defective mutants. The C753A mutants are catalytically inactive forms of both E3s, where the active site cysteine has been mutated to alanine. The NleL F569A mutant lacks a functional phenylalanine residue that supports binding of NleL to the E2 UBE2L3 and subsequent Ub transfer[50]. FP data shown are normalized to a 'no E3' control. Data represent a single experiment.

6) control mixtures) from Steps 1-3 to the 384-well plate. Begin the FP time-course experiment and record the baseline FP signal of each sample for 5-10 cycles.

7) Pause the FP experiment on the plate reader. Remove the plate, and add 5 µL of the DUB (or buffer as the negative control), mix, and quickly resume the FP experiment in the plate reader (see Note 4). Each DUB used to cleave the +ATP master mix should also be added to a 'no ATP' master mix as the positive control (see Note 5). Monitor the experiment for 1-2 hrs, or until no further change in FP signal is observed (see Note 6).

8) Analyze and plot the data to compare the kinetics of each DUB treatment (**Fig. A1.3**) (see Section A1.3.4).

A1.3.3 UbiReal to quantify inhibitor potency

1) Prepare the inhibitor at concentrations at least 40X above the highest desired final value (see Note 7).

2) As starting material, generate the appropriate Ub complex that is the target of the inhibitor. For example, if the inhibitor targets a DUB, generate Ub chains as in Steps 1-3 of Section A1.3.2. In this example, the drug PYR-41 inhibits formation of the E1~Ub complex (**Fig. A1. 1**), and so a mixture of apo E1 and T-Ub in the absence of ATP is the starting material (**Fig. A1. 4**) (see Note 8).

3) In the 384-well plate, add the starting material (without inhibitor) and begin the FP time-course experiment, recording the baseline FP signal of each sample for 5-10 cycles.

4) Pause the experiment and add 0.5 µL of the inhibitor dilutions into the sample wells,

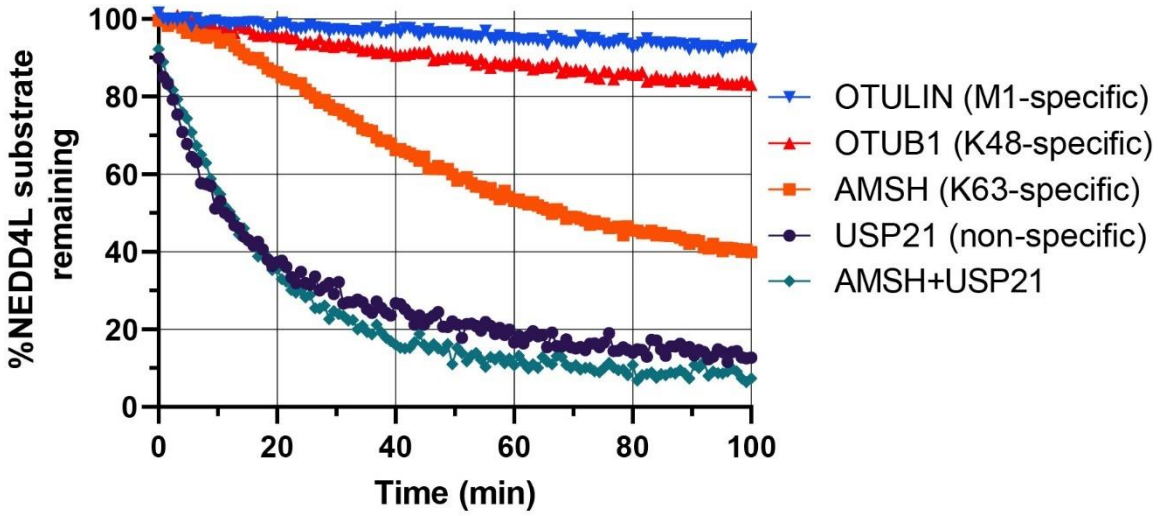

Figure A1. 3 Application to DUBs

Ubiquitin deconjugation assay using starting material generated by the E3 ubiquitin ligase NEDD4L that is cleaved using several different DUBs with varied linkage specificities. Since K63-specific AMSH cleaves a large amount of substrate, these data support the K63-specificity of NEDD4L[47]. AMSH appears unable to cleave the terminal ubiquitin linkage on the substrate (NEDD4L in this case) and so the difference between the AMSH and non-specific USP21 may indicate the relative presence of polyUb vs. mono-ubiquitinated NEDD4L (see ref.[138]). FP data shown are normalized to positive and negative controls (see Section 3.4). Data represent a single experiment.

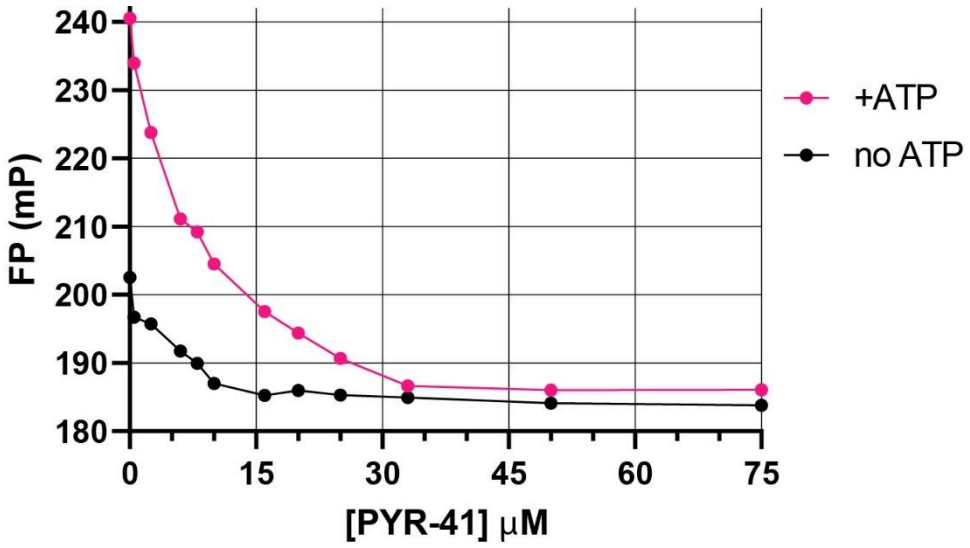

Figure A1. 4 Application as a drug screen

PYR41-mediated inhibition of E1~Ub complex formation. E1 and T-Ub were incubated with dilutions of PYR-41 and formation of the E1~Ub complex was monitored following addition of ATP. The negative control of 'no ATP' is shown for reference. Raw FP data are shown. Data represent a single experiment.

5) mix, and again record the baseline FP signal for 5-10 cycles (see Note 4).

6) Pause the experiment one last time, add the missing substrate to initiate the reaction and mix. For example, if studying a DUB inhibitor, then add the DUB now. In this experiment, the missing substrate is ATP, and so ATP is added now to initiate the reaction (see Note 4).

7) Quickly return the plate to the plate reader, and let the experiment proceed for 1-2 hrs, or until no further change FP signal is observed (see Note 6).

8) Analyze and plot the data to observe the inhibitor potency (**Fig. A1. 4**) (see Section A1.3.4).

A1.3.4 Data analysis

1) Data analysis for each experiment is simple but relies on appropriate positive and negative controls (which will vary for each experiment) to be able to appropriately normalize the data.

2) Section A1.3.1, which explores the effect of functional mutations on ligation activity for an E3 Ub ligase, requires a positive control (WT E3) representing the highest possible signal, as well as a negative control ('no E3', or a catalytically inactive form of the E3) representing the lowest possible FP signal. Data can be presented as in **Fig. A1. 2**, where it is normalized to only the negative control to determine the change in FP over time, or normalized using Equation 1 (see below).

3) Section A1.3.2 requires a negative control (no DUB) representing the highest possible FP signal and a positive control (DUB with the ligation mixture lacking ATP) representing the lowest possible signal and maximum DUB cleavage (this

control is specific to each DUB).

4) Each data point may be normalized as in **Fig. A1. 3** using the following equation:

   a. Equation 1: $\left[{(X_t - LC_t)}\Big/{(HC_t - LC_t)}\right] * 100\%$

   b. Where X represents the sample of interest, HC represents the control with the highest possible signal, and LC represents the control with the lowest possible signal, calculated at each time point t. (see Note 9.)

5) Section A1.3.3, and normalizing inhibitor data in general, requires a control sample with minimal inhibition as well as a control sample with maximum inhibition. For example, in **Fig. A1. 4** PYR-41 prevents E1~Ub complex formation, and so maximum inhibition is the lowest possible FP signal (T~Ub alone) and minimal inhibition is the maximum possible FP signal (E1~T-Ub) (**Fig. A1. 1**). In order to achieve these controls with the equivalent buffer conditions in Section A1.3.3 and **Fig. A1. 4**, the maximum inhibition control is a sample of E1, T-Ub, and the maximum dose of PYR-41 but lacking ATP, while the minimum inhibition control is a sample of E1, T-Ub and ATP given DMSO alone instead of PYR-41. The exact controls needed to properly normalize the data for a specific experiment will differ on a case-by-case basis.

Assay Notes

1) Enzyme concentrations should be adjusted to suit enzyme kinetics and the desired reaction step. For characterizing E3s, using a concentration of the E3 that consumes the entirety of the Ub substrate in 1-2 hrs is generally ideal.

2) Delayed addition of unlabeled Ub produces a higher signal from the early transfer

of T-Ub, as done in **Fig. A1. 1**, while in this example the T-Ub and unlabeled Ub are mixed together prior to initiating the reaction. Ub mutants can also be utilized to explore chain specificity of a Ub ligase. For example, for a K63-specific ligase like NEDD4L[47], using a panel of Ub mutants where one lysine is mutated to arginine and therefore non-conjugatable at that residue, the K63R mutant should only allow mono-auto-ubiquitination modifications, while the WT Ub substrate or any other K-to-R mutant will allow Ub chain ligation and result in a higher FP signal (see ref.[138]).

3) Allowing each master mix/substrate to reach room temperature (the operating temperature of the plate reader in these experiments) will prevent erroneous FP signal changes due to temperature fluctuation.

4) Note that, if screening a large number of samples, use of a multi-channel pipette will improve efficiency and limit the time between addition of ATP/DUB and returning the plate to the plate reader. Simply pipette the reagent into multiple small-volume tubes or a trough prior to addition.

5) The 'no ATP' control should resemble the FP signal of the T-Ub substrate alone, and the +ATP samples should be much higher (50-200 mP relative to the control). The 'no ATP' control will be important to determine the minimal FP signal of the reaction mixture in the presence of the DUB, as some DUBs have been observed to have moderate affinity for monoUb which may result in an artificially high FP signal[105].

6) The 384-well plates in these experiments are open, and so evaporation will occur over time. We observed that experiments exceeding 2 hrs begin to noticeably

decrease in volume, which could produce erroneous changes to the observed FP signal. If longer incubations are needed (i.e., if using an enzyme with slow kinetics), the plate should be sealed throughout the experiment, a solution which other groups have utilized successfully[50].

7) Should the drug require DMSO to be dissolved (as is the case for PYR-41), it is best practice to dilute this into the assay as far as possible and include a matched vehicle control, since the DMSO itself may impair enzymatic activity.

8) The difference in FP signals varies between different (E1-E2-E3)~Ub states, but typically a larger FP difference will aid in characterizing the drug and observing FP changes generally. In order to increase this FP difference and improve the z' of the inhibition assay, a solubility tag such as GST or SUMO may be added to the target to increase its size and resultant FP signal when conjugated to the fluorescent Ub.

9) This equation can also be used to normalize the data in **Fig. A1. 2** and **Fig. A1. 4**.